7-1-1992

Mathematical modeling of incompressible flow through a collapsible tube

Jennifer L. Lowdermilk

MATHEMATICAL MODELING OF INCOMPRESSIBLE FLOW THROUGH A COLLAPSIBLE TUBE

by

Jennifer L. Lowdermilk

A thesis submitted to the Faculty of
Rochester Institute of Technology
in partial fulfillment of the requirements
for the degree of

MASTER OF SCIENCE

July 1992

Approved by:

Dr. Mark H. Kempski, Thesis Advisor
Mechanical Engineering Department
Rochester Institute of Technology

Dr. Alan H. Nye
Mechanical Engineering Department
Rochester Institute of Technology

Dr. Joseph S. Török
Mechanical Engineering Department
Rochester Institute of Technology

Dr. Charles W. Haines, Department Head
Mechanical Engineering Department
Rochester Institute of Technology

I, Jennifer L. Lowdermilk, do hereby grant permission to Wallace Memorial Library, of Rochester Institute of Technology, to reproduce my thesis in whole or in part. Any reproduction will not be for commercial use or profit.

July 29, 1992

ABSTRACT

An in-depth examination of eight articles pertaining to collapsible tube phenomenon is provided. Experimental models and mathematical models are explored. Two mathematical models are developed by the author, each of which attempt to reproduce experimental data provided by Lyon [37]. Respective models produce sets of coupled differential equations, and Advanced Continuous Simulation Language (ACSL) is utilized to solve these equations. Neither of the author's models provides total numerical reproductions of the experimental data under consideration. However, general trends are obtained which correspond to those observed in Lyon's data. General responses to variations in system parameters are provided for both models.

ACKNOWLEDGMENTS

I would like to express my gratitude to my parents Ron and Carol Horwath, and David and Ann Lowdermilk, and to my sister Leslie Lowdermilk for their love, support and most of all encouragement through the completion of this work. I love you all very much.

TABLE OF CONTENTS

LIST OF FIGURES

LIST OF SYMBOLS

ρ - fluid density

μ - fluid absolute viscosity

α - area ratio ($\alpha=A/A_0$)

ν - Poisson's ratio

τ_W - tube wall shear stress

A_0 - nominal cross-sectional area of collapsible tube

A - altered cross-sectional area of collapsible tube

A_i - inlet cross-sectional area of tube segment

A_o - outlet cross-sectional area of tube segment

c - wave speed

D_0 - nominal diameter of collapsible tube

E - Young's Modulus of collapsible tube

f_L - laminar skin friction coefficient

f_T - turbulent skin friction coefficient

H - collapsible tube wall thickness

K_p - tube stiffness factor

L - length of collapsible tube segments

M - momentum of flowing fluid

n - tube law index

P - pressure of flowing fluid inside collapsible tube

P_{atm} - atmospheric pressure

P_e - external pressure

P_i - inlet pressure

P'_i - inlet pressure measured in rigid tube

P_o - outlet pressure

P'_o - outlet pressure measured in rigid tube

P_{TM} - transmural pressure ($P_{TM} = P - P_e$)

P^*_{TM} - dimensionless transmural pressure ($P^*_{TM} = P_{TM}/K_p$)

Q - fluid flow rate

rad - nominal radius of collapsible tube

R_{in} - resistance of upstream rigid tube

R_o - outflow resistance

R_e - Reynolds number

S - speed index (S=u/c)

u - fluid velocity

V - volume of collapsible tube segment

1.0 INTRODUCTION

The phenomenon of incompressible flow in collapsible tube segments has been investigated by engineers, physiologists, and mathematicians for years. Understanding pressure-flow characteristics and how they relate to the tube properties is relevant to flow in coronary arteries and veins, pulmonary veins and airways, and hydraulic systems.

This research seeks to investigate collapsible tube phenomena as it relates to transmural myocardial blood flow. 'Myo' is a prefix denoting muscle and 'cardi' is a prefix denoting heart, therefore myocardium is muscle of the heart. More specifically, the myocardium is the middle of three layers that form the heart wall. The inner layer is a delicate membrane that lines the heart and is referred to as the endocardium. The outer layer is a serum containing a membrane that envelopes the heart and is referred to as the epicardium. Located within the myocardium are the blood vessels which deliver blood to the heart itself, and are collectively referred to as the coronary vasculature. Coronary blood flow is phasic and pulsitile due to the pumping nature of the heart, and interactions between intramyocardial blood vessels and mechanical forces generated within the myocardium.

The cardiac cycle consists of two phases, systole and diastole. Systole is the period during which the heart contracts. Blood in the heart chambers is ejected into the arteries for distribution throughout the body. Diastole is the period between

contractions where the myocardium relaxes, allowing the heart chambers to refill with blood.

1.1 Coronary Flow Alteration

Intramyocardial pressure (IMP) is defined as "the hydrostatic pressure in the soft tissue surrounding the myocardial fibers" [1]. Intramyocardial pressure surrounding peripheral coronary blood vessels may rise markedly during systole. If IMP exceeds vascular perfusion pressure, compliant intramyocardial blood vessels may be subject to collapsible tube behavior. Such a situation may alter blood flow through the vessel, as well as in vascular segments

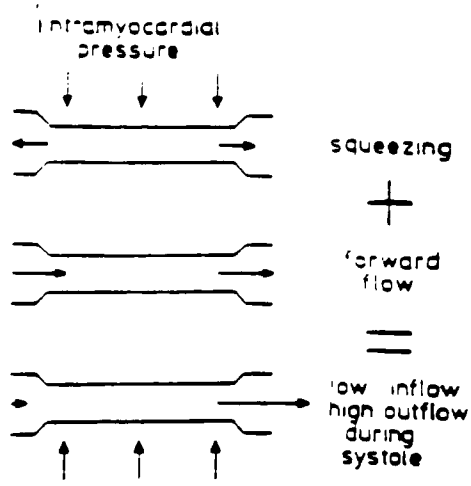

FIGURE 1 - Effect of constriction on a blood vessel (From Arts [1])

upstream and downstream of the collapsed segment. A mechanistic hypothesis for flow augmentation is depicted in Figure 1. The constriction plus normal forward flow results in low blood inflow and high blood outflow, as shown. If the difference between outflow and inflow is great enough, an interruption of blood flow to the tissue may occur. This interruption of flow reduces delivered oxygen to the tissue, defined as ischemia, and may be a contributing factor in the pathogenesis of myocardial infarction [24].

1.2 Collapsible Tube Flow

Transmural pressure, P_{TM}, is defined as the difference between the internal and external pressures of a tube segment.

$$P_{TM} = P - P_e \tag{1}$$

If the external pressure exceeds the internal pressure, transmural pressure becomes negative and tube collapse may occur. Collapse may be partial or complete and is defined as any condition between a (nominally) circular cross-section and total closure. Regardless of the degree of collapse, pressure-flow relationships are affected. Likewise, if transmural pressure becomes positive, the tube may become distended and pressure-flow relationships are again affected.

1.3 Physiological Application - The Starling Resistor

Blood flow in a coronary vessel is analogous to a collapsible

tube segment carrying an incompressible fluid, for example water, with an external pressure supplied to mimic IMP. Any vessel which undergoes collapse is characterized as a "Starling resistor", taking its name from E.H. Starling. He first utilized a collapsible tube segment suspended between rigid tubes in a pressure-controlled compartment in his heart-lung experiments [30]. Since that time, many experiments have been performed on some variation of his apparatus, investigating many aspects of pressure-flow relationships. These include experiments looking at general pressure-flow relationships [14], self-excited oscillations [2,26] and their link to choking [3], high [39] and low [38] Reynolds number flow, fluctuating upstream pressure [36], oscillatory external pressure [56], branching tubes [15], thick-walled tubes [5], microtubes [49], the effect of wall thickness and strain [4], the effects of tube diameter, length, tension, and of fluid viscosity [37], and the application of collapsible tube flow to cardiac assist devices [34]. In addition, physiological canine experiments are often performed to investigate pressure-flow relationships [8,9,12,13,24,26,35,51,57]. Other investigators have utilized rats [50], rabbits [31], and cats [23].

The earliest mathematical model of flow through a collapsible tube was referred to as the "waterfall model" by Permutt and Riley [41]. They postulated that when a vessel is partially collapsed, the flow through that vessel is independent of outflow pressure, just as flow over a waterfall is independent of waterfall height. Many diversified mathematical models have since emerged, each

trying to model the many complicated facets of collapsible tube phenomenon. Investigators have looked at unidimensional steady flow [7], stenotic collapsible tubes [32], flow limitation [43], the filling of a partially collapsed tube [27], post buckling behavior of elastic tubes [21], time-dependent blood perfusion [6], skeletal muscle microcirculation [33], branching tubes with stenoses [44], steady and nonsteady flow in pulmonary airways [29], nonlinear elastic response of large arteries [17], tube oscillations in a separated flow model [11], the development of a nonlinear wave equation [54], flow in the fully dilated coronary vasculature [10], forced expiration [19], and the development of a tube law for the bronchial airways [18]. Algebraic manipulation of equations [46], finite differencing schemes [20,40], finite elements methods [42], electrical analog models [52,53], Windkessel model [55], fourth- and fifth-power laws [58], and iterative processes [47] have all been employed to solve the resulting equations.

Although the main emphasis on collapsible tube phenomenon has been biomedical, this phenomenon is also present in submarine and aeronautical hydraulic systems, among others.

1.4 Summary of Intent

The object of this investigation is to mathematically model a single collapsible tube segment perfused with water and subject to a constant external pressure. Once simplified modeling is successful, nonlinear components can be introduced, and the results

compared to the published experimental data of Lyon [37]. With good comparison between experimental and mathematical results, external pressure can be implemented in a time-varying manner, which is consistent with coronary flow alteration.

2.0 LITERATURE REVIEW

Many articles have been published that investigate the pressure-flow relationships of collapsible tube flow, and several pertinent experimental and mathematical studies are presented here.

2.1 Conrad [14]

One of the earliest experimental investigations of steady and non-steady flow was performed by Conrad [14] using what has since become the standard apparatus for such analyses, as depicted in Figure 2. A collapsible tube, typically Penrose (latex) tubing, is suspended in an airtight box between rigid tubes. The pressure inside the airtight box (external pressure), P_e, can be modified during experimentation. Pressures upstream and downstream of the collapsible tube, P_i and P_o respectively, are measured, as is the fluid flow rate, Q, through the tube. Resistances are often applied by clamping a segment of tubing spliced into the rigid inlet (R_1) and outlet (R_2) sections of the collapsible tube.

Experiments were conducted by varying flow while keeping the external pressure and downstream resistance constant. The variation in flow was produced by either modifying the upstream resistance, or by utilizing a variable speed piston pump. Upstream and downstream pressures were allowed to vary freely.

A general characterization of the pressure-flow relationship of Conrad's Starling resistor subject to constant external pressure is shown in Figure 3. In Region I, $P_e > P_i > P_o$, the tube is

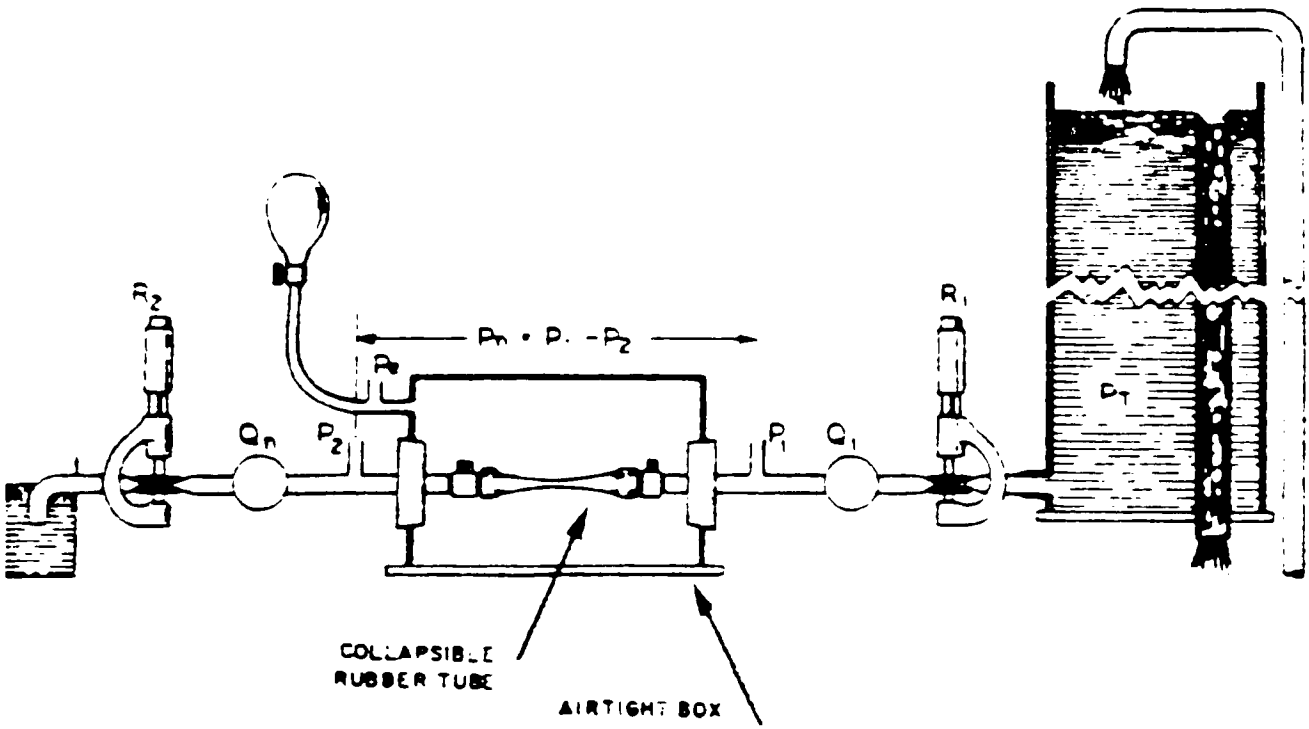

FIGURE 2 - Typical collapsible tube experimental apparatus (From Conrad [14])

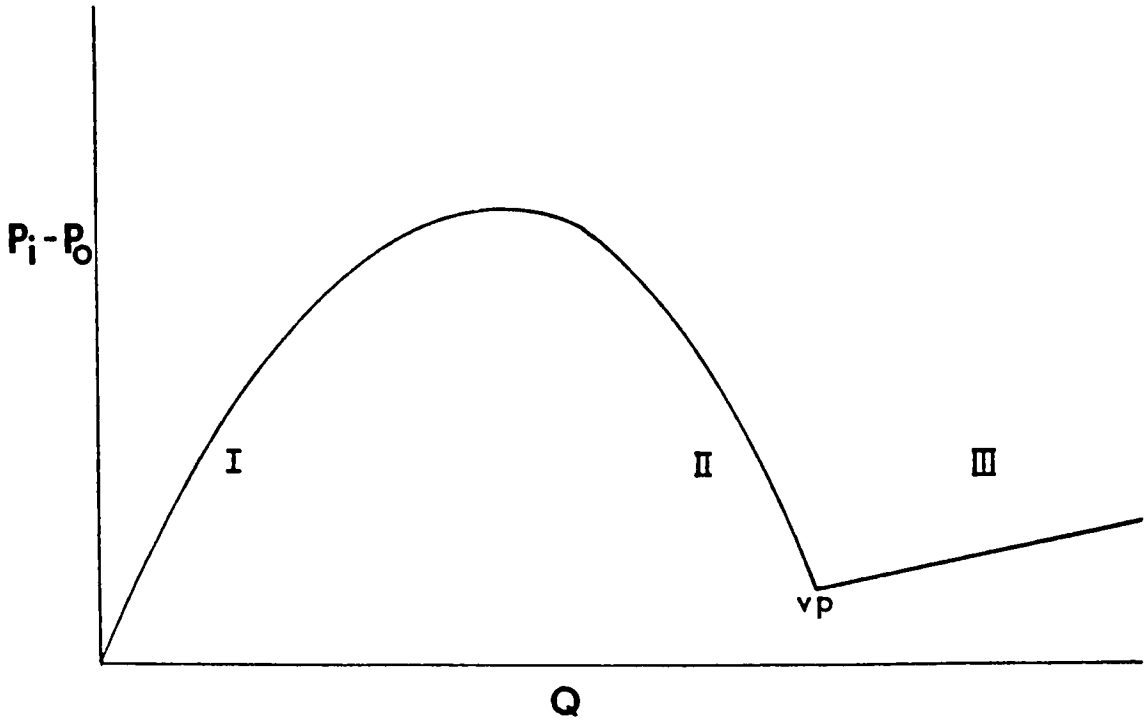

FIGURE 3 - Characterization of the pressure-flow relationship of the Starling resistor when P_e is held constant (From Lyon [37])

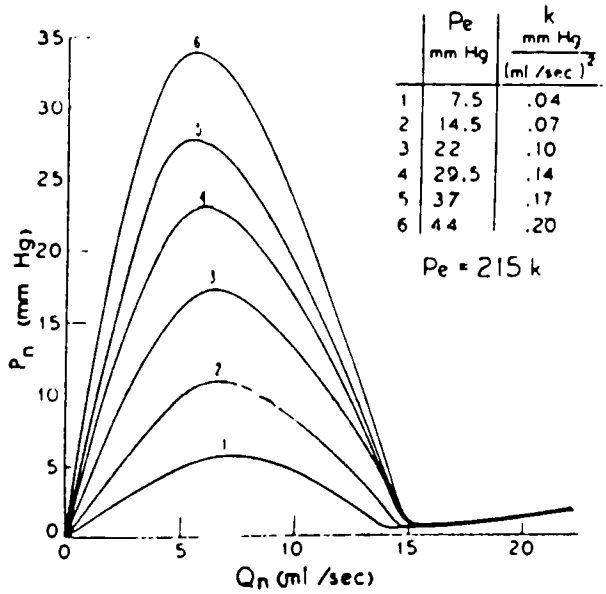

FIGURE 4 - Characteristic pressure-flow relationship (From Conrad [14])

collapsed with a high resistance to flow. Compliance is defined as the ability to undergo changes in cross-sectional shape. At collapse, tube compliance is at a maximum because changes in volume are made by bending the tube walls rather than stretching them. As flow rate increases, the collapsed tube transforms its cross-section from a dumbbell shape (with opposite sides in contact) towards a more elliptical cross-section (see Figure 10). As P_e increases, the slope of the pressure-flow relation in Region II increases as does the maximum difference between upstream and downstream pressure ($P_i - P_o$) [37].

In Region II, $P_i > P_e > P_o$, the partially collapsed tube alters its cross-section from an ellipse to its original circular shape. The negative slope in Region II indicates that driving pressure ($P_i - P_o$) decreases with increased flow rate. This "negative resistance region" indicates the collapsible tube is analogous to an electrical flow-controlled nonlinear resistance (QNLR) and is thus similar in operation to tunnel diodes and other "negative resistance" systems [14]. However, if P_e is held constant while P_o is allowed to vary, transmural pressure changes, so the conclusion of a "negative resistance" is merely a product of Conrad's experimental methodology [37].

The sharp transition point between Region II and Region III was referred to as the valley point (VP). Here P_o is approximately equal to P_e and the tube has its original cross-sectional shape and area.

In Region III, $P_i > P_o > P_e$, the tube is distended, and flow is

similar to Poiseuille flow through a rigid tube. Thus tube characteristics play a limited role in the pressure-flow relationships in this region. The tube inflation stiffness is much greater than the tube collapse (bending) stiffness, as depicted by the tube law (see Figure 10).

Flow for the entire experiment is assumed to be laminar, since the approximate Reynolds numbers never exceed 2000.

Self-excited oscillations occur in Region II of the curve depicted in Figure 3. Here P_e is sufficiently greater than P_o to cause an instantaneous collapse of a segment of the tube. This collapse occurs towards the distal end of the tube, cutting fluid flow out of the tube. Continued flow into the tube thus increases the internal pressure until it is great enough to overcome the external pressure causing collapse. The collapsed segment opens, and allows fluid to flow out of the tube. This loss of fluid results in a decrease of pressure and the collapse cycle begins again. Self-excited oscillations are observed only within Region II, and are not observed outside this critical region. This relates to intramyocardial pressure and coronary flow, since flow conditions analogous to those in Region II may cause self-excited oscillations in coronary vessels.

Under steady flow conditions at the threshold of oscillation, a series of pressure vs. flow curves are produced as shown in Figure 4, where P_n is defined to be the difference between upstream and downstream pressure. Here, external pressure is proportional to the constant 'k'. The value of 'k' depends on fluid viscosity,

and represents the energy loss for the downstream resistance. These curves indicate that as external pressure of the tube increases for any given flow rate, the difference between upstream and downstream pressures increases. Self-excited oscillations are observable in the region of negative slope (Region II) of all curves.

If flow rate is progressively increased, the pressure difference varies linearly in Region III with flow rate. What may seem counterintuitive is that once the valley point of the curves is surpassed, the pressure difference settles out to the same numerical value, regardless of the external pressure. This is related to the increased tube inflation stiffness.

Tube collapse can occur when transmural pressure reaches a 'critical' value [37]. This critical value is dependent upon tube characteristics, such as the elasticity of the wall, tube length to diameter ratio, and tube diameter to wall thickness ratio.

Conrad used the self-excited oscillations as well as forced oscillations to examine nonsteady flow. When the operating point of the apparatus was in aforementioned Region II but the tube was not oscillating, a compliant structure was inserted between the tube and the outflow resistance to produce oscillations. This compliance, in effect, isolated the downstream circuit from the collapsible tube.

An oscillation build up, which is the gradual increase in the oscillation amplitude, was obtained by varying either the upstream or downstream resistance until the oscillations stopped. Self-

excited oscillations could then be restored if the resistance was returned to the original state. Conrad observed that as the flow rate increased through Region II, the period of oscillation increased, the build up was more rapid, and the oscillations became more nonsinusoidal. In addition, as the downstream resistance was increased, a higher flow rate was required before oscillations were observed, analogous to increased venous resistance.

2.2 Lyon [37]

Extensive experiments on an apparatus similar to that of Figure 2 were studied in an attempt to verify and unify seemingly conflicting observed data trends. Of particular interest were the effects of outflow resistance, tube length, fluid viscosity, tube diameter and applied tension on pressure-flow relationships.

Pressure-flow relationships for Penrose tubing are graphically depicted in Figure 5. Minimal outflow resistance and constant pressure differences between P_e and P_o are shown. In Figure 5, three phases of the pressure-flow relationships can be seen. First, there exists an initial rising phase at low flow rates, followed by a plateau phase where $P_i - P_o \cong P_e - P_o$ at moderate flow rates, and finally a late rising phase at high flow rates. Using a series of these relationships, a three-dimensional surface of pressure-flow relationships can be generated (Figure 6). When downstream pressure exceeds external pressure, the fully distended tube behaves as a rigid tube, exhibiting a linear relationship between pressure and flow. Similar behavior is noted when the

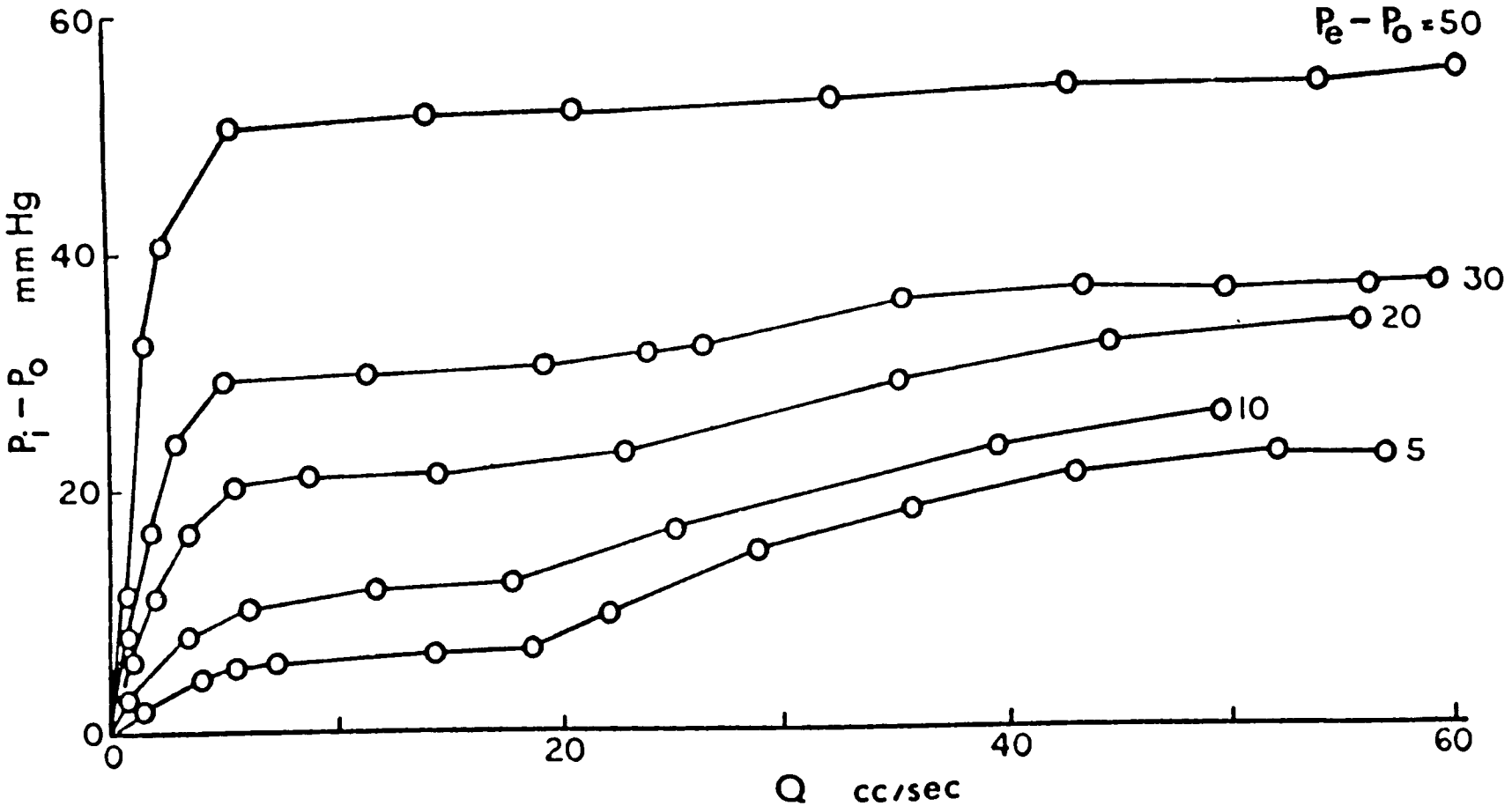

FIGURE 5 - Pressure-flow relationship of Penrose tubing
(From Lyon [37])

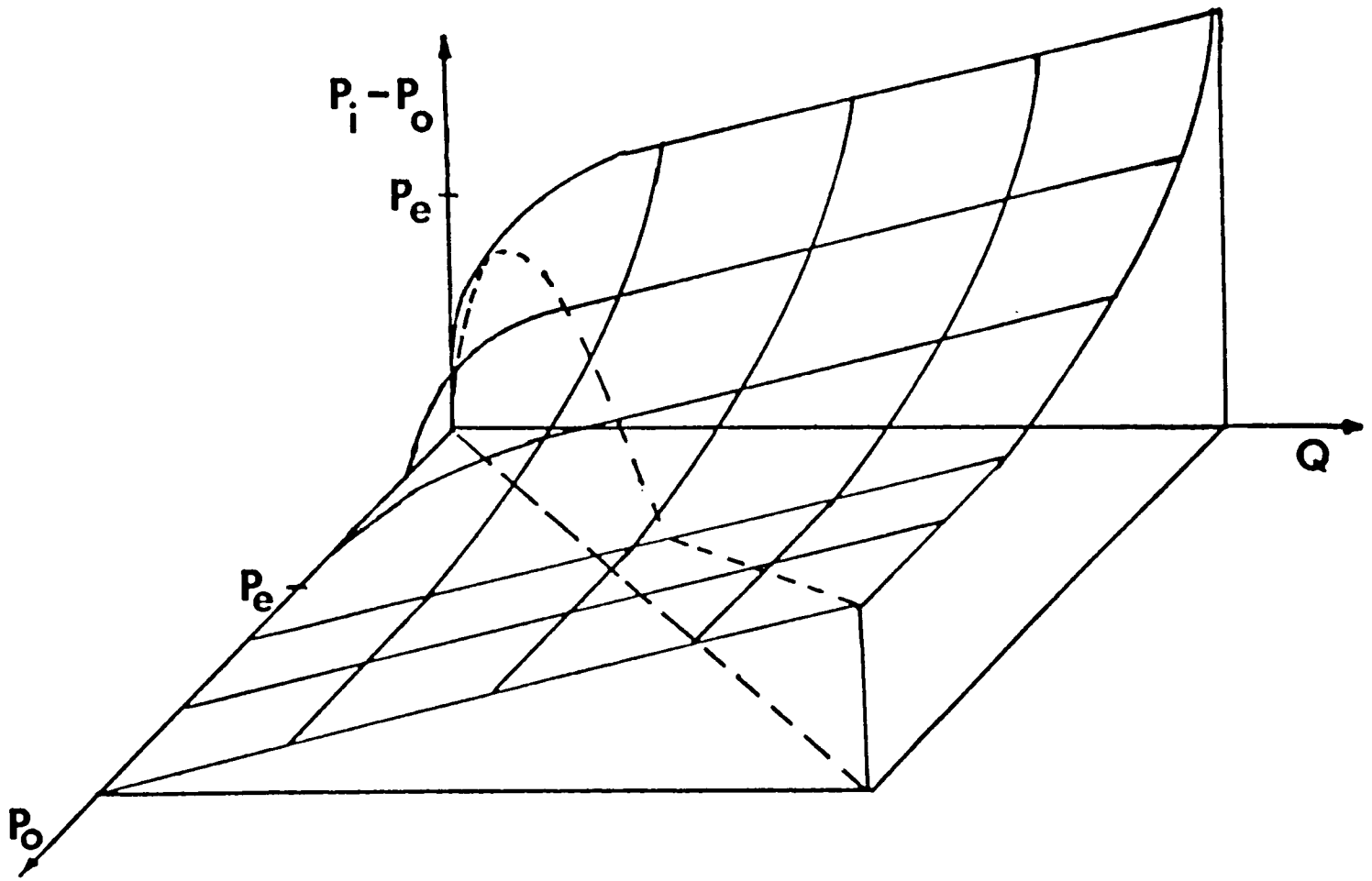

FIGURE 6 - Three-dimensional surface of pressure-flow relationship of Penrose tubing (From Lyon [37])

pressure loss along the length of the tube (ie. $P_i - P_o$) is greater than the external pressure. However, whenever external pressure exceeds either the downstream pressure or the pressure loss along the length of the tube, a nonlinear relationship between pressure and flow develops. The dashed line cutting across the surface is obtained when P_e, rather than $P_e - P_o$, is held constant and outflow resistance is high. This dashed pressure-flow relationship is identical to the curves produced by Conrad [14] (Figure 3).

2.2.1 Penrose Tubing Observations

Many observations can be made using the data of Figure 5, as well as tabulated results. In particular:

1. The slope of the initial rising phase increased as the parameter $P_e - P_o$ increased.
2. For a given flow rate, increasing outflow resistance, R_o, caused P_o to increase and $P_i - P_o$ to decrease.
3. Increasing the length of the tube increased the slope of initial rising phase of the pressure-flow curves.
4. Decreasing the diameter decreased the flow rate at which the three phases occurred.
5. Longitudinal stretching of the tubing, which produced tension in the tube wall, decreased the slope of the early rising phase, but increased the slope of the late rising phase.
6. Both the initial slope and the length of the plateau phase increased when the parameter $P_e - P_o$ was increased.

7. Higher viscosity fluids produced pressure-flow relationships closer to that of the waterfall model. (See below.)
8. Oscillations appeared at the beginning of the plateau phase and increased in pressure amplitude as flow increased, and the magnitude of the late rising phase was proportional to the pressure amplitude of the oscillations.
9. The frequency of oscillation increased with flow rate, which agrees with Conrad's findings.
10. With $P_e - P_o$ held constant, outflow resistance decreases the frequency and amplitude of self-excited oscillations, thereby decreasing the slope of the late rising phase.
11. Tension increased the pressure amplitude of the oscillations.
12. Stretch (combined tension and increased tube length) produced fairly inconsistent results. An analysis of variance proved that the pressure amplitude of the oscillations was always greater in stretched tubing than in unstretched tubing.

2.2.2 Waterfall Analog

The three-dimensional surface shown in Figure 7 illustrates the pressure-flow relationship predicted by the vascular waterfall model. Comparing this surface to the one generated from Penrose tubing (Figure 6), shows the shortcomings of the waterfall model in

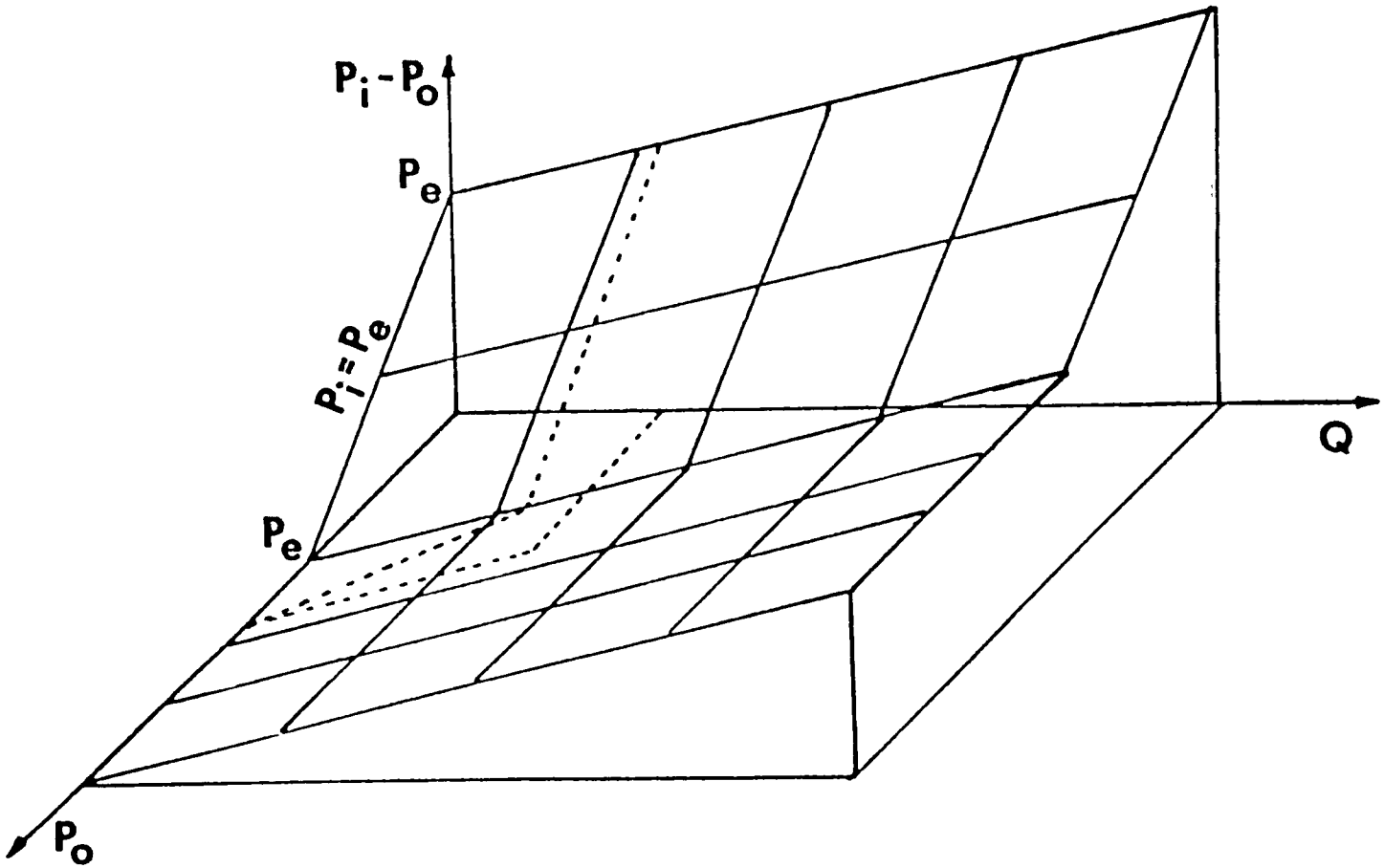

FIGURE 7 - Three-dimensional pressure-flow relationship predicted by the vascular waterfall model

predicting (latex) tube phenomena. The vascular waterfall model does not depict either the initial rising phase or the late rising phase of Lyon's experimental data (Figure 5).

2.3 Lyon, et al. [38]

These experiments determined if pressure-flow relationships from the Starling resistor model resemble those of the waterfall model for low Reynolds number flow ($R_e < 2000$), consistent with the microcirculation. Fluids of different viscosities (0.01, 0.5, 10.0 stoke) were used to vary the Reynolds number in the standard physical model (Figure 2) to approach the microcirculation's Reynolds number of 0.01. The flow rate, Q, was determined by time-collection:

$$Q = \frac{W}{\rho T} \tag{2}$$

where W is the collected fluid weight and T is the elapsed time. Accuracy of these readings was given to be ±5%.

Pressures were recorded in the rigid tubes, upstream and downstream of the collapsible tube (Figure 2). Since the actual pressures of interest were those at either end of the collapsible tube segment, inflow and outflow pressures were corrected using the recorded pressures and Poiseuille's Law:

$$P_i' - P_i = P_o - P_o' = 128 \frac{L_p \mu Q}{\pi d^4} \tag{3}$$

where

P_i' = measured upstream pressure

P_o' = measured downstream pressure

L_p = distance from collapsible tube to respective port

d = inner diameter of rigid tube

A difference of less than 10% between the experimental pressure loss and theoretical pressure loss was obtained for both the 0.5-stoke fluid and the 10.0-stoke fluid.

Reynolds number was calculated as:

$$R_e = \frac{4\rho Q}{\pi d \mu} \qquad (4)$$

where ρ is fluid density, and μ is fluid viscosity, and a low flow rate was produced by varying the upstream resistance (Figure 2). Pressure inside the air-tight box was adjusted to yield a constant, predetermined value for $P_c - P_o$. After the system stabilized, pressures, times and weights were recorded. The flow was then increased, and P_c was once again adjusted to maintain the same value for $P_c - P_o$. This produced a family of curves indicating the variance of $P_i - P_o$ with Q (Figure 5).

For the collapsible tube perfused with water (0.01 stoke), the representative graph of the pressure-flow relationships indicated an initial rising phase, during which the tube's appearance changed

from a flattened dumbbell shape to fully distended. This shape change resulted in a non-linear pressure-flow relationship. The larger the constant value of $P_e - P_o$, the sharper this initial phase. The curves then moved into a plateau region, where self-excited oscillations began. The frequency of these oscillations increased as the flow rate increased. The tube was fully distended in this region and produced a linear pressure-flow relationship, nearly parallel to the flow axis, with $P_i - P_o \approx P_e - P_o$. The Reynolds number for these curves reached a maximum of 2000 for $Q = 20$ ml/sec.

When a 0.5-stoke fluid was utilized in the same manner, the curves produced were similar in nature, with an initial rising phase and a plateau region. However, the initial rising phase was much sharper. In addition, the self-excited oscillations began at a higher flow rate and occurred with a lower oscillatory pressure amplitude than with the water perfusion experiments. For this fluid, the maximum Reynolds number was approximately 40.

Perfusion with a 10.0-stoke fluid produced curves (Figure 8) radically different from those previously discussed, since there existed no initial rising phase and no plateau. Instead, the results produced straight lines whose y-intercepts ($P_i - P_o$) were equivalent to the constant $P_e - P_o$. The slopes of these lines were slightly larger than the values calculated from Poiseuille's Law. No oscillations were observed, and the maximum Reynolds number for this fluid was 2.

Although a Reynolds number of 0.01 was not achieved, these

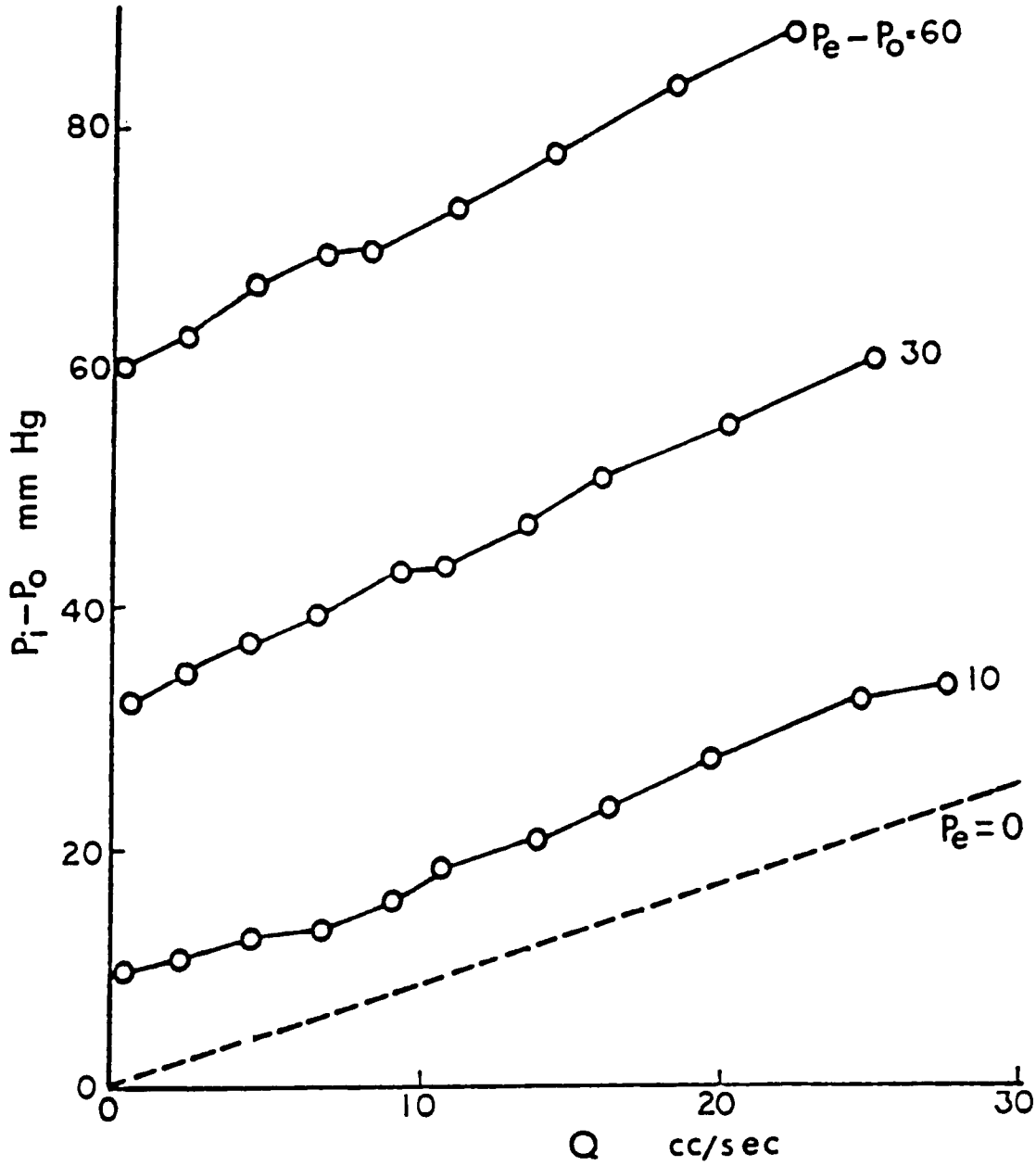

FIGURE 8 - Pressure-flow relationship for 10.0 stoke fluid (From Lyon [38])

data suggest that the waterfall model is applicable in very low Reynolds number flow. Here, collapsible tube properties, tube size, and method of mounting seem to be secondary factors. Self-excited oscillations diminish to zero as the Reynolds number decreases, and pressure-flow relationships are distinctly different for low and high Reynolds number flow. Therefore, results from various investigations should not be randomly applied to other experiments or hypotheses until Reynolds number compatibility has been confirmed.

2.4 Lyon, et al. [39]

High Reynolds number flow (R_e > 2000) was investigated to further examine the effects of tubing diameter, length, tension, and stretch of the collapsible tube segment on the pressure-flow relationships. The apparatus used was very similar to the one discussed above, but incorporated a flow meter to more accurately determine flow rate.

High Reynolds number flow (without incorporating any other variables) produces pressure-flow graphs similar to earlier water perfusion experiments (Figure 5) where an initial sharp rising phase is followed by a plateau region. However, for high Reynolds number flow, a late rising phase occurs at flow rates greater than 20 ml/sec. The slope of this late rising phase is much less than the initial rising phase, and occurs at higher flow rates for higher $P_e - P_o$. As in the previous experiment [38], self-excited oscillations occur during the plateau phase, but the amplitude of

the pressure fluctuations caused by the oscillations increases during the late rising phase. The maximum Reynolds number was 6000 at a flow rate of 60 ml/sec.

Increasing the outflow resistance (via use of a clamp on latex tubing) increases all pressure measurements, decreases the slope of the late rising phase, reduces the frequency of the self-excited oscillations, and reduces the pressure amplitude of the oscillations. The use of increased outflow resistance also serves to prolong the plateau stage.

To examine the effect of tube diameter on pressure-flow relationships, water perfused two collapsible tube segments, one twice the diameter of the other. Comparison of pressure-flow relations shows that diameter reduction increases the slope of the initial rising phase, and shifts the start of the plateau phase to lower flow rates, as depicted in Figure 9. Self-excited oscillations initiate at the beginning of the plateau phase and continue as the flow rate increases for both diameters, but the late rising phase begins at a lower flow rate for reduced diameter. The maximum Reynolds number for this smaller diameter tube was 4000.

The effects of longitudinal tension and the effects of changes in vessel length were investigated separately and then jointly. To investigate longitudinal tension, the distance between the rigid tubes to which the collapsible segment was mounted was kept constant while the tube was mounted at various tension levels. This produced an "applied tension" to the collapsible segment,

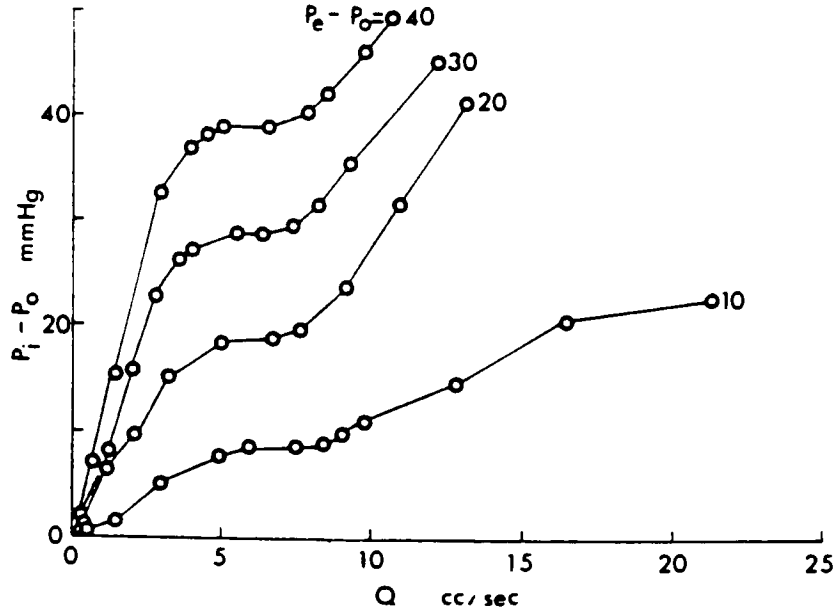

FIGURE 9 - Pressure-flow relationship for 0.635 cm diameter tubing (From Lyon [39])

which decreases the slope of the initial rising phase but increases the slope of the late rising phase. This tension also increases the pressure amplitude of the oscillations while slightly decreasing their frequency.

To investigate the effect of changes in vessel length, the distance between the rigid tubes was varied, as was the length of the collapsible segment, so no "applied tension" was present. The results obtained for these experiments do not indicate any clear trends. For a high flow rate, as the length of the collapsible tube segment increases, the frequency and pressure amplitude of oscillation increases and then decreases. In addition, the effect on the three phases of the pressure-flow relationships is variable.

To examine the combined effect of "applied tension" and changes in vessel length, which has been defined as stretch, a

collapsible tube segment of fixed length was attached to the rigid mounts with no applied tension. The distance between these mounts was then gradually increased, producing both increased tension and length. The results show that the effects of tension and length are not additive. A statistical analysis of the data indicates that stretch increases the pressure amplitude of the oscillations, but has a variable effect on the frequency of oscillation.

In general, these experiments show that the amplitude of the oscillations increases when flow, tension, and/or stretch increase, and these parameters had varying effects on the frequency of oscillation. It is also determined that the pressure-flow relationships of collapsible tubes for high Reynolds number flow are greatly affected by instabilities such as oscillatory phenomenon and high pressure gradients. Longitudinal tension and stretch increase these instabilities, while increased diameter, length and outflow pressure decrease these instabilities.

2.5 Low and Chew [36]

The effects of upstream pressure fluctuations on the pressure-flow relationships in collapsible tubes were examined using an experimental apparatus similar to that of Lyon, et al. [38,39]. The downstream pressure P_o was gradually reduced while the upstream mean pressure was fixed. A piston-type pulsatile pump was used to obtain the fluctuating component of P_i, although the upstream pressure amplitude and frequency were maintained at a constant value for each set of results. Upstream pressure fluctuations were

on the order of 1250 Pa.

The following dimensionless parameters are defined to aid in results presentation:

1. the tube stiffness factor:

$$K_p = \frac{E H^3}{\left[\frac{3}{2} D_0^3 (1-\nu)^2\right]} \tag{5}$$

2. the wave speed

$$c = \sqrt{\frac{n K_p \left(\frac{A}{A_0}\right)^{-n}}{\rho}} \tag{6}$$

where E is the Young's Modulus of the collapsible tube, H is the tube wall thickness, ν is Poisson's ratio, D_0 is the nominal diameter of the collapsible tube, A_0 is the nominal cross-sectional area of the tube, A is the altered cross-sectional area of the tube, and n (approximated to be 1.5) is the tube law index (see Figure 10).

Generally, the tube wall begins to oscillate when the downstream transmural pressure approaches zero. With a steady upstream pressure, the oscillations are in the traverse direction. However, with a fluctuating upstream pressure the oscillations also have an axial component superposed on the traverse oscillations.

Even when the tube reaches the collapsed state and the traverse oscillations cease, the axial oscillations continue.

When the upstream pressure fluctuates, the downstream pressure fluctuates as well albeit out of phase by approximately 45°. Decreasing the flow rate to produce a fully collapsed tube reduces the amplitude of the downstream pressure waves. However, the frequency of the downstream waves remains the same as the upstream pressure waves, with a small component of a higher harmonic present.

Steady upstream pressure and gradual reduction of downstream pressure allows the flow rate to initially increase, then reach an asymptotic value which remains independent of downstream pressure, indicative of flow-limitation (choked flow).

Tube collapse occurs when $(P_i - P_e)/K_p$ is approximately zero, as expected. Compared to steady upstream pressure conditions, the pressure fluctuations cause the flow limitation to occur at higher values of $(P_o - P_e)/K_p$ and lowers the maximum flow rate. This maximum flow rate decreases as P_e increases.

Speculation is made that the fluctuating upstream pressure gives rise to a fluctuating transmural pressure throughout the collapsible tube segment, producing an instantaneous negative transmural pressure which triggers tube collapse. Tube collapse may therefore occur more readily with unsteady flow conditions. This is an area of interest to physiologists studying coronary blood flow, since unsteady flow conditions may be present in coronary flow and resulting vessel collapse may lead to ischemia.

Quasi-steady flow was considered, characterized by a reduced velocity parameter, u/(fL). This parameter is the ratio of the time for the fluid to convect along the tube vs. the period of oscillation (1/f). A large reduced velocity, usually greater than 10, indicates quasi-steady flow. Calculations show that quasi-steady behavior may indeed occur, but should be expected only at the throat where the effective radius is very small. The results, however, do not indicate the presence of quasi-steady flow.

Low and Chew concluded that increasing the amplitude or frequency of the fluctuating upstream pressure reduces the mean value of the maximum flow rate, and the quasi-steady considerations may not be applicable even if the reduced velocity at the throat is high. This implies that increasing the rate of the cardiac cycle actually decreases the rate of blood flow through a collapsible blood vessel.

2.6 Shapiro [46]

One of the earliest mathematical models utilized two coupled partial differential equations and an algebraic equation to look at one-dimensional, unsteady inviscid flows in a compliant tube.

The equation of motion is given as:

$$-\frac{1}{\rho}\frac{\partial P}{\partial x} = \frac{\partial u}{\partial t} + u\frac{\partial u}{\partial x} \qquad (7)$$

where P is the pressure of the flowing fluid, u is fluid velocity,

and x is longitudinal distance along the tube.

The continuity equation for incompressible fluids in a compliant tube is:

$$\frac{\partial A}{\partial t} + \frac{\partial}{\partial x}(Au) = 0 \qquad (8)$$

The final equation necessary to completely define the system, commonly referred to as the tube law, relates transmural pressure to the cross-sectional area of the tube, where $A = A(P-P_e)$.ratio, $\alpha = A/A_0$. Figure 10 shows a typical graphical representation of the tube law utilized by various mathematical models. Although neither mathematical formula shown in Figure 10 predicts the tube behavior exactly, The following equation is generally accepted:

$$P^*_{TM} = 1 - \alpha^{-\frac{3}{2}} \qquad (9)$$

where

$$\alpha = \frac{A}{A_0} \qquad (10)$$

For positive dimensionless transmural pressure, P^*_{TM} (defined as P in Figure 10), the tube is distended ($\alpha>1$) and the pressure difference is supported by hoop tension. For negative dimensionless transmural pressure, however, the tube is in some state of collapse ($\alpha<1$), the severity of which increases with decreasing transmural pressure. The pressure difference in the

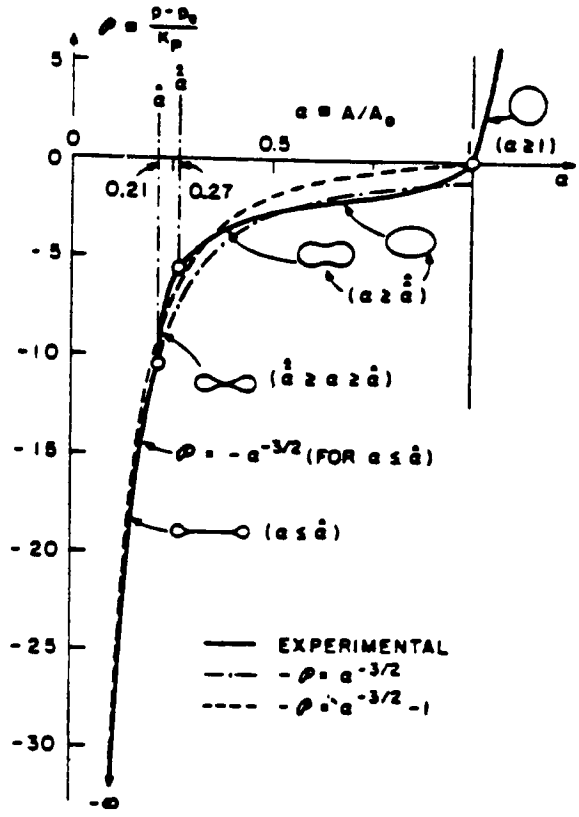

FIGURE 10 - Tube law for Penrose (latex) tubing
(From Shapiro [46])

collapsed state is supported by the bending stiffness of the tube wall. Note the highly nonlinear nature of the tube law and the existence of an transition point at α=1. The behavior of the tube law near zero transmural pressure (α=1) is dependent on whether the tube is truly round in the unstressed state.

Shapiro defines the wave speed to be:

$$c^2 = \frac{A}{\rho}\frac{dP}{dA} = \frac{A}{\rho}\frac{d(P-P_e)}{dA} \qquad (11)$$

Incorporating the tube law (Eq. 9) into the above equation, the final form of the wave speed becomes:

$$c = \sqrt{\frac{nK_p\alpha^{-n}}{\rho}} \tag{12}$$

The important dimensionless parameter for flow through a compliant tube is the speed index, S, analogous to the Mach number of compressible flows. This speed index is defined as the ratio of fluid velocity to wave speed, or

$$S = \frac{u}{c} \tag{13}$$

Flow is defined as either subcritical (S<1) or supercritical (S>1), and at S=1, flow limitation (choking) occurs.

Wall friction stress was also considered in this analysis, and was incorporated into the momentum equation. For fully-developed turbulent flow, the turbulent skin friction coefficient, f_T, is defined in terms of the wall shear stress, τ_W, as:

$$\tau_W = f_T \frac{\rho u^2}{2} \tag{14}$$

Thus, the wall friction force per unit cross-sectional area, acting in the length dx is expressed as:

$$\frac{\tau_w s\, dx}{A} = \frac{\rho u^2}{2}\left[\frac{4 f_T\, dx}{D_e}\right] \tag{15}$$

where s is the perimeter of the tube, and D_e, the equivalent hydraulic diameter, is defined as:

$$D_e = \frac{4A}{s} \tag{16}$$

For fully developed laminar flow, the laminar friction coefficient, f_L, is defined as:

$$f_L = \frac{\tau_w D_e}{\mu u} \tag{17}$$

thus producing the following equation for wall force per unit cross-sectional area, acting in the length dx:

$$\frac{\tau_w s\, dx}{A} = \frac{\mu u}{D_e}\frac{4 f_L\, dx}{D_e} \tag{18}$$

Incorporating the wall friction stress, the resulting momentum equation is:

$$-A\, dp - \tau_w \cdot s\, dx - \rho g A\, dz = \rho A u\, du = \rho A u^2\, \frac{du}{u} \tag{19}$$

where z is elevation and g is gravitational force. Substitution is

made for τ_w with Eq. 15 or Eq. 18 for turbulent or laminar flow, respectively.

Shapiro's analysis is through algebraic manipulation of the above equations, and investigates how certain parameters vary with respect to other parameters. His observations are summarized here:

1. As P_e increases, both A and P decrease in subcritical flow, but increase in supercritical flow.
2. Friction causes A to decrease in subcritical flow and to increase in supercritical flow.
3. Friction produces a pressure rise in supercritical flow and a velocity increase in subcritical flow.
4. Friction always reduces the stagnation pressure.
5. If the nominal tube area increases along the length of the tube, then the area A and the area ratio α both increase in subcritical flow but decrease in supercritical flow.

In addition, Shapiro investigated shock waves. His simple description of a wave is that a rapid area increase causes flow separation and a jetlike flow which passes through an eddying region. The flow then gradually refills the passage until the flow becomes uniform again. The viscous losses associated with the eddies and the passage filling are the dissipative mechanisms producing stationary waves. Associated head losses depend on the shape of the divergent section. This shape is influenced by the longitudinal tension and curvature of the wall, and the structural mechanics of the wall are coupled to the pressure distribution

produced by the flow. This may have impact on flow into and out of a collapsed segment suspended from rigid supports.

Algebraic manipulation of equations utilizing the aforementioned tube law yields the following for the inlet speed index:

$$S_1^2 = \frac{1-\beta^n}{n\beta(1-\beta)} \tag{20}$$

where the ratio between the inlet and outlet area ratios is expressed as $\beta = \alpha_1/\alpha_2$, and n is an arbitrary constant. The outlet speed index is expressed as:

$$S_2 = \frac{V_2}{c_2} = \frac{V_2}{V_1} \cdot \frac{V_1}{c_1} \cdot \frac{c_1}{c_2} \tag{21}$$

where V_i is the speed of the wave relative to the fluid into which it is advancing (ie. a speed differential). Given the above equations, the relationship between inlet and outlet speed indices eventually becomes:

$$S_2^2 = S_1^2 \left(\frac{\alpha_1}{\alpha_2}\right)^{2-n} \tag{22}$$

The following are Shapiro's observations:

1. For n = 1 : $S_1 > 1$ and $S_2 = 1$
2. For n = 2 : $S_1 > 1$ and $S_2 = S_1$
3. For n = 1.5 : $S_1 > 1$ and $S_2 > 1$ (but $S_1 \neq S_2$)

He also suggested that if $S_2 > 1$, there can be multiple shocks with S_2 never becoming less than unity. However, the combination of two shocks is not equivalent to a single larger shock. This may be the qualitative results of a sharp or pseudosharp transition through a stenosis.

Although not directly related to the present investigation, Shapiro examined another aspect of collapsible tube flow. He looked at flow with combined friction and gravity, and defined the following term to identify the ratio of gravity to frictional forces:

$$\Gamma_r = \frac{1}{3} \frac{\left(\frac{\alpha}{S^{-4}}\right)^2 \rho g D_e}{f_T K_p \sqrt{\frac{A_0}{A}}} \tag{23}$$

For a tube with a constant downward slope, he defines:

$$S_{lim} = (-\Gamma_r \sin\theta)^{1/10} \tag{24}$$

where θ is the angle of decline. The following are the results of this analysis:

1. For $S_{lim} < 1$:
   - A. When $S > S_{lim}$:S goes toward unity; choking ultimately occurs
   - B. When $S < S_{lim}$:S goes toward zero; no choking

2. For $S_{lim} = 1$:

   A. When $S < 1$:S goes away from unity; no choking

   B. When $S > 1$:S goes toward unity; smooth transition from subcritical to supercritical flow rather than choking

3. For $S_{lim} > 1$:

   A. When $S > S_{lim}$:S decreases asymptotically to S_{lim}; no choking

   B. When $1 < S < S_{lim}$:S increases asymptotically to S_{lim}; no choking

   C. When $S < 1$:S decreases to zero; no choking

The basic conclusions from this are:

- When $S < S_{lim}$, gravity dominates and S goes away from unity
- When $S > S_{lim}$, friction dominates and S goes toward unity

2.7 Ku, et al. [32]

Using a mathematical model, one-dimensional steady inviscid flow through a compliant tube with a stenosis is investigated. A stenosis is defined as the abnormal narrowing of a passage or opening, such as atherosclerotic plaque. In this study, coupled equations of steady, incompressible, and inviscid flow through collapsible tubes adapted from Shapiro [46] and Elad, et al. [16] are solved. The conservation of mass is presented as:

$$\frac{\partial Au}{\partial x}=0 \tag{25}$$

and the momentum equation as:

$$u\frac{\partial u}{\partial x}= -\frac{1}{\rho}\frac{\partial P}{\partial x} \tag{26}$$

The final form of the coupled equations solved using a fourth-order Runge-Kutta finite difference method are:

$$\frac{d\alpha}{dx}=\frac{\alpha}{1-S^2}\left[\frac{S^2}{A_0}\frac{dA_0}{dx} - \frac{P^*_{TM}}{\rho c^2}\frac{dK_p}{dx}\right] \tag{27}$$

$$\frac{dS^2}{dx}=\frac{S^2}{1-S^2}\left[\frac{[-2+(2-M)S^2]}{A_0}\frac{dA_0}{dx} + \left(\frac{M P^*_{TM}}{\rho c^2}-\frac{1-S^2}{K_p}\right)\frac{dK_p}{dx}\right] \tag{28}$$

where M is defined as:

$$M = 3 + \alpha\left[\frac{\left(\frac{d^2P^*_{TM}}{d\alpha^2}\right)}{\left(\frac{dP^*_{TM}}{d\alpha}\right)}\right] \tag{29}$$

and P^*_{TM}, the dimensionless transmural pressure difference is defined by the tube law as:

$$P^*_{TM} = \frac{P-P_e}{K_p} = \alpha^{n_1} - \alpha^{-n_2} \qquad (30)$$

The area ratio, α, and tube stiffness factor, K_p, are defined as in Eqs. 10 and 5 respectively, and n_1 and n_2 are numerical constants, chosen by the authors to be 20 and 1.5, respectively. Equation 30 differs from Equation 9 in that the addition of α^{n_1} allows for a smooth transition through α=1.

A solution is possible when there is a smooth transition from subcritical (S<1) to supercritical (S>1) flow at the throat of the stenosis, and the flow rate for this solution is called the "critical flow".

The local wave speed of small disturbance, c, is defined as:

$$c^2 = \frac{A}{\rho}\frac{\partial P}{\partial A} \qquad (31)$$

Once $\alpha(x)$ and $S(x)$ have been determined, the values for $u(x)$, $c(x)$, and $P(x)$ can be determined.

The shape of the stenosis is modeled using the following:

$$\frac{A_0}{A_{0i}} = 1-\lambda_A \sin^2\left(\frac{\pi(x-x_1)}{(x_2-x_1)}\right) \tag{32}$$

where A_{0i} is the nominal inlet tube area, λ_A is the reduction of the stenosis, x is the length coordinate, and x_1 and x_2 are the end-points of the stenosis.

The stiffness of the stenosis is allowed to vary according to the relationship below:

$$\frac{K_p}{K_{pi}} = 1-\lambda_{K_p} \sin^2\left(\frac{\pi(x-x_1)}{(x_2-x_1)}\right) \tag{33}$$

where K_{pi} is the inlet stiffness, and λ_{Kp} is the amplitude of the stiffness perturbation. If λ_{Kp} is positive, the stenosis is less stiff than the inlet tube; if λ_{Kp} is negative, the stenosis is stiffer than the inlet tube; if λ_{Kp} is zero, the stiffness is constant.

The inlet and outlet pressures of the tube can be varied to simulate various physiological conditions, but the external pressure is held constant at zero so that the transmural pressure is the internal pressure of the tube.

The first investigation was of a system with constant

stiffness ($\lambda_{Kp} = 0$). For a 90% stenosis by area, the speed index, S, varies greatly along the length of the stenosis. It increases above its inlet value as the distance to the throat of the stenosis is approached. This is due to the simultaneous fall in wave speed, c, from the decreasing tube radius and a rise in fluid velocity, u, from conservation of mass. At the throat, S=1, and a smooth transition to supercritical flow causes the tube to collapse downstream of the throat. The wave speed in the collapsed segment is very low, producing a very high speed index. The fluid velocity in this segment remains relatively constant. The static pressure along the stenosis varies due to the acceleration of fluid in the throat. At the point of minimum pressure, there is a rapid transition from supercritical to subcritical flow. This is defined as an elastic jump, and it is the only mechanism of significant energy dissipation in the inviscid solution, resulting in the sudden expansion of the tube. It was determined that for a given set of critical flow stenosis conditions, α at the throat is governed mainly by the inlet pressure.

Next, different degrees of stenosis were investigated. The results are summarized here:

1. As the degree of stenosis increases, the critical flow rate decreases and the length of tube subject to collapse is shortened. The location of the elastic jump is also affected by the severity of the stenosis.
2. Doubling the length of the stenosis doubles the length of the collapsed segment.

3. Increasing the outlet pressure moves the point of collapse upstream, and decreases the collapse length. However, if the outlet pressure becomes too great, a solution with S=1 in the throat does not exist. Conversely, if the outlet pressure is too low, no jump occurs and the tube remains in the collapsed state, unless some other force (such as longitudinal tension or tethering) is applied to cause the tube to expand.
4. Increasing the inlet pressure increases the critical flow rate and moves the elastic jump downstream.

The effects of increasing the stenosis stiffness were then investigated. It was discovered that as the stiffness of the stenosis increases:

1. the critical flow value decreases
2. the maximum value for the speed index, S, decreases
3. the minimum area in the collapsed segment decreases
4. the length of the collapsed segment decreases
5. the area ratio, α, at the throat decreases
6. the pressure at the throat decreases

Finally, the importance of the variables used in the tube law were examined by varying K_p, n_1, and n_2. Increasing n_1 produces a highly distensible tube law, and moves the onset of collapse and the elastic jump slightly downstream. Doubling or halving K_p produces less than 0.1% change in critical flow rate or length of

collapse. Critical flow and length of collapse are altered by roughly 15% by similar variations in n_1. These same changes in n_2 do not affect the critical flow rate, but change the length of collapse by approximately 5%. These fairly insignificant variations suggest that the model is well adapted for most arterial segments.

2.8 Siebes and D'Argenio [47]

Pulsatile flow through a partially collapsible tube with a stenosis, subject only to positive transmural pressure was mathematically modeled. Three severities of area reduction (50%, 80%, and 90%) with four degrees of flexible wall (0, 1/4, 1/3, and 1/2 of the circumference) were used to model the stenoses. These variables produce stenoses shapes that ranged from rigid and concentric to highly flexible and eccentric.

This model assumes that the pressure-flow relationship is essentially linear over a wide range of flow rates, and that the instantaneous distal resistance remains constant regardless of the stenosis modeled. The flow is assumed to be fully-developed, quasi-steady, and laminar; the fluid is assumed to be incompressible and Newtonian; the system is assumed to be free of capacitive and inductive elements, thus containing only resistive elements.

The vessel circumference is divided into two portions, a flexible portion, C_{flex}, and a rigid portion, C_{fix}. The area of the plaque (stenosis), A_{pl}, is assumed fixed and is determined by the

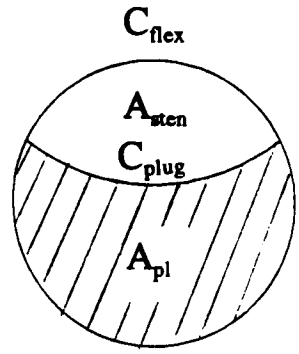

severity of the stenosis modeled, as shown above. The total potential luminal area, A_{pot}, defined as the internal cross-sectional area of the tube, is given by:

$$A_{pot} = \frac{C_{flex}^2 + C_{fix}^2}{4\pi} \tag{34}$$

The remaining luminal area at the stenosis location is thus:

$$A_{sten} = A_{pot} - A_{pl} \tag{35}$$

The hydraulic diameter is used for all calculations since the stenosis is not round, and that is defined as:

$$D_{hyd} = \frac{4A_{sten}}{C_{flex} + C_{plug}} \tag{36}$$

where C_{plug} is the wetted rigid part of the stenosis modeled and is determined by the severity of the stenosis modeled.

Total pressure loss is divided into three sections, the first between the inlet pressure port and the stenosis, the second over the stenosis, and the last from the stenosis to the outlet pressure port. The pressure losses in the first and third sections are assumed small and are calculated as Poiseuille losses for the whole length of the section. However, since the pressure loss along the stenosis is expected to be significant, this segment is divided into thirteen sections to compute the pressure loss. The remaining intraluminal pressure at the end of each increment, P_k, is calculated by subtracting the viscous and kinetic losses from the pressure at the entrance of the stenosis, P_{inp}, as:

$$P_k = P_{inp} - \sum_{j=1}^{k} C_1 \frac{32\ \mu\ \Delta L}{D_{hyd_j}^{\ 2}\ A_j} Q + C_2 \frac{\rho}{2} \frac{1}{A_k^{\ 2}} Q^2 \qquad for\ k=1...13 \qquad (37)$$

where C_1 and C_2 are dimensional constants, and ΔL is the length of the k^{th} tube section.

Since intraluminal distending pressure is lost as flow passes through the vessel, the stenotic area, A_{stn}, is at a minimum at the end of the stenosis. This area is used to calculate the overall stenotic pressure drop, ΔP_{stn}, as the sum of the viscous and turbulent exit losses:

$$\Delta P_{sten} = C_1 \frac{k_v \mu}{D_{prox} A_{prox}} Q + C_2 \frac{k_t}{2} \frac{\rho}{A_{dist}^2} \left(\frac{A_{dist}}{A_{sten}} - 1 \right)^2 Q^2 \qquad (38)$$

where the subscript 'prox' denotes proximal to the stenosis, and the subscript 'dist' denotes distal to the stenosis. The terms k_v and k_t represent the viscous and turbulent loss coefficients, respectively. Both coefficients incorporate entrance effects and are given by:

$$k_v = 32 \left[0.45 \left(\frac{D_{prox}}{D_{hyd_{sten}}} \right)^2 \frac{A_{prox}}{A_{sten}} + 0.86 \int_0^{L_{sep}} \left(\frac{D_{prox}}{D_{hyd_x}} \right)^2 \frac{A_{prox}}{A_x} \frac{dx}{D_{prox}} \right] \qquad (39)$$

$$k_t = 1.21 + 0.08 \frac{L_{sep}}{D_{dist}} \qquad (40)$$

In the above equations, L_{sep} is the stenotic length at the separation point. Although an exact definition is not given for this length, it is assumed that L_{sep} is the length from the stenosis to the flow separation point. The flow separation point is the location within the fluid where the fluid layers contiguous to the tube wall come to rest and the remaining fluid layers continue to flow, thus

producing a separation of flow [22].

An iterative process is utilized to find the maximum achievable flow rate through a given stenosis, the total pressure loss, the downstream intraluminal pressure, and the geometric changes along the stenotic vessel. The results of this study are best summarized as follows:

1. Mean flow rate decreases with increasing stenosis severity and with increasing degree of flexible wall circumference, while the respective pressure losses increase.
2. Exit losses dominate over viscous losses for the rigid models, but the reverse is true for the more compliant models.
3. Upon comparison of the calculated results with previously performed experiments [48], the mean flow rate and pressure drop are predicted within 13% of the experimental values.

Siebes and D'Argenio concluded that utilizing the properties of the latex tubing produced most of the discrepancies between calculated and experimental results. Unlike the linearly elastic properties of the (distended) latex tubing, the arterial wall, with its highly nonlinear nature, becomes progressively more compliant at lower (positive) transmural pressure.

3.0 MATHEMATICAL MODEL 1

3.1 Description of Model 1

The first model used to investigate collapsible tube phenomenon compared a collapsible tube segment to an electrical R-C-L circuit. Due to the variations in area, the tube has resistance; due to the flexible walls, the tube has capacitance; due to the inertial properties of the conveyed fluid, the system has inductance.

In a collapsible tube, the resistance is a function of fluid viscosity and tube geometry, and is defined as:

$$R = \frac{8 \mu \pi L}{A^2} \tag{41}$$

where μ is fluid viscosity and L is the length of the tube. This is the Hagen-Poiseuille relationship, using tube area, A, instead of tube diameter since the shape of the tube is not circular once collapse begins. In addition, the dynamic pressure associated with the kinetic energy of the fluid is incorporated into the model as another resistance which is a function of flow rate, defined by the Bernoulli equation:

$$R_b = \frac{\rho Q^2}{2} \left(\frac{1}{A_o^2} - \frac{1}{A_i^2} \right) \tag{42}$$

where ρ is fluid density, and A_o and A_i are tube inlet and outlet area, respectively. Note that for a rigid tube, where $A_i = A_o$, the above equation goes to zero.

Upstream and downstream resistances, equivalent to R_1 and R_2 of Figure 2, will be referred to as R_{in} and R_{out}.

Inertial effects of the flowing fluid are defined by the following equation [28]:

$$I = \rho \int_0^L \frac{dx}{A(x)} \tag{43}$$

where A(x) is the cross-sectional area at a longitudinal distance x in the tube. For tube segments where the inlet and outlet areas were not equal, a linear taper was assumed, and the inertial equation becomes:

$$I = \frac{\rho L}{A_{avg}} \tag{44}$$

where $A_{avg} = \frac{1}{2}(A_i + A_o)$ of each segment.

For constant resistance and inductance, a constant area of A_0 was utilized in Eq. 41 and Eq. 44. When nonlinearities were to be included, the tube law (see below) was then incorporated.

Due to the flexibility of the tube segments, fluid capacitance is an important component of the pressure-volume relationship. In

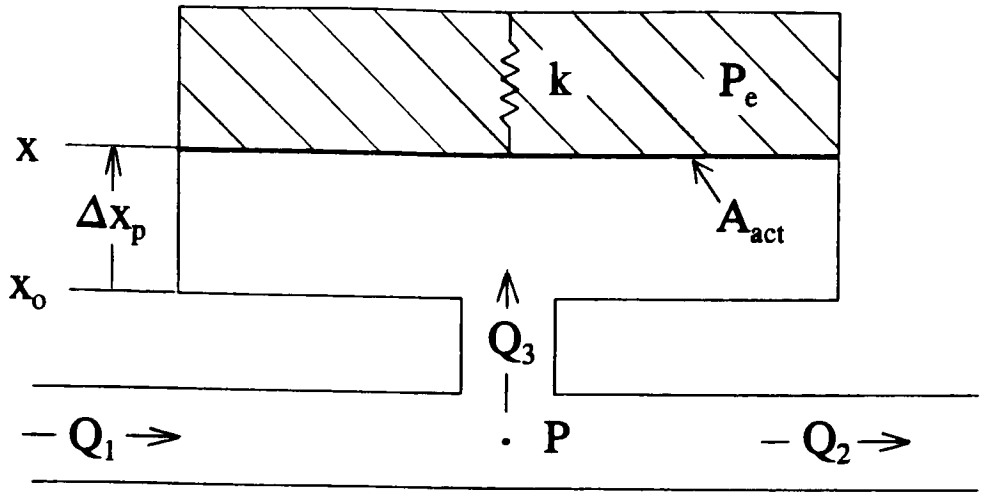

FIGURE 11 - Spring-loaded accumulator

the linear case,

$$P = \frac{1}{C} V \tag{45}$$

where the capacitive value C is defined by the specific system under consideration. For this modeling, consider the spring-loaded accumulator shown in Figure 11 as the net effect of tube volume changes due to wall flexibility. Any increase in volume in the accumulator (tube wall expansion) must overcome a spring force (wall elasticity). In the accumulator system:

$$F_{on\ plate} = A_{act}\ P_{TM} = k\ \Delta x_p \tag{46}$$

and

$$V = A_{act}\,\Delta x_p \tag{47}$$

where $P_{TM} = P - P_e$ and A is the area the force acts upon. Combining these two equations:

$$\Delta x_p = \frac{A_{act}\,P_{TM}}{k} = \frac{V}{A_{act}} \tag{48}$$

Rearranging:

$$P_{TM} = \frac{k}{A_{act}^{\,2}}\,V \tag{49}$$

Thus the definition of capacitance becomes:

$$C = \frac{A_{act}^{\,2}}{k} \tag{50}$$

For a collapsible vessel, the area the force acts upon is the product of the circumference and the segment length, or

$$A_{act} = \pi D_0 L \tag{51}$$

During any state of collapse when opposing sides of the tube are in contact, this A_{act} is reduced since flow is through two conduits. However, for the present investigation, this area is assumed constant, regardless of the state of collapse.

The "spring constant" for a collapsible tube is derived from the following free body diagram:

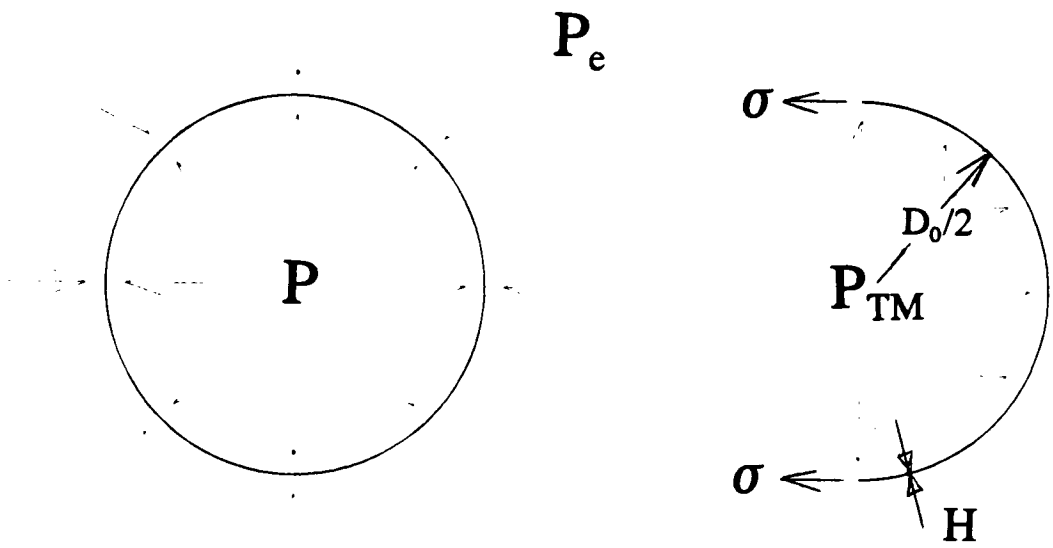

Transmural pressure is defined as usual, σ is hoop stress, and H is tube wall thickness. Force balance in the thin hoop segment gives the following:

$$2\sigma L_0 H_0 = P_{TM} L_0 D_0 \qquad (52)$$

where L_0, H_0, and D_0 are nominal tube length, wall thickness, and diameter, respectively.

From Hooke's law:

$$\sigma = E\epsilon \tag{53}$$

where E is Young's Modulus and ϵ is hoop strain, and by definition

$$\epsilon = \frac{\Delta D}{D_0} \tag{54}$$

Therefore, combining Equations 52, 53, and 54 yields:

$$P_{TM} = \frac{2H\,E}{D_0^{\,2}}\Delta D \tag{55}$$

Since pressure is defined as a force divided by the area it acts over, Eq. 55 may be redefined as:

$$\frac{2H\,E}{D_0^{\,2}}\Delta D = \frac{F}{A_{act}} = \frac{F}{\pi D_0 L} \tag{56}$$

Rearranging:

$$F = \left(\frac{2\pi H\,E\,L}{D_0}\right)\Delta D \tag{57}$$

which is analogous to the force equation (Eq. 46) of the

accumulator system discussed above. Thus, the effective spring constant, k, becomes:

$$k = \frac{2\pi H E L}{D_0} \tag{58}$$

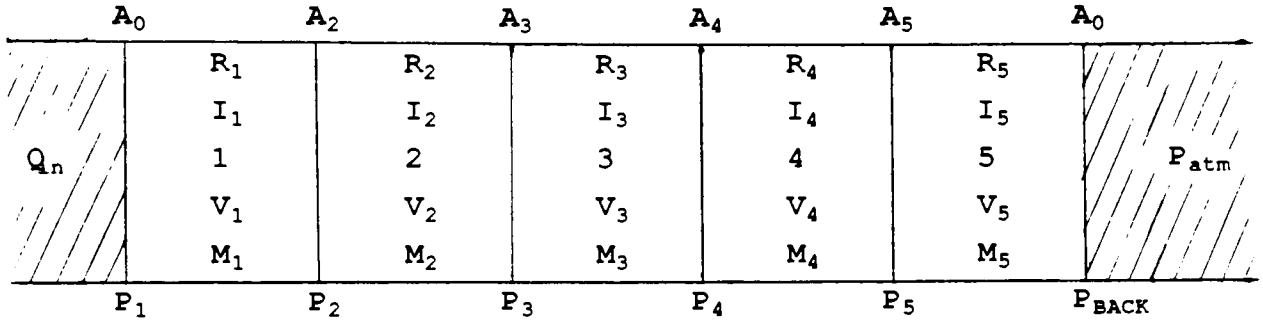

Model 1 nomenclature

Using these definitions and assuming a lumped-parameter philosophy, the collapsible tube can be divided into any number of tube segments, each segment having the above properties. Nomenclature for this model is shown above. With the exception of the two end segments, all of the segments will have the same defining equations for the pressure-flow relationship. The end segments differ only because the tube is attached to a rigid tube at either end and is thus held open.

Bond graph theory [45] was utilized to determine the governing coupled differential equations of this system. For each segment of

the tube, the following bond graph was applied:

where R_T is the sum of the viscous and Bernoulli resistances. The complete bond graph for this system is provided in APPENDIX A. Using this as the basis for the model, the following governing equations resulted:

$$\frac{dV_i}{dt} = \dot{V}_i = \frac{M_{i-1}}{I_{i-1}} - \frac{M_i}{I_i} \tag{59}$$

$$\frac{dM_i}{dt} = \dot{M}_i = \frac{V_i - V_0}{C_i} - R_i Q_i - \frac{V_{i+1} - V_0}{C_{i+1}} \tag{60}$$

Energy state variables, M and V, represent fluid momentum and tube volume, respectively, and V_0 is nominal tube segment volume. In addition, the standard tube law (Figure 10) was utilized in equation form. For the collapsed states:

$$\alpha = \left(1 - \frac{P_{TM}}{K_p}\right)^{-\frac{2}{3}} \tag{61}$$

where

$$K_p = \frac{1}{12}\left[\frac{E\left(\frac{H}{rad}\right)^3}{(1-\nu^2)}\right] \tag{62}$$

For the distended states, a linear relationship adapted from Siebes and D'Argenio [47] was utilized:

$$D - D_0 = 0.000634 P_{TM} \tag{63}$$

where 0.000634 is the slope of the pressure-diameter relationship. To incorporate this equation into the mathematical model, it was redefined in terms of area, and the final form that resulted was:

$$A = \frac{\pi}{4}\left[(0.000634\ P_{TM}) + \sqrt{\frac{4A_0}{\pi}}\right]^2 \tag{64}$$

These equations were solved simultaneously using Advanced Continuous Simulation Language (ACSL) software, which employed a second order Runge-Kutta method. The complete program is provided

in APPENDIX B. Reynolds number for a flow rate of 10 cc/sec is less than 1000.

3.2 Results of Model 1

Problems incorporating the Bernoulli resistor proved to be insurmountable in the present study due to numerical instabilities it produced. Therefore, the resistance that was applied in each segment was only that which arose from area changes of the tube.

3.2.1 Single Segment Analysis

First, the tube segment was examined in its entirety (ie. as one element), with a step flow rate of 10 cc/sec, zero external pressure, and a downstream resistance of 0.0125 mm Hg/(cc/sec). This value of downstream resistance was taken from noted rigid tube resistance in Lyon [37]. Pressure and volume responses for constant resistance and inductance are shown in Figure 12. Initial oscillations with a frequency of 3 Hz decay to steady-flow conditions, with a volume oscillation amplitude less than 1 cc/sec and pressure oscillation amplitude less than 1 mm Hg.

To analytically verify the accuracy of the model, the natural frequency and period of oscillation were calculated, with good agreement between the analytical and mathematical modeled results.

Doing a sensitivity analysis, nonlinear resistance was added, via incorporation of the tube law, and the results are shown in Figure 13. Adding this nonlinear resistance acts as a damping factor, slightly increasing the frequency while reducing the

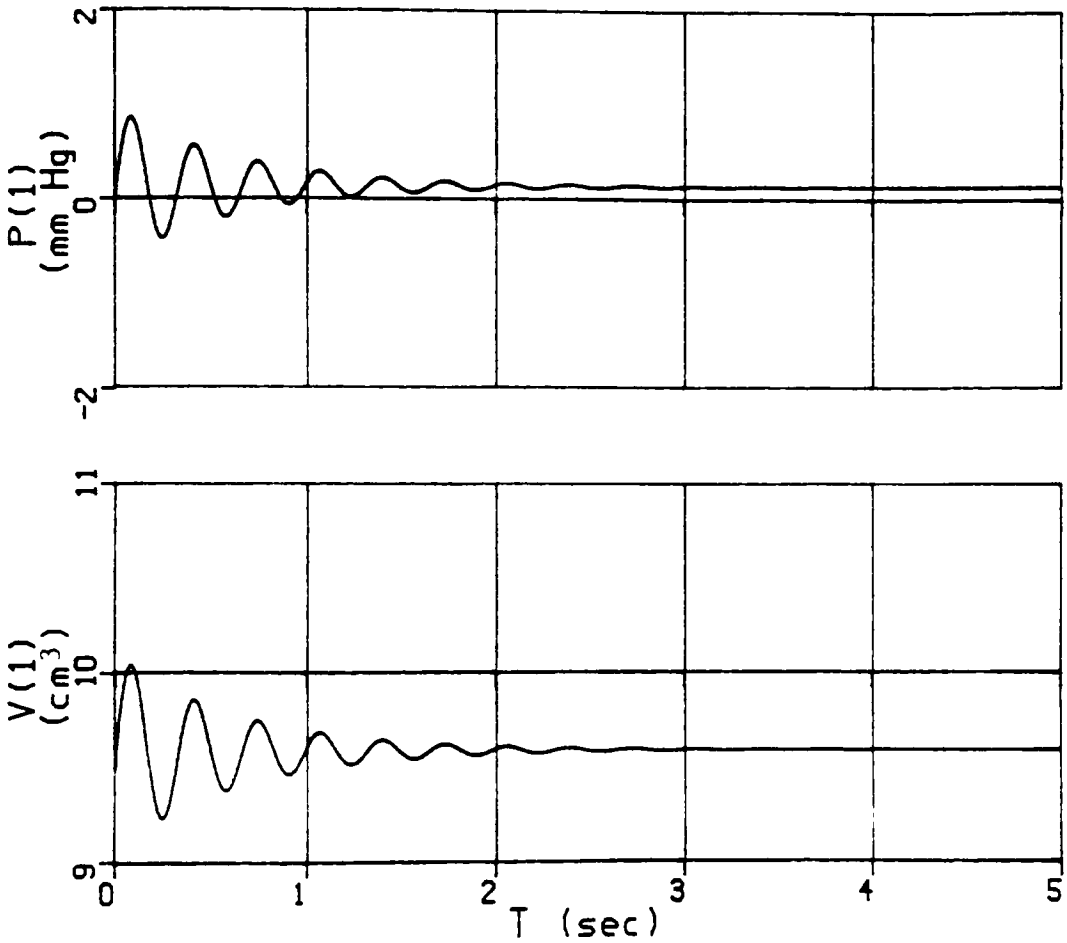

FIGURE 12 - Model 1: 1 element pressure and volume time responses for constant resistance and inductance

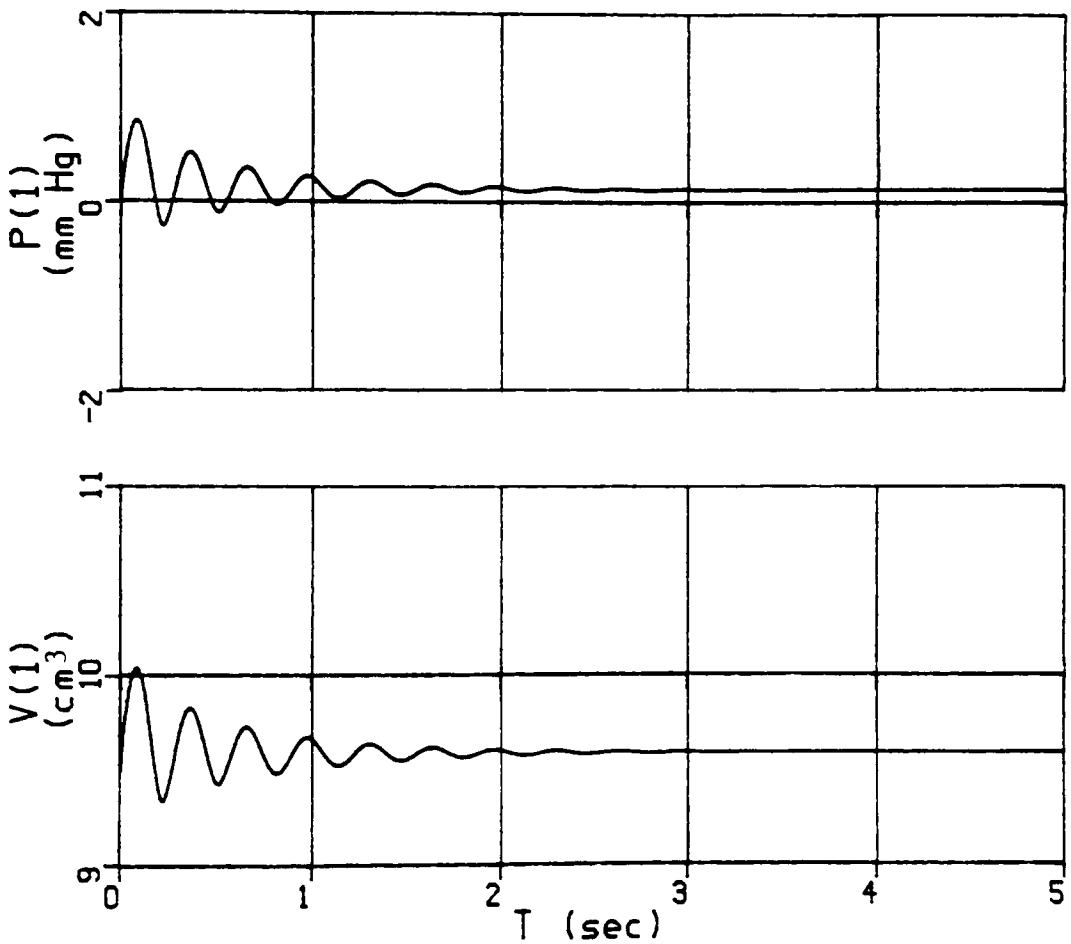

FIGURE 13 - Model 1: 1 element pressure and volume time responses for nonlinear resistance and constant inductance

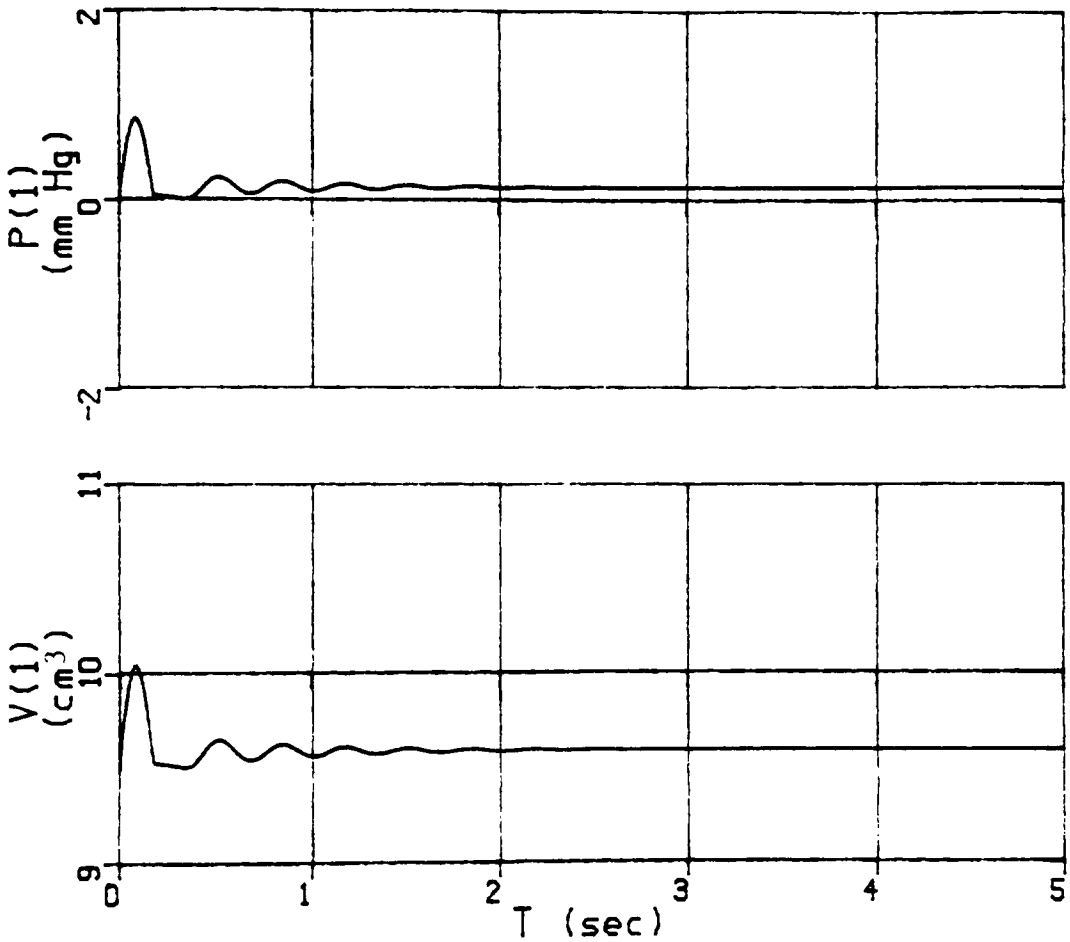

FIGURE 14 - Model 1: 1 element pressure and volume time responses for constant resistance and nonlinear inductance

amplitude of oscillations. Figure 14 shows the pressure and volume responses for constant resistance and nonlinear inductance, as given by Equations 41 and 44, respectively. This nonlinear inductance acts to truncate early oscillations that occur at approximately 0.3 seconds, but this anomaly disappears in the later oscillations. Figure 15 shows the pressure and volume responses with both nonlinear resistance and nonlinear inductance. Note, that the nonlinear inductance allows the system to reach steady state faster than the linear case, as shown by comparing Figures 12 and 13 with Figures 14 and 15. It is evident that the nonlinear inductance is dominant over the resistance in terms of controlling the pressure-flow relationships.

To determine the accuracy of Model 1 for predicting collapse phenomena, comparisons were made with Lyon's [37] experimental data. Recall that her study showed that as downstream resistance increased, $P_i - P_o$ decreased at any given flow rate. This is shown graphically in Figure 16 and is representative for $P_e - P_o$ = 10 mm Hg. In addition, P_o increased with increasing downstream resistance. Although Lyon did not provide numerical values for these resistances, Figure 17 and Figure 18 show qualitative agreement between Model 1 and Lyon's [37] experimental data for high flow rates, although the three distinct phases (initial rise, plateau, and late rise) are not present. Also, Lyon's data showed that for a very high outflow resistance, $P_i - P_o$ remained constant with increasing flow rate. Although "very high" was not empirically defined, Figure 19 shows the mathematical model

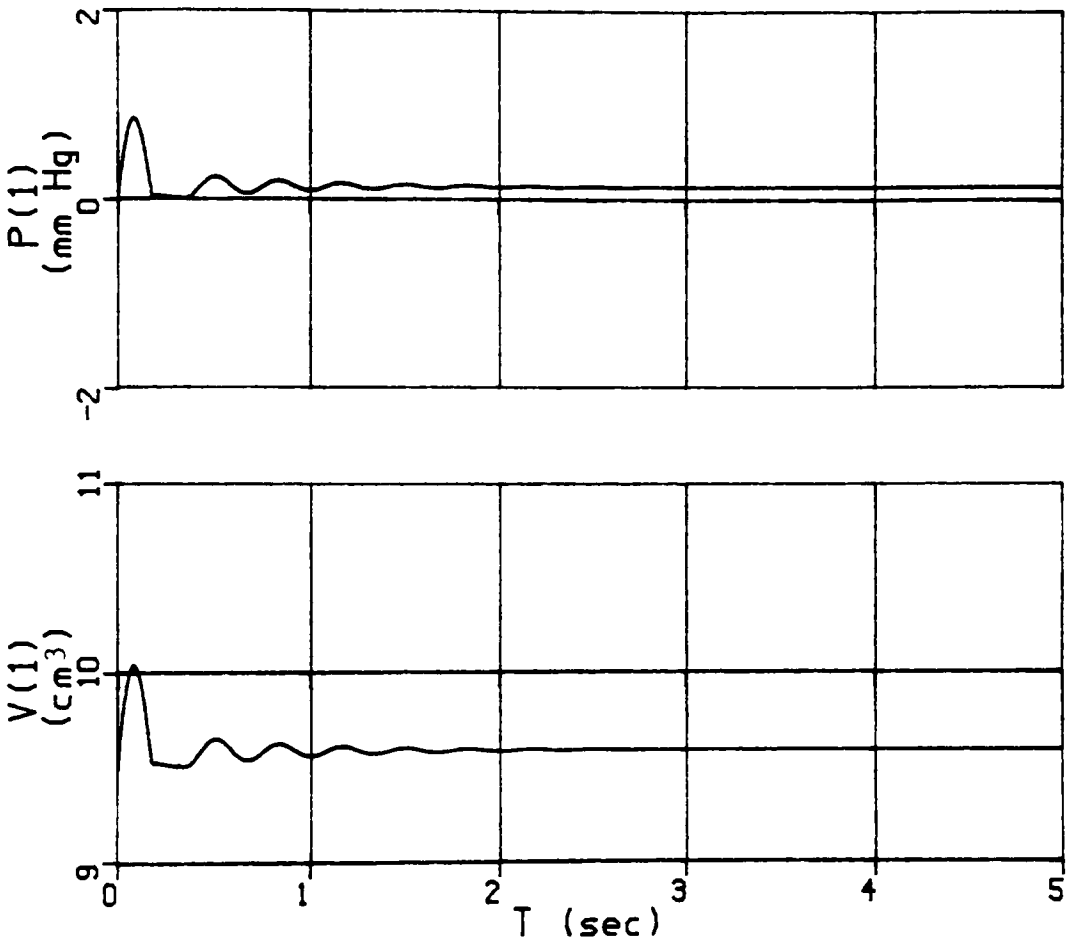

FIGURE 15 - Model 1: 1 element pressure and volume time responses for nonlinear resistance and inductance

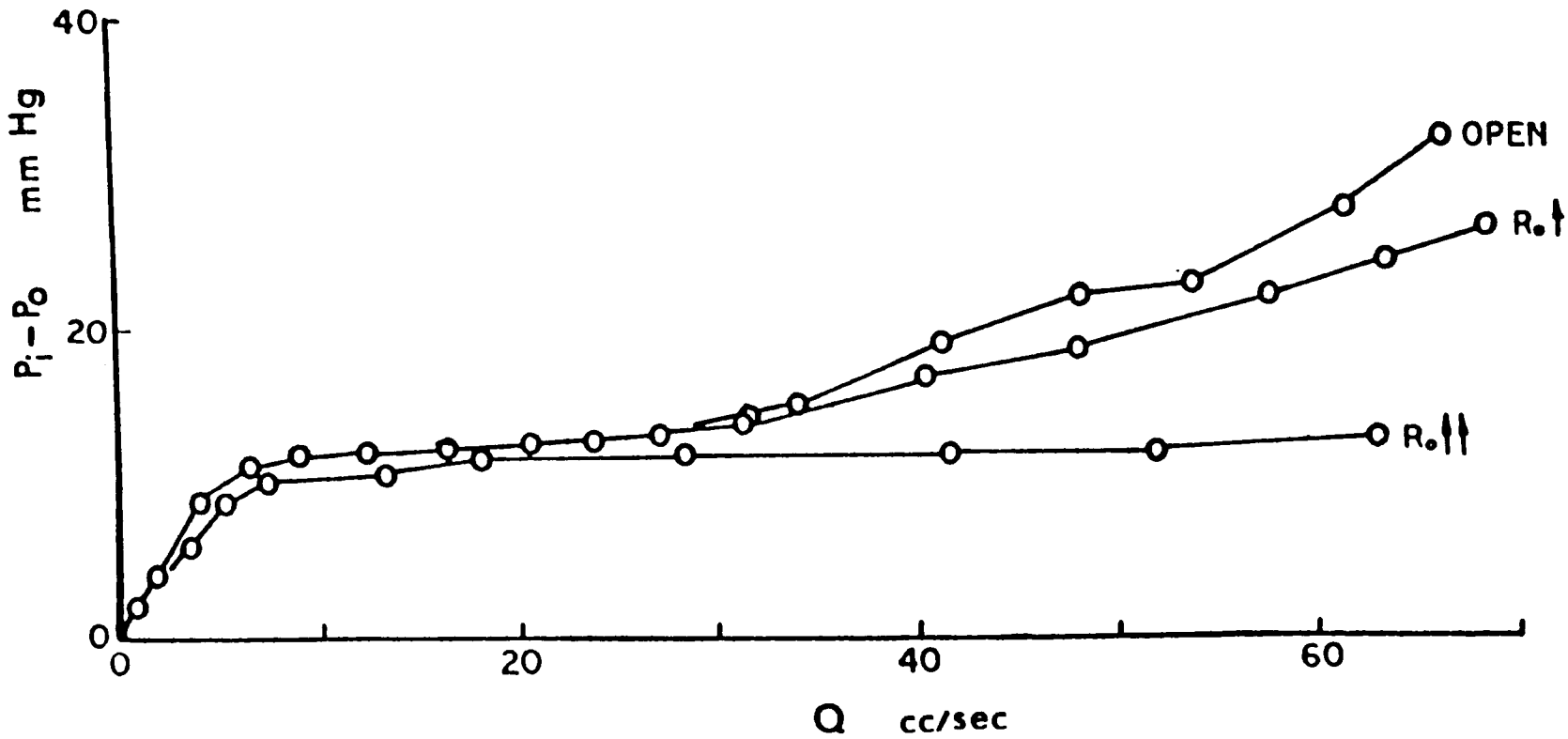

FIGURE 16 - Lyon's [37] results of the effect of outflow resistance on P_i - P_o

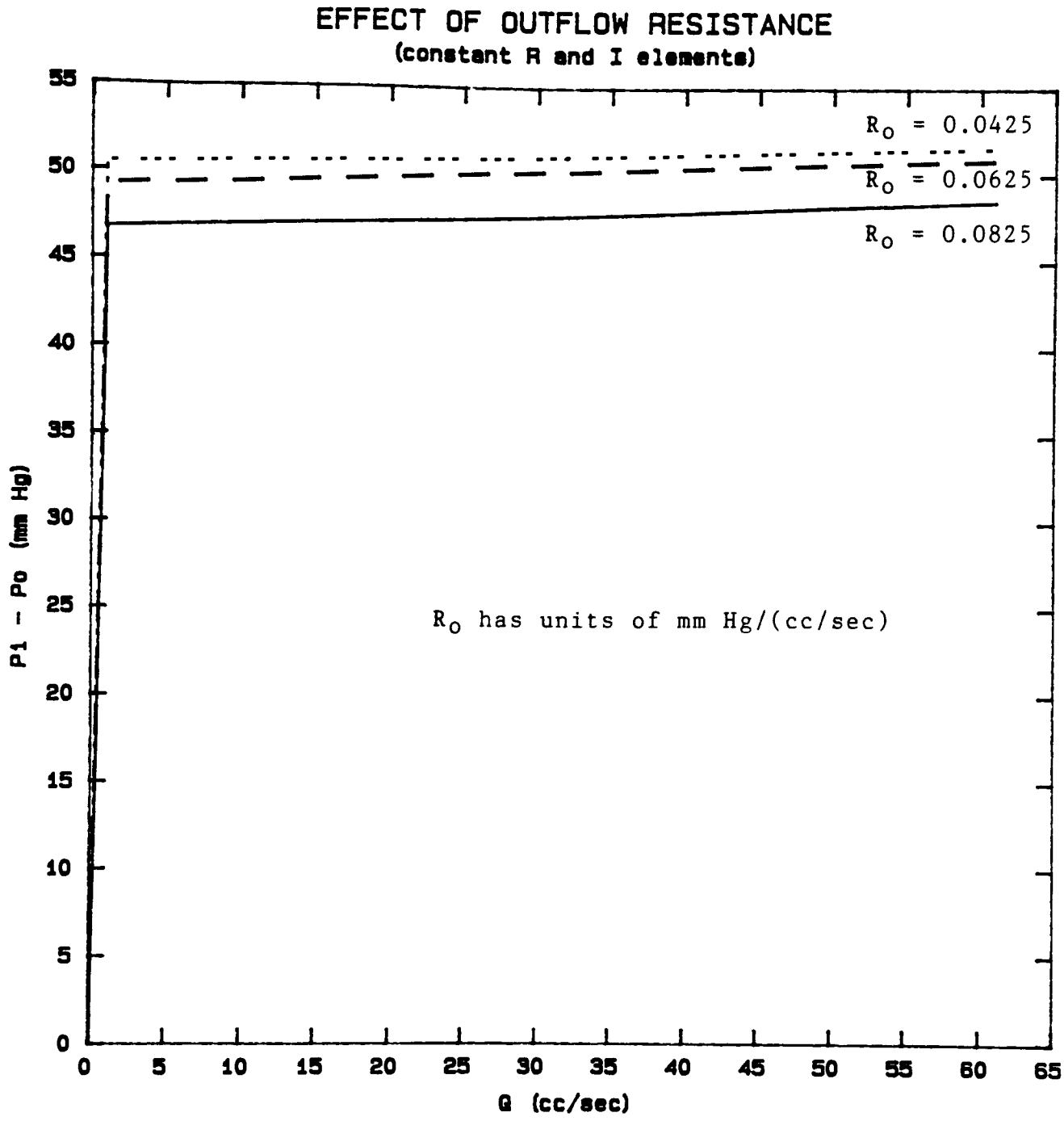

FIGURE 17 - Model 1: 1 element effect of outflow resistance on $P_i - P_o$

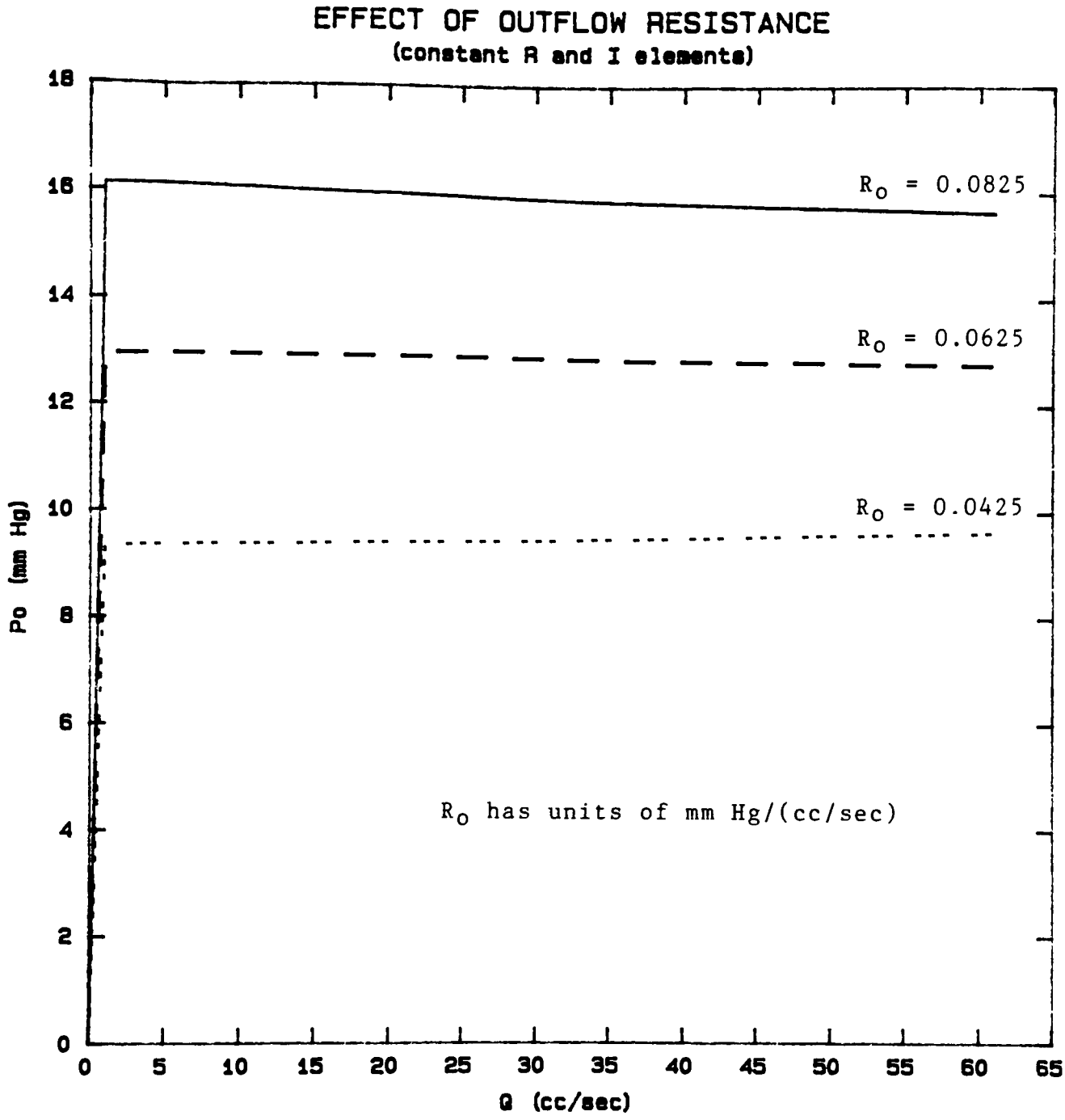

FIGURE 18 - Model 1: 1 element effect of outflow resistance on P_o

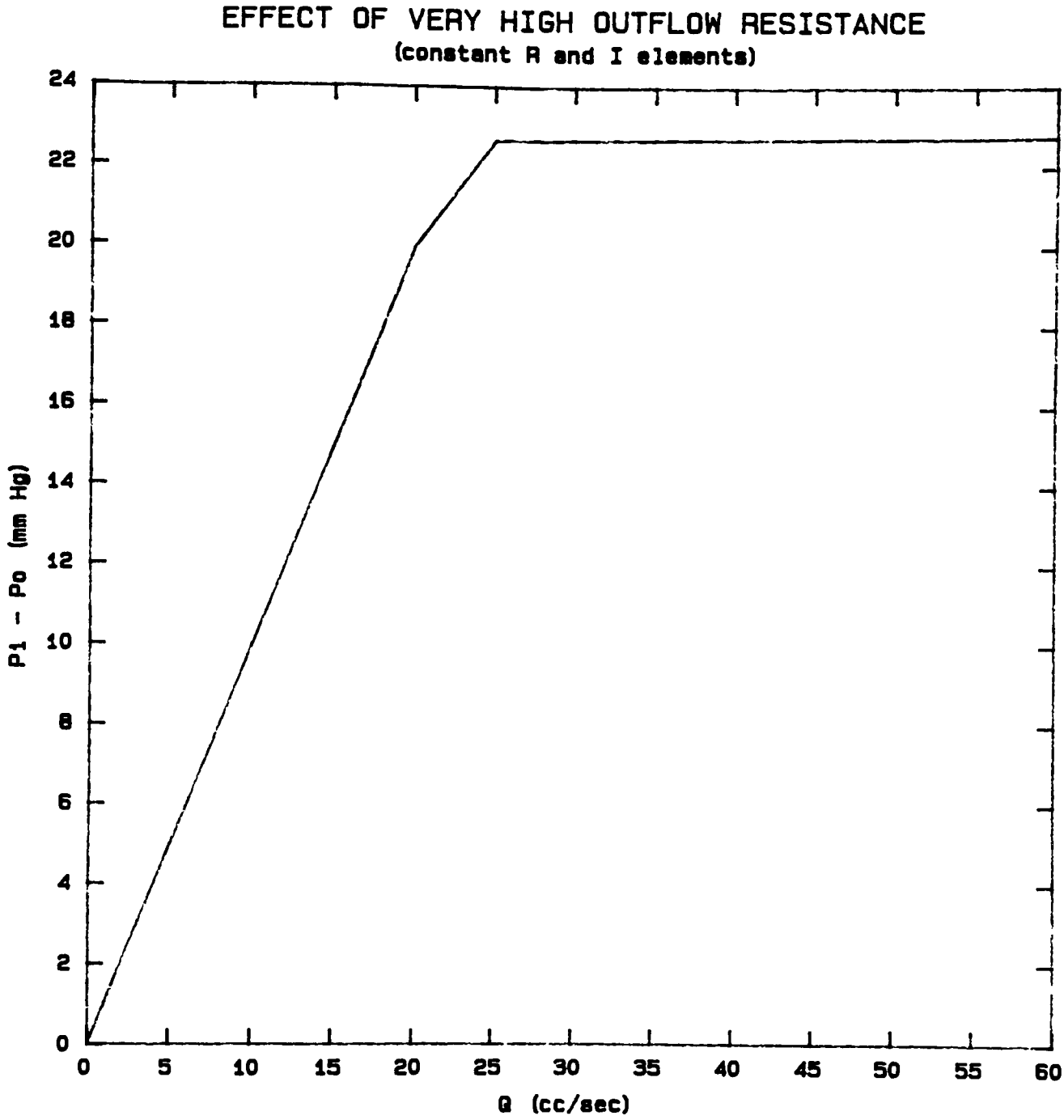

FIGURE 19 - Model 1: 1 element effect of very high outflow resistance on $P_i - P_o$

predicts the same response for an estimated outflow resistance of 1.0 mm Hg sec/cm^3, but again, only qualitatively. However, note the re-emergence of the initial rising phase and plateau phase.

A probable explanation for the discrepancy is that the mathematical model does not allow the difference $P_c - P_o$ to be held at a constant value. Instead, P_c is a set value and P_o varies with the system. This is also the reason other comparisons to Lyon's data could not be obtained. Lyon's results were functions of pressure differences, something that could not be controlled in the present model. In addition, Lyon's [37] results were obtained on a trial and error basis; it was necessary to tweak the downstream resistance to initiate oscillations, thus making exact determination of a resistive value impossible.

Accepting the model as qualitatively correct, the effect of input flow rate is shown in Figure 20. This shows that the steady state volume and internal pressure increase with increasing inlet flow rate. The amplitudes of the oscillations in pressure and volume are increased but the frequencies of oscillation are unaffected when compared to Figure 12.

Figure 21 shows that, like increasing the flow rate, increasing the outflow resistance increases the steady state volume and internal pressure when compared to Figure 12. This increased outflow resistance also acts as a damping device, and the amplitude of oscillations is decreased, but the frequency of oscillations is unaffected.

To investigate the effects of external pressure, it was

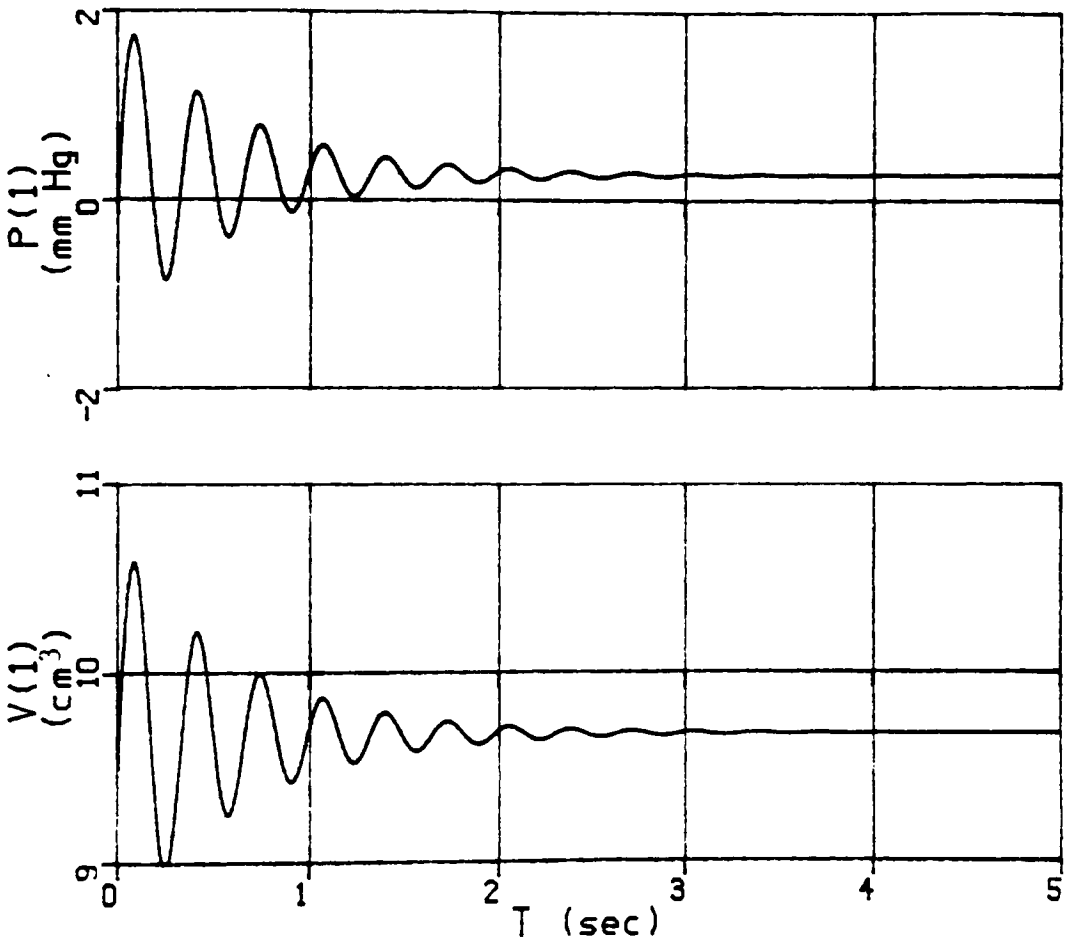

FIGURE 20 - Model 1: 1 element effect of increased step input flow rate

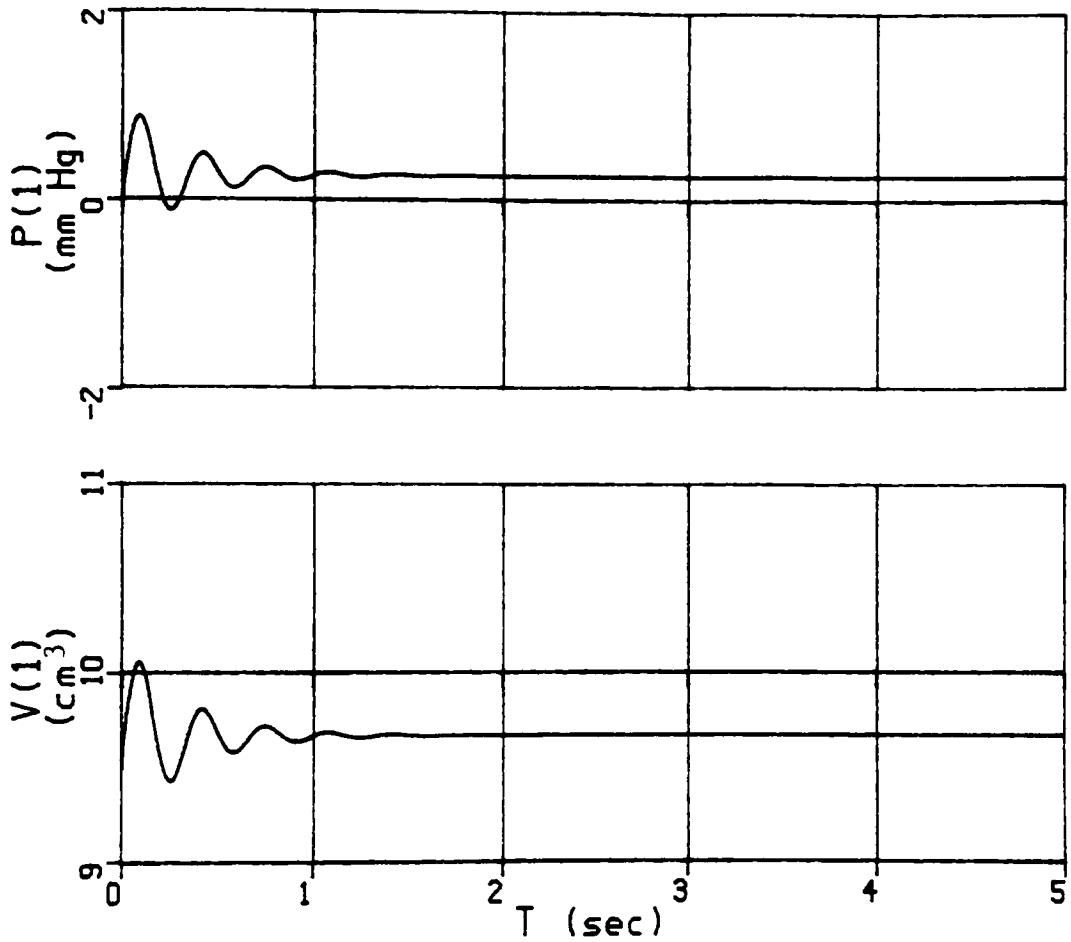

FIGURE 21 - Model 1: 1 element effect of increased outflow resistance

necessary to utilize nonlinear resistive and inductive elements. Figure 22 shows the pressure and volume time responses for an external pressure of 10 mm Hg, with a step input flow rate of 10 cc/sec, and outflow resistance of 0.0125 mm Hg/(cc/sec). Increased external pressure decreases the steady state volume and increases the internal pressure (comparison of Figure 22 with Figure 15). It also dampens the amplitude of oscillations as well as the frequency.

Increased external pressure and increased outflow resistance were then investigated. Both steady state volume and internal pressure increase negligible amounts (when compared to Figure 22) with an outflow resistance of 0.025 mm Hg/(cc/sec). Also, the amplitude and frequency of oscillation appear unaffected, as shown in Figure 23.

For increased external pressure the final variable perturbed was flow rate. The outflow resistance was reduced to its original value (0.0125 mm Hg/(cc/sec), and the step input flow rate was increased to 20 cc/sec. The resulting pressure and volume time responses are shown in Figure 24. Increasing the flow rate increases both steady state volume and internal pressure (when compared to Figure 22). The amplitude and frequency of oscillations before steady state is achieved are again unaffected.

3.2.2 Multiple Segment Analysis

To further investigate the pressure and volume time course data in a collapsible tube, with the hopes of predicting self-

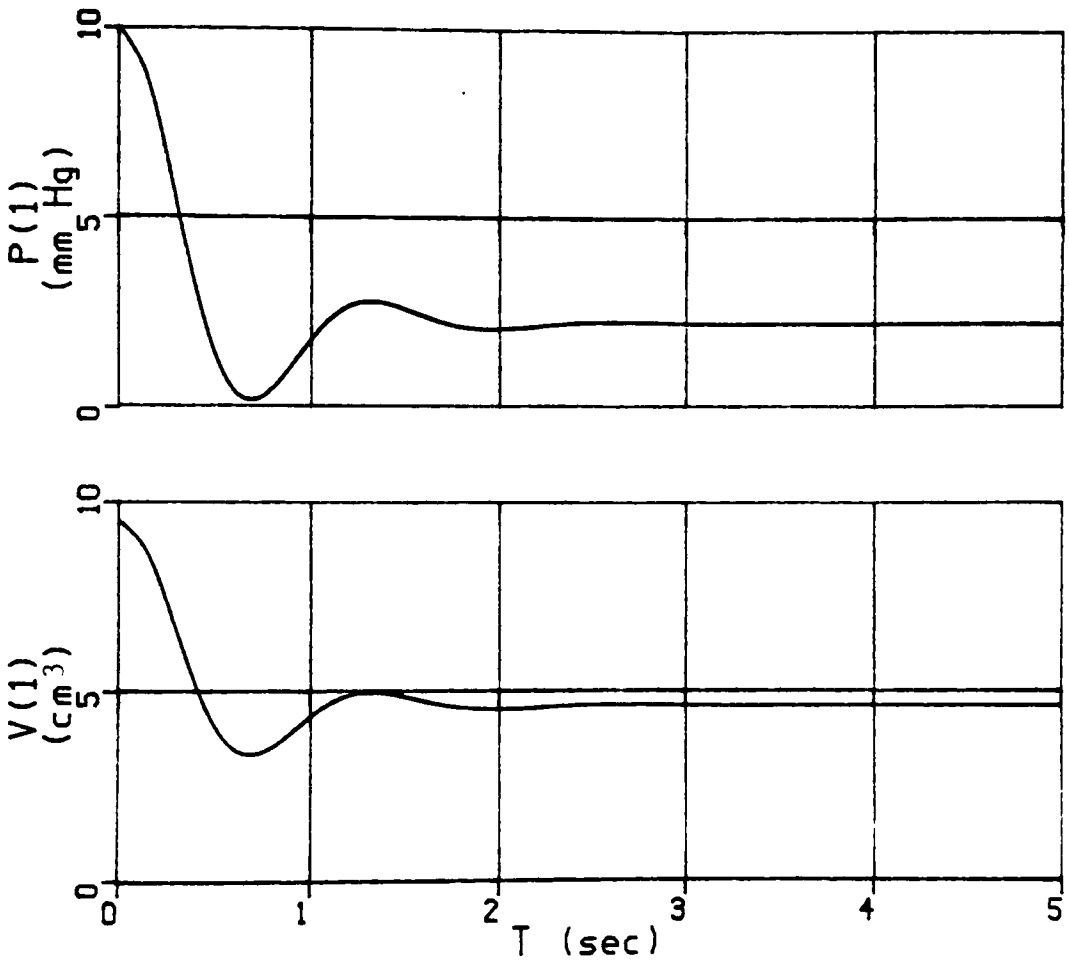

FIGURE 22 - Model 1: 1 element effect of increased external pressure

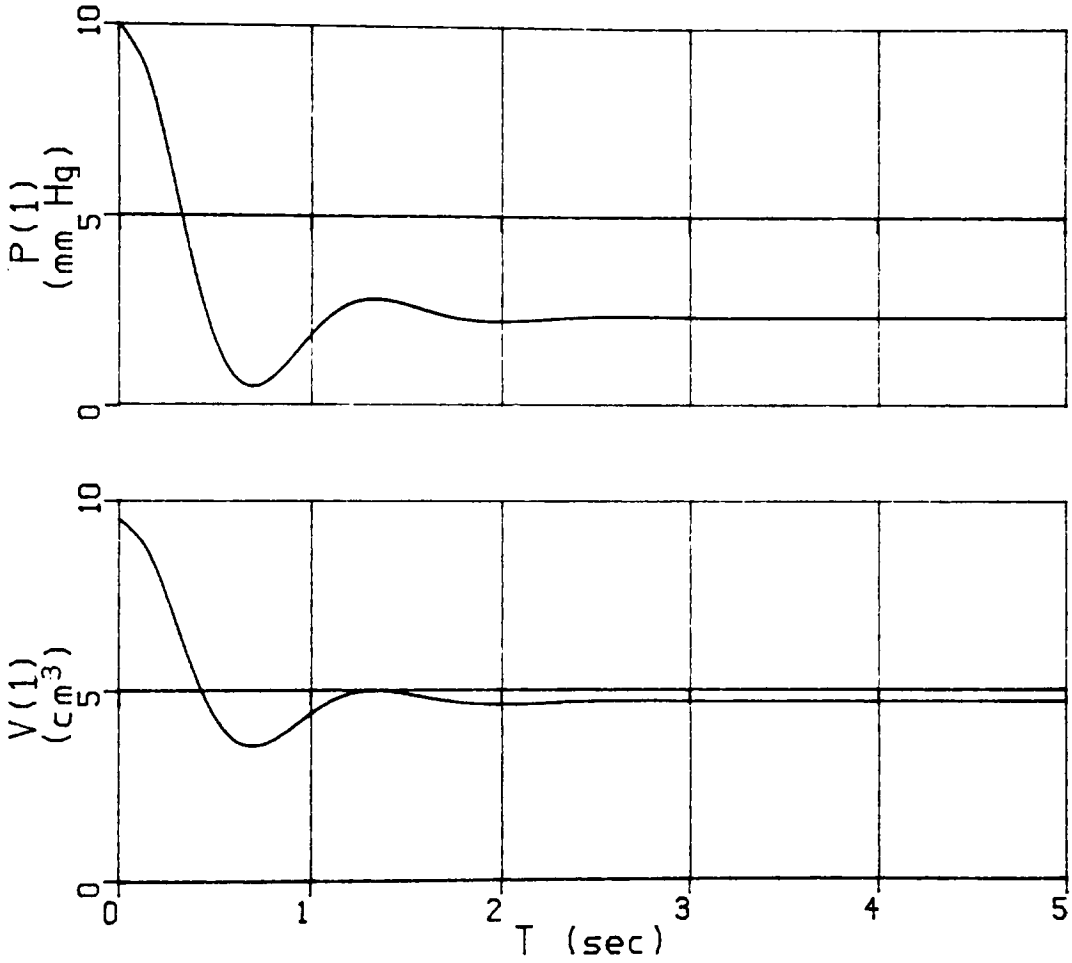

FIGURE 23 - Model 1: 1 element effect of increased outflow resistance with increased external pressure

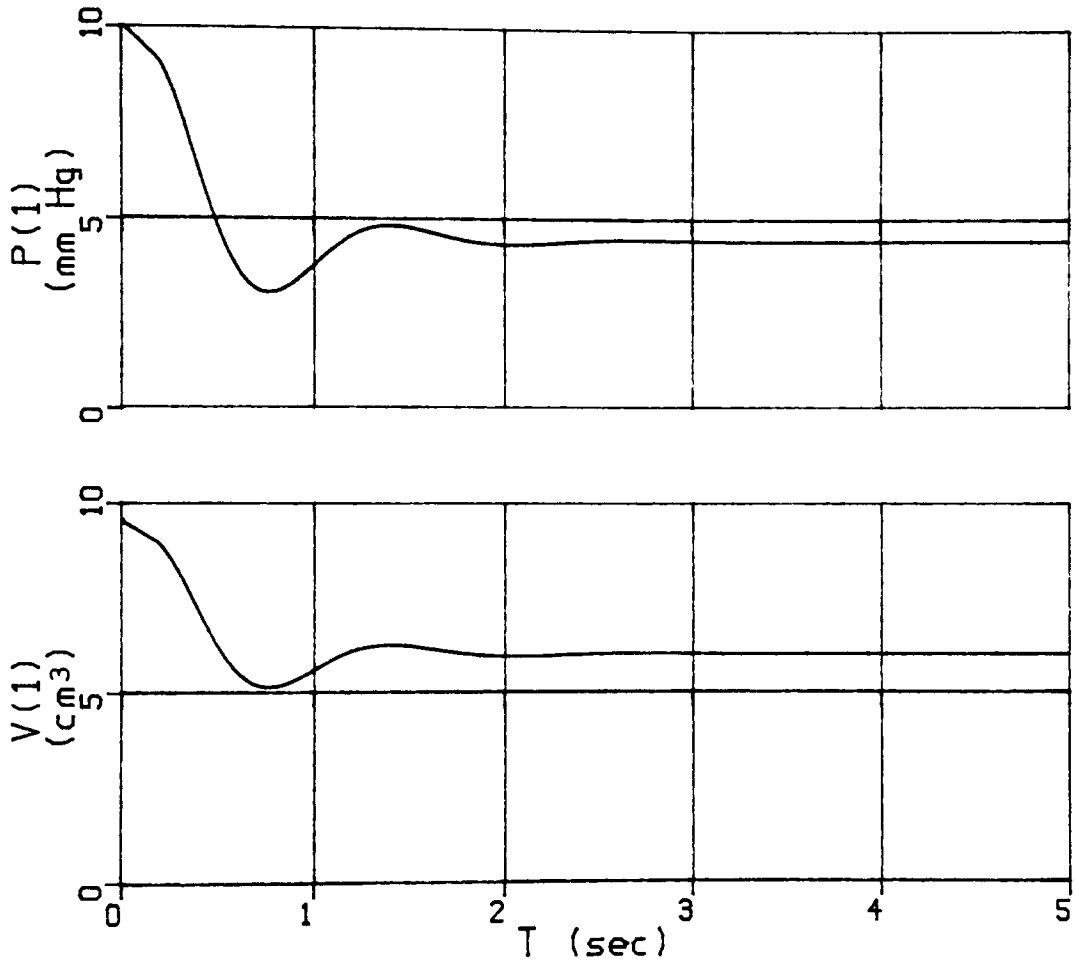

FIGURE 24 - Model 1: 1 element effect of increased step input flow rate with increased external pressure

excited oscillations, the tube was divided into five sections and a similar analysis performed. Figure 25 shows that the amplitude of oscillations due to start-up transients diminish along the length of the tube (segment 1 to segment 5) and the frequency becomes slightly out of phase. However, the general pressure and volume time responses are fairly similar in all five segments of the tube. For this reason, segment 1 will be used to depict the pressure and volume time responses for perturbation in resistive and inductive elements. The relationship produced using constant resistance and inductance is shown in Figure 26. Pressure and volume waveforms are no longer simple exponentially decaying sinusoids, as they were for the one element model. Note the slight steady state oscillations that indicate interaction between the elements.

The model was next adapted to include both nonlinear resistive and inductive elements. Once again, an outflow resistance of 0.0125 mm Hg/(cc/sec), and a step input flow rate of 10 cc/sec were used, but numerical instabilities arose with zero external pressure, so P_e was set constant to 2 mm Hg. The pressure responses for both the first and last elements are shown in Figure 27, and the volume responses are shown in Figure 28. This comparison is made to show that the amplitude of oscillation increases along the length of the tube (trace V(1) vs. V(5)). Initially, it appears that the system is unstable, then suddenly the system reaches steady state. There is no obvious reason for the timing of the onset of steady state, however, there appears to be a constructive-

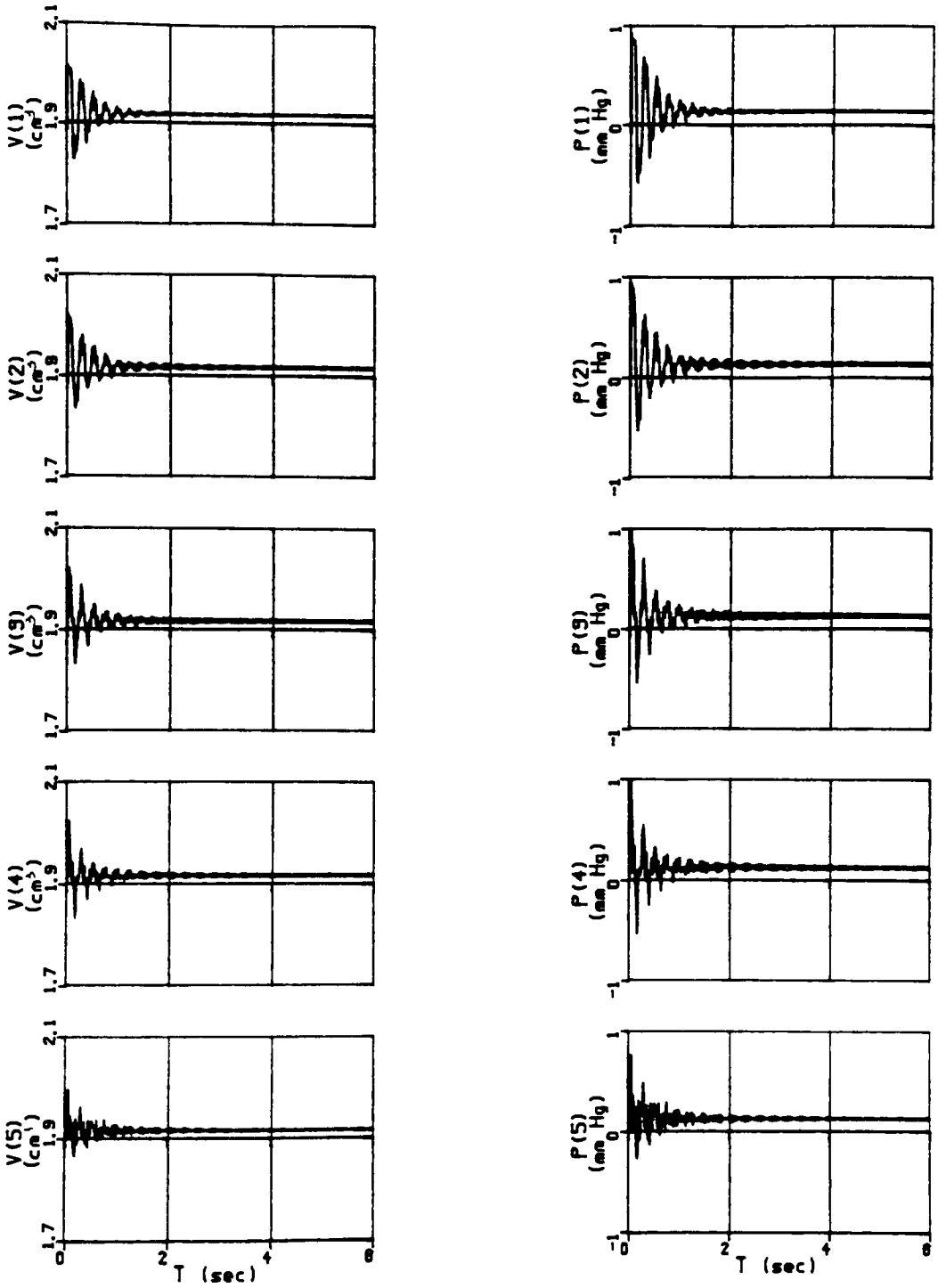

FIGURE 25 - Model 1: 5 element pressure and volume time responses with constant resistance and inductance

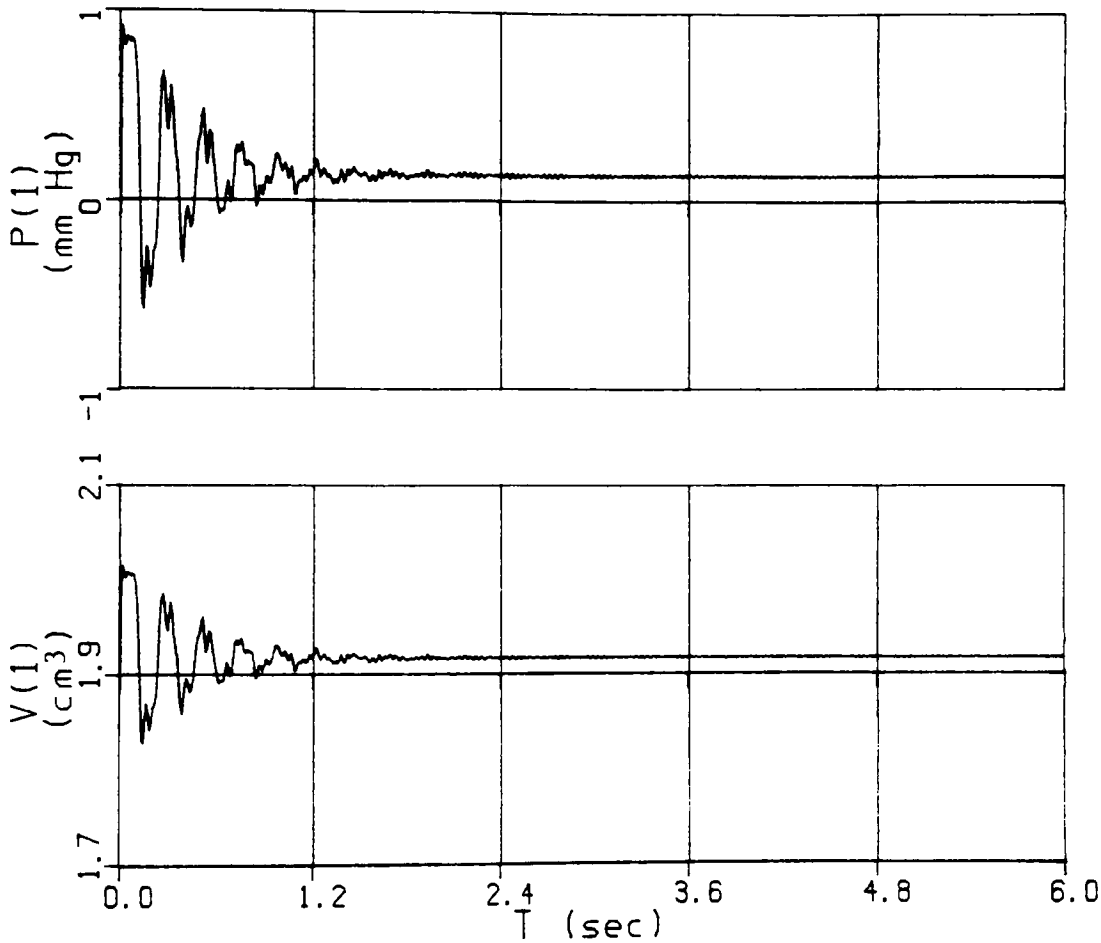

FIGURE 26 - Model 1: segment 1 pressure-flow relationship for constant resistance and inductance

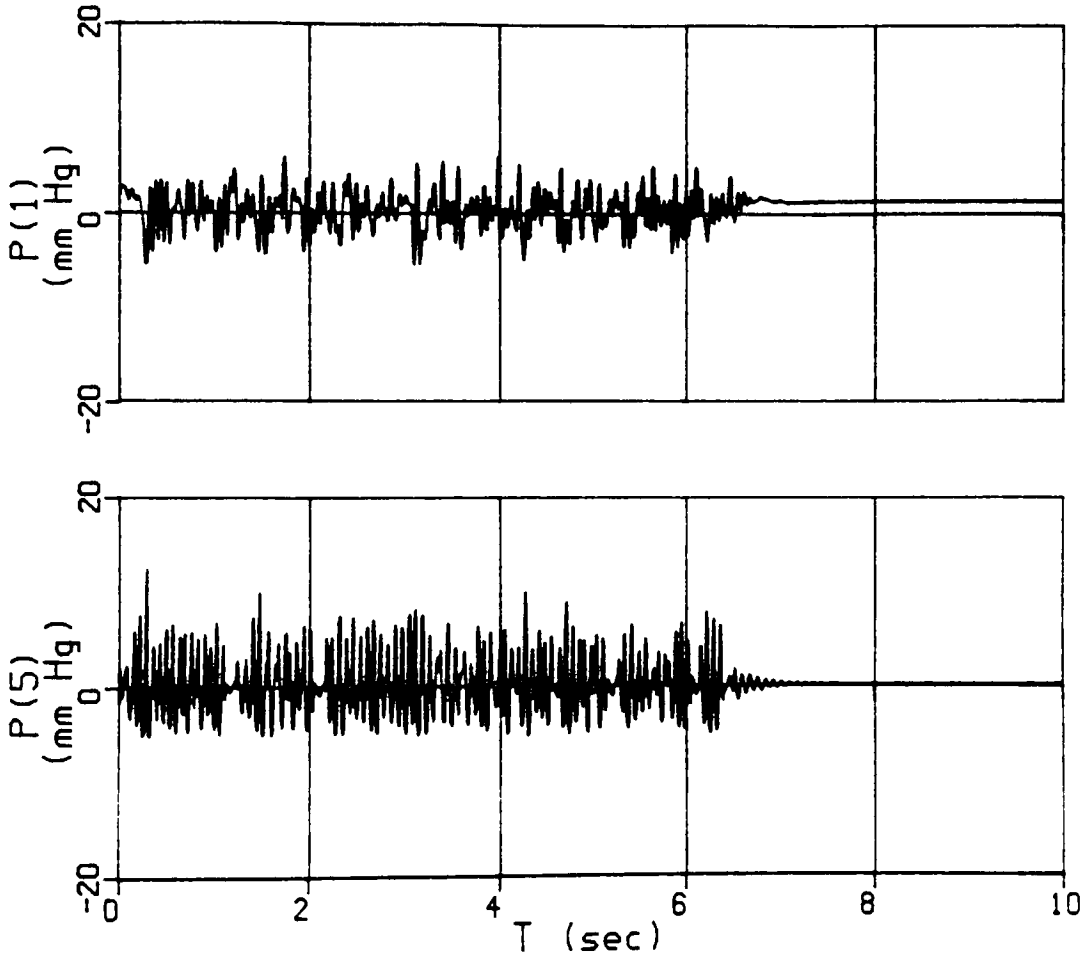

FIGURE 27 - Model 1: elements 1 and 5 pressure responses for nonlinear resistance and inductance

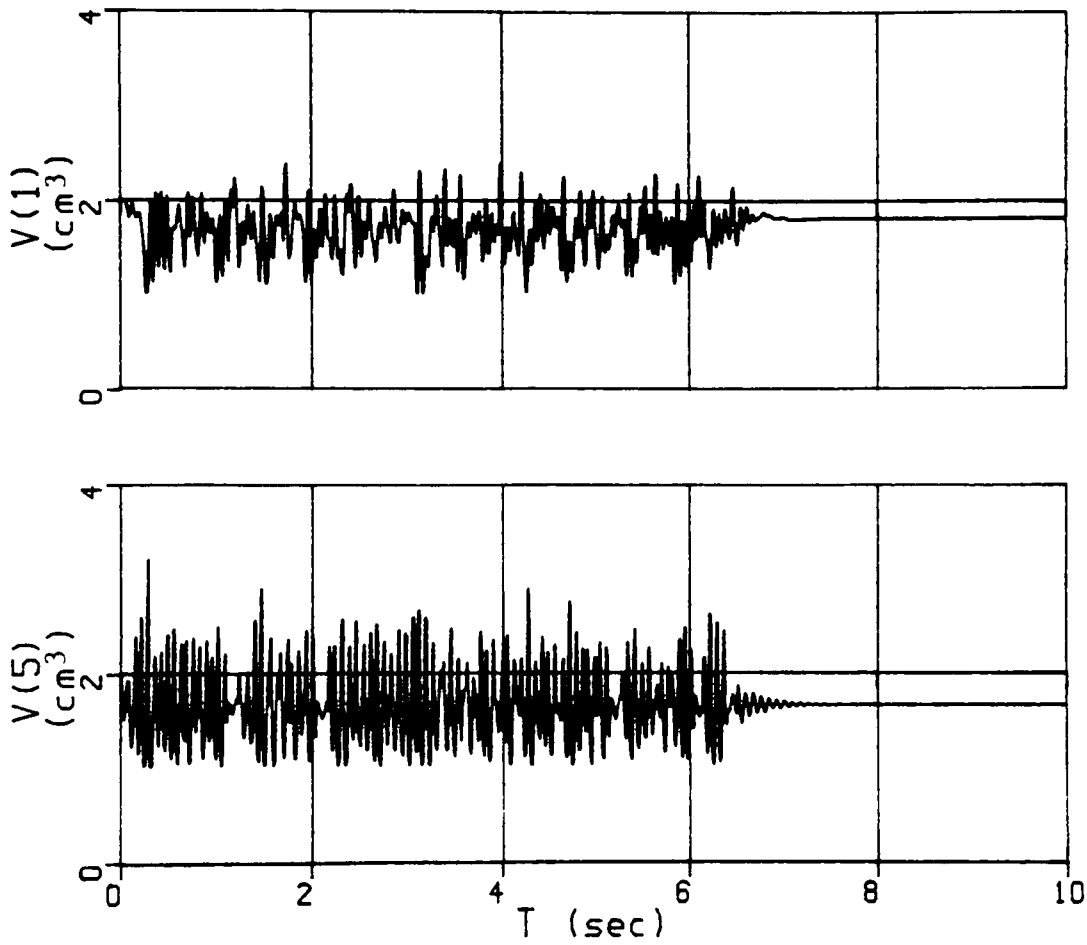

FIGURE 28 - Model 1: elements 1 and 5 volume responses for nonlinear resistance and inductance

destructive interference pattern in the oscillations.

Further increasing the external pressure or the outflow resistance dampens the oscillations drastically, and total collapse of the tube occurs. An increase in the step input flow rate again increases the amplitude of oscillations, but the numerical solution becomes unstable and halts. Steady state is never achieved.

It is theorized that if the input flow rate is increased, and the external pressure is increased to an appropriate value, then the solution will be stable. This is because the external pressure must equally oppose the increased pressure from the elevated input flow rate. Once this balance has been achieved, steady state can ensue. This is shown to be true by the experimental results of Conrad [14] and Lyon [37,38,39], which show stable operating conditions for increased flow rate with increased external pressure. Unfortunately, the correct balance was not achieved in this study. Many other factors, such as tube properties, outflow resistance, and the accuracy of the tube law may have such impact on the modeling that with the currently defined values, a balance was not possible.

4.0 MATHEMATICAL MODEL 2

4.1 Description of Model 2

The second mathematical model utilized Shapiro's [46] equations previously discussed. Recall the coupled differential equations for inviscid flow:

$$-\frac{1}{\rho}\frac{\partial p}{\partial x} = \frac{\partial u}{\partial t} + u\frac{\partial u}{\partial x} \tag{65}$$

$$\frac{\partial A}{\partial t} + \frac{\partial (Au)}{\partial x} = 0 \tag{66}$$

The tube law utilized in Model 1 (Eq. 61) was employed inversely in Model 2; given the area ratio, the internal pressure was determined. For the collapsed state:

$$P_{TM} = K_p \left(1 - \alpha^{-\frac{3}{2}}\right) \tag{67}$$

and for the distended state [7]:

$$P_{TM} = K_p \, [1016.5743*(\alpha - 1)] \tag{68}$$

Backward differencing and forward differencing methods of solving these equations produced numerical instabilities, so a central differencing method was used. Using velocity and area as state variables, the resulting equations became:

$$\dot{u}_i = \frac{P_{i-1} - P_{i+1}}{2\rho L} + u_i \frac{u_{i-1} - u_{i+1}}{2L} \tag{69}$$

$$\dot{A}_i = \frac{A_i}{2L} (u_{i-1} - u_{i+1}) + \frac{u_i}{2L} (A_{i-1} - A_{i+1}) \tag{70}$$

for i = 1...N number of elements. Since both ends of the collapsible tube are connected to rigid tubing:

$$\begin{aligned} A_1 &= A_{n+1} = A_0 \\ \dot{A}_1 &= \dot{A}_{n+1} = 0 \end{aligned} \tag{71}$$

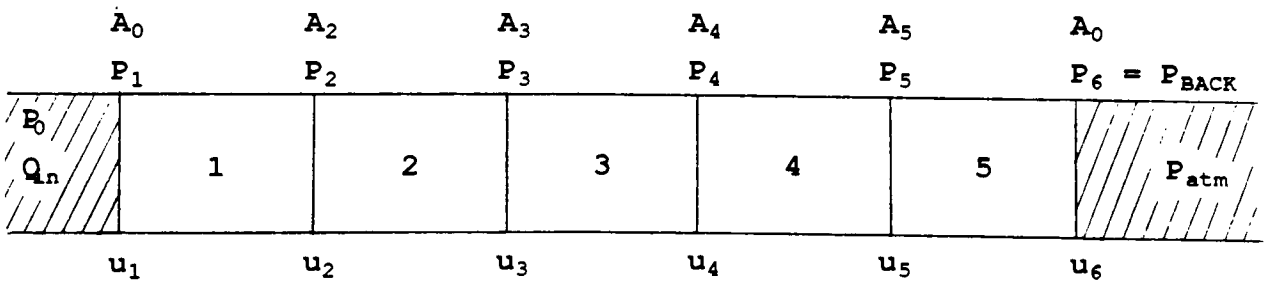

Model 2 nomenclature

The nomenclature utilized is depicted above. At the beginning of the collapsible tube (node 1):

$$\dot{u}_1 = \frac{P_0 - P_2}{2\rho L} + u_1 \frac{u_0 - u_2}{2L} \tag{72}$$

where

$$P_0 = R_{in}\, Q_{in} = R_{in}\, A_0\, u_1 \tag{73}$$

and

$$\begin{aligned} u_0 &= u_1 \\ R_{in} &= \frac{8\mu\pi L}{A_0^2} \end{aligned} \tag{74}$$

At node 2:

$$\dot{u}_2 = \frac{P_1 - P_3}{2\rho L} + u_2 \frac{u_1 - u_3}{2L} \tag{75}$$

and

$$\dot{A}_2 = \frac{A_2}{2L}(u_1 - u_3) + \frac{u_2}{2L}(A_1 - A_3) \tag{76}$$

where P_1 must be explicitly defined in the model.

Equations for all middle segments are of the generic form, as

given previously.

At node n:

$$\dot{u}_n = \frac{P_{n-1} - P_{n+1}}{2\rho L} + u_n \frac{u_{n-1} - u_{n+1}}{2L} \tag{77}$$

and

$$\dot{A}_n = \frac{A_n}{2L}(u_{n-1} - u_{n+1}) + \frac{u_n}{2L}(A_{n-1} - A_{n+1}) \tag{78}$$

where P_{n+1} is defined as:

$$P_{n+1} = R_{out} A_0 u_{n+1} + P_{atm} \tag{79}$$

At node n+1:

$$\dot{u}_{n+1} = \frac{P_n - P_{n+2}}{2\rho L} + u_{n+1} \frac{u_n - u_{n+2}}{2L} \tag{80}$$

However:

$$\begin{aligned} P_{n+2} &= P_{atm} \\ u_{n+2} &= u_{n+1} \end{aligned} \tag{81}$$

Since gage pressure was utilized in the model, $P_{atm} = 0$.

Unlike Model 1, inductive elements are not defined explicitly, but rather they are inherently nonlinear and defined by the tube law (see Figure 10). Again, ACSL was utilized to solve these

equations. The complete computer program is provided in APPENDIX C.

A step input fluid flow rate proved to cause numerical instabilities, so the feathered step of Equation 82 was utilized. As in Model 1, Reynold's number for a flow rate of 10 cc/sec was less than 1000.

$$Q_{\epsilon} = \frac{B}{2} \{\cos[(\omega T) + \pi] + 1\} \qquad (82)$$

where B was the amplitude of the sinusoid, and ω was the period of oscillation.

4.2 Results of Model 2

Because of the nature of the computer program, it was not possible to obtain volume information for the tube examined in its entirety (i.e., as one element). Therefore, the tube was initially divided into two segments to make a comparison between Lyon's experimental data and the predictions of the mathematical model.

4.2.1 Two Segment Analysis

Recall that Lyon [37] showed that as downstream resistance was increased, pressure loss along the length of the tube, $P_i - P_o$, decreased, while downstream pressure, P_o, increased. Figures 29 and 30 show that the mathematical model under consideration produces qualitatively the same results. These plots are for a defined upstream pressure of 10 mm Hg, and zero external pressure. Modifying the upstream pressure produces curves identical in shape

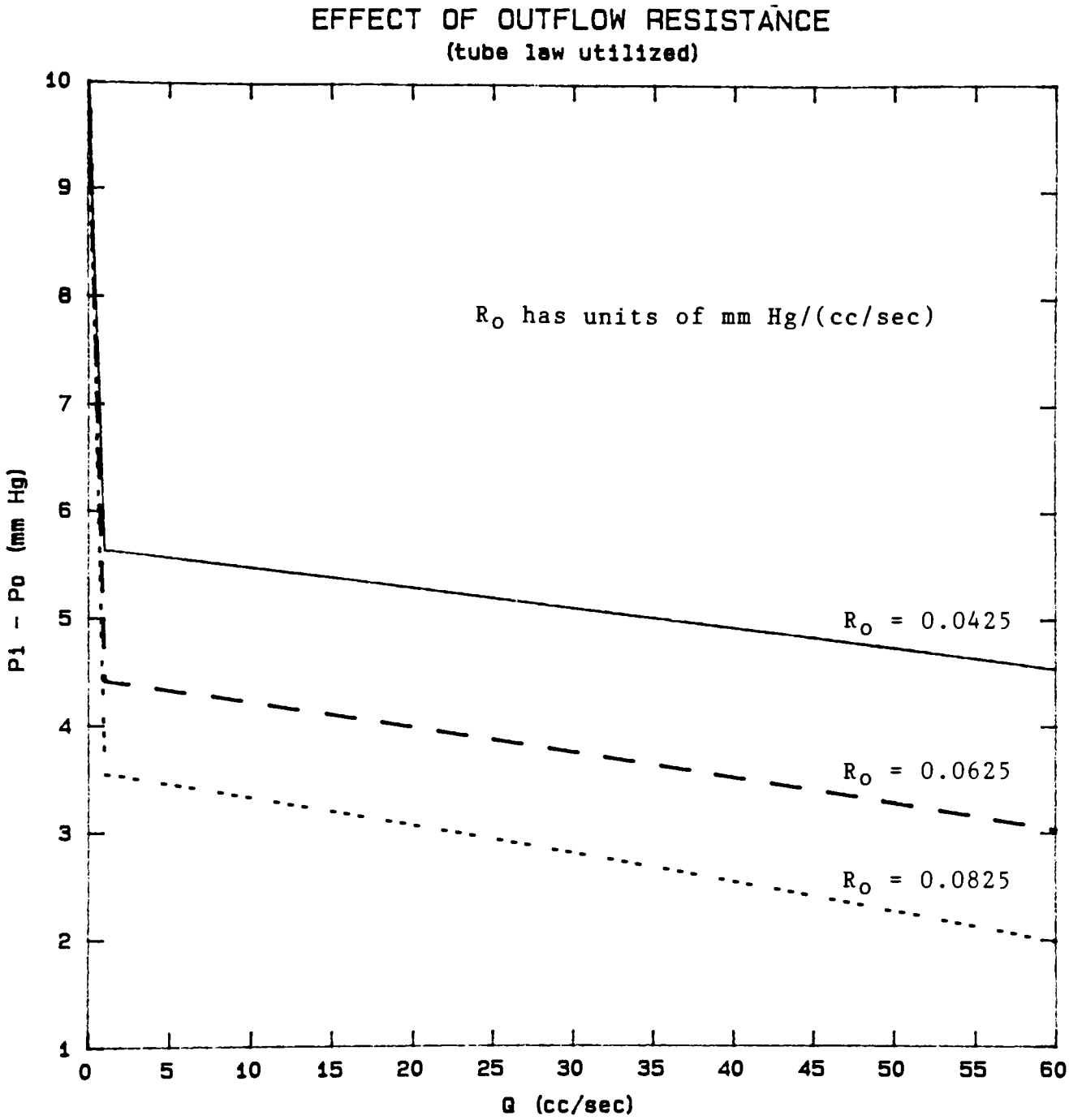

FIGURE 29 - Model 2: 2 element effect of outflow resistance on $P_i - P_o$

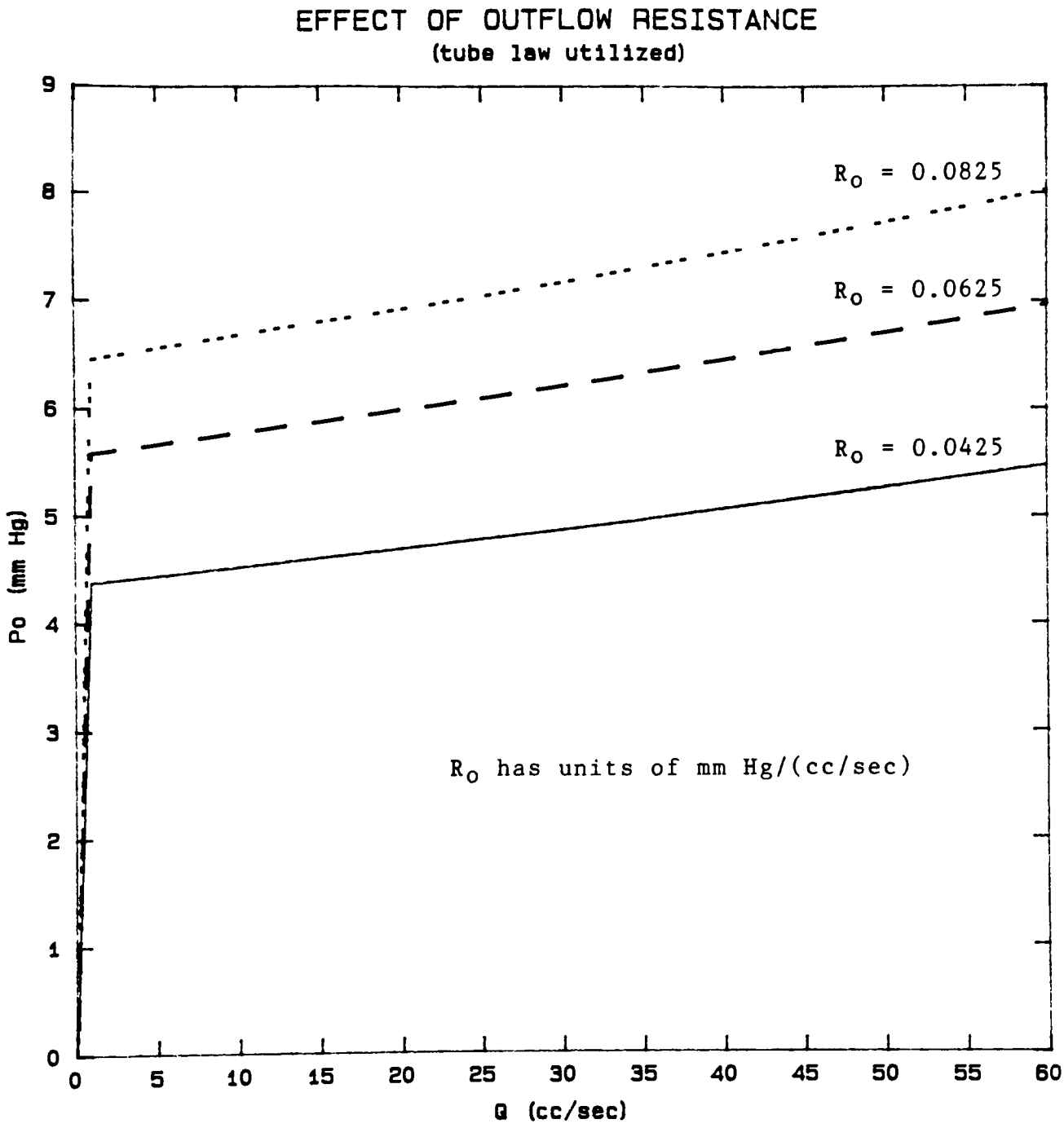

FIGURE 30 - Model 2: 2 element effect of outflow resistance on P_o

to, but numerically different from, the curves depicted in Figures 29 and 30.

The model did not produce a constant pressure loss along the length of the tube for "very high" outflow resistance. This could be due to the fact that both the upstream pressure and the input flow rate had to be increased to avoid numerical instability when the outflow resistance was greatly increased. The parameters were then not comparable.

Because of the nature of the present mathematical model, it was not possible to mimic more of Lyon's experimental data due to the presentation method of her results. Again, as in Model 1, it was not possible to maintain a constant $P_e - P_o$ value, and therefore, comparison with Lyon's data was not possible.

4.2.2 Multiple Segment Analysis

Since the model qualitatively predicts the pressure-flow relationships in a collapsible tube, the tube was then divided into five elements (to be consistent with Model 1).

The model was first examined with a downstream resistance of 0.0125 mm Hg/(cc/sec), input flow rate of 10 cc/sec, upstream pressure of 10 mm Hg, and zero external pressure. Figure 31 shows the volume and internal pressure for each segment. Note that with the exception of the first segment, the volume in all segments reaches approximately the same mean value after one second. Note that the volume data oscillate about this mean with an "envelope" period of approximately one second, with a secondary superposed

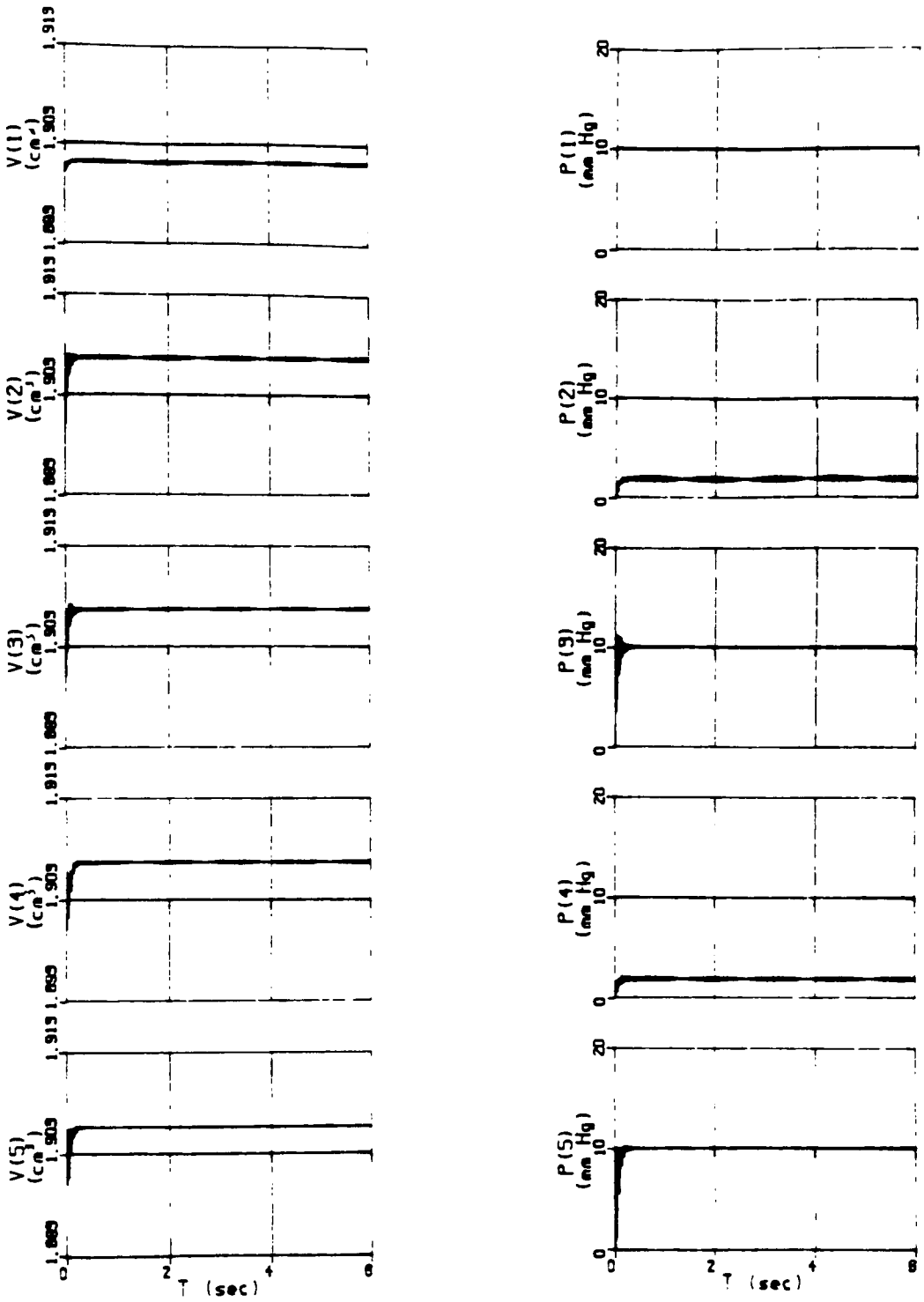

FIGURE 31 - Model 2: 5 element pressure and volume time responses

high frequency. Note also that prior to one second both pressure and volume time courses reflect the feathered step input. The internal pressure in each segment, however, is the same in every *other* segment (i.e. segment 4 mirrors segment 2, and segment 5 mirrors segment 3). (The pressure in segment 1 reflects the defined upstream pressure.) Segments 2 and 3 will be utilized as representative segments to examine changes in parameters. Figures 32 and 33 are enlarged portrayals of the pressure and volume time responses shown in Figure 31 for segments 2 and 3. Segment pressure and volume oscillations before one second are damped prior to reaching steady state. Segments 2 and 3 oscillate pressure while all segments oscillate volume. However, in the pressure response of segment 2, a secondary low frequency oscillation persists. This oscillation is present in the volume responses as well, but the amplitude is not easily observed. This oscillation physically represents a flutter of the tube wall.

Figures 34 and 35 show the system response for the increased input flow rate of 30 cc/sec. This increased flow rate had no effect on the magnitude of the steady state volumes and pressures. However, the frequency envelope at steady state is increased. This is more evident in the pressure response, shown in Figure 36.

The effects on segment internal pressure and volume for an outflow resistance increased to 0.025 mm Hg/(cc/sec) are shown in Figures 37 and 38. These graphs show that an increase in outflow resistance increases the amplitude of the envelope oscillations, but has no effect on their frequency.

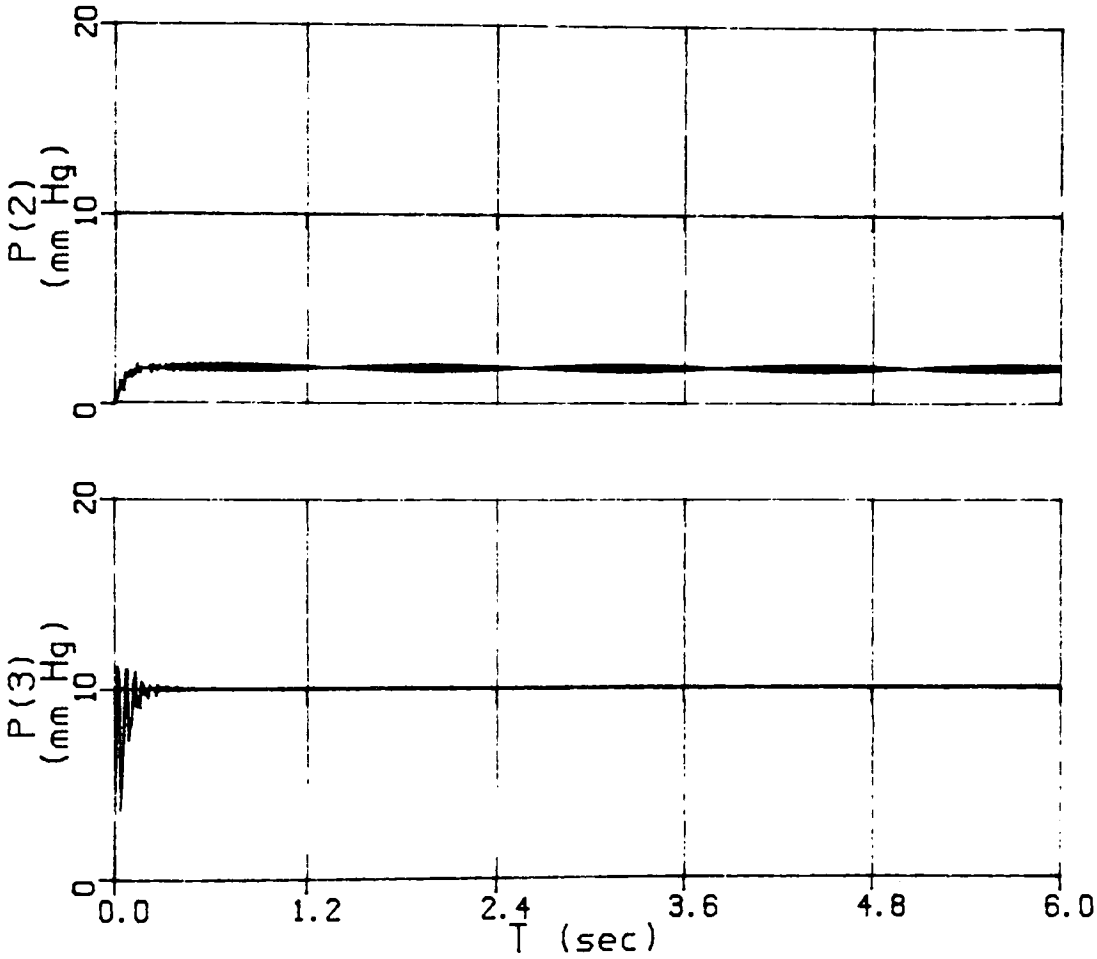

FIGURE 32 - Model 2: 5 element internal pressure responses for segments 2 and 3

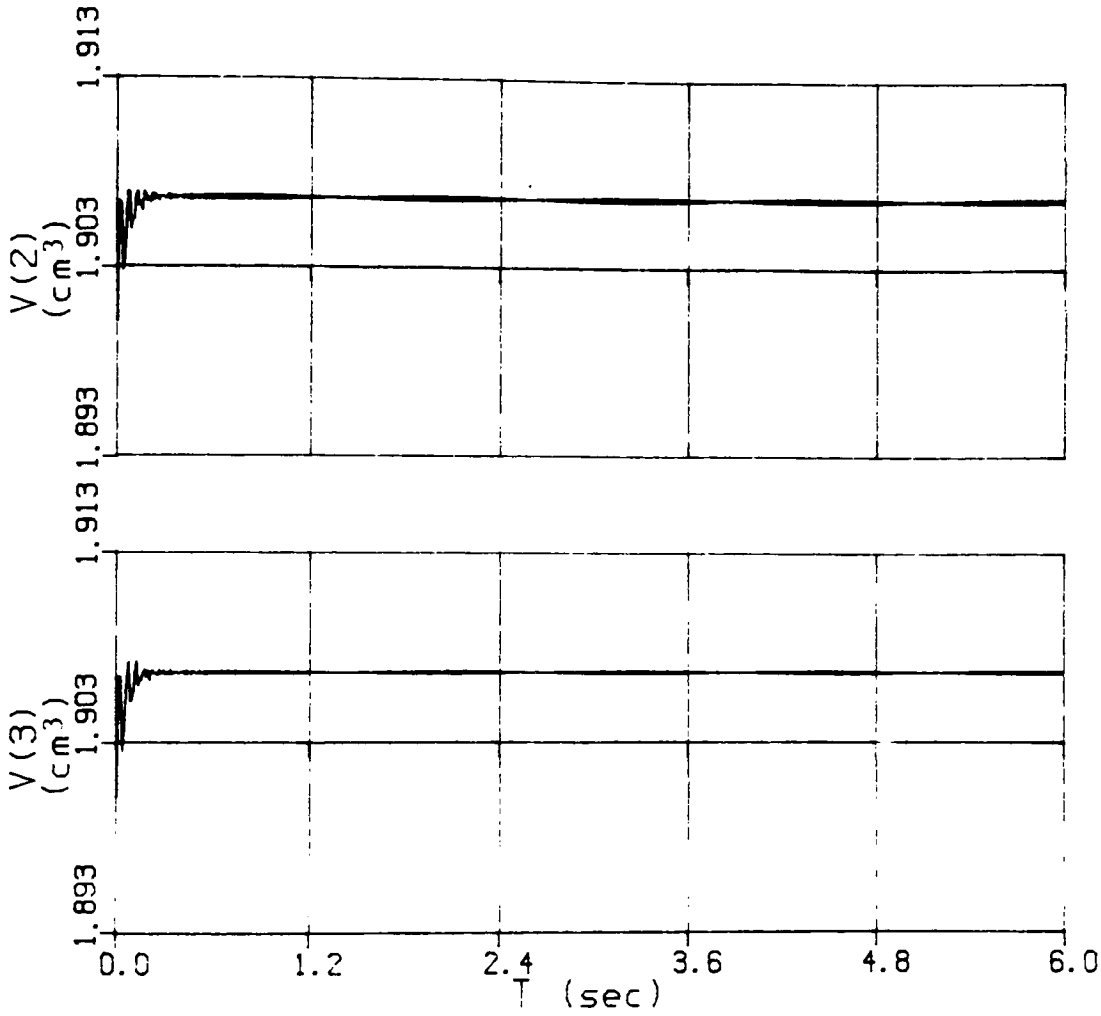

FIGURE 33 - Model 2: 5 element volume responses for segments 2 and 3

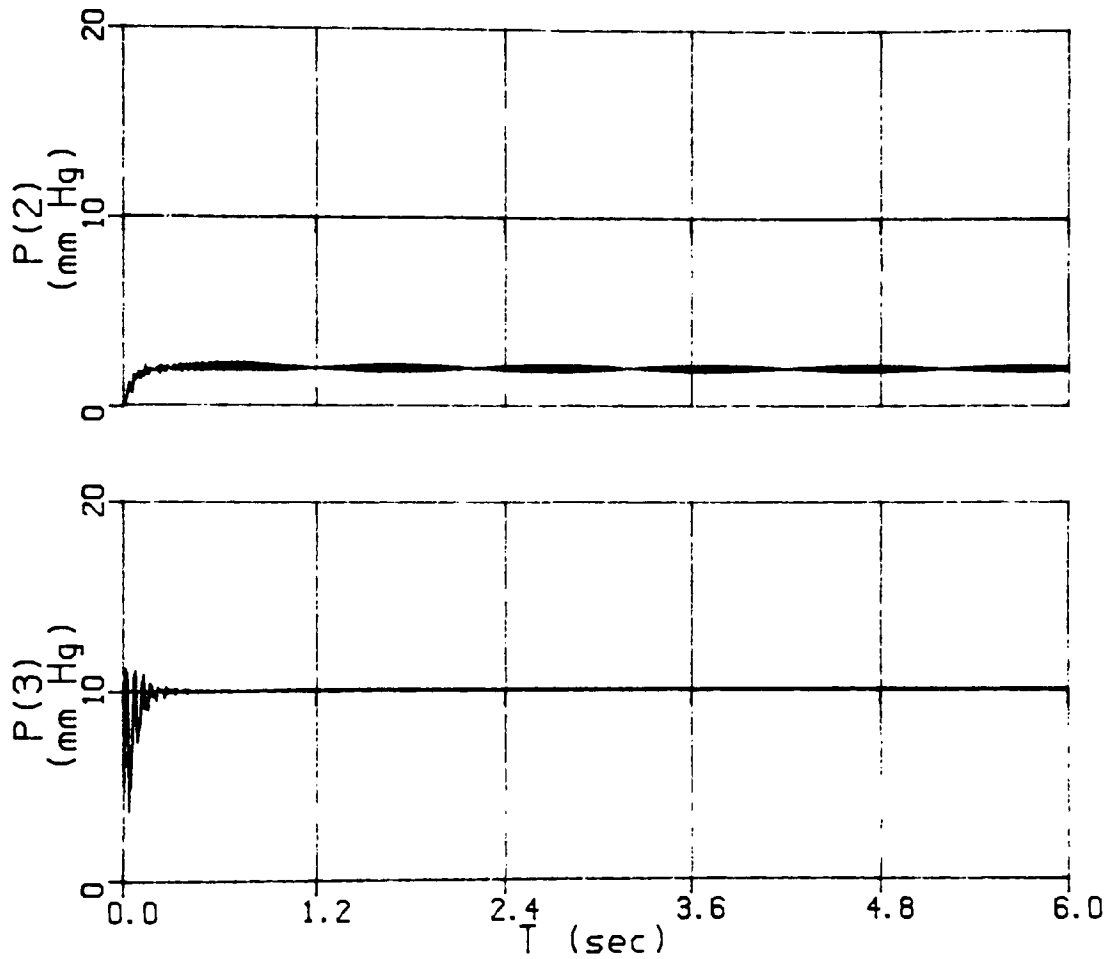

FIGURE 34 - Model 2: 5 element effect of increased flow rate on internal pressure

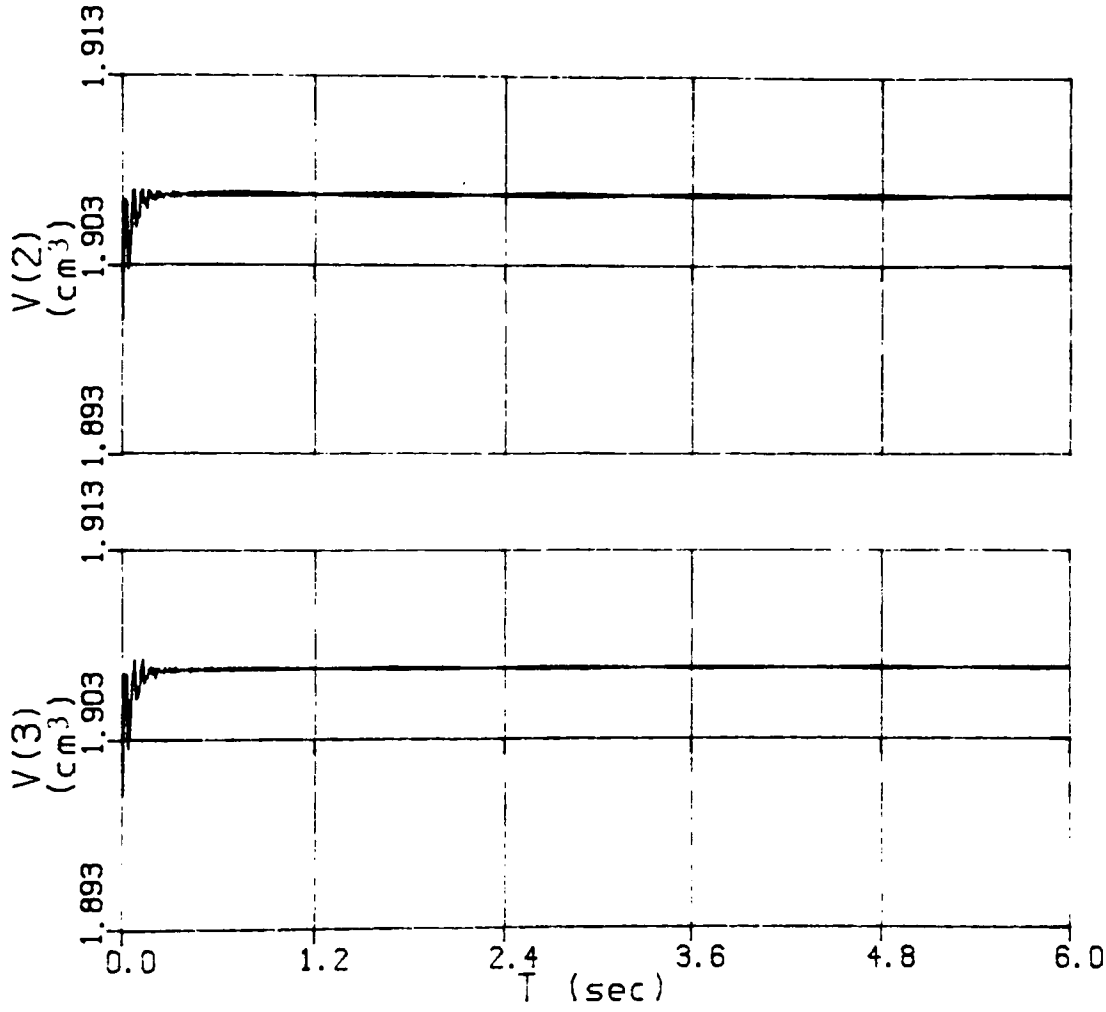

FIGURE 35 - Model 2: 5 element effect of increased flow rate on volume

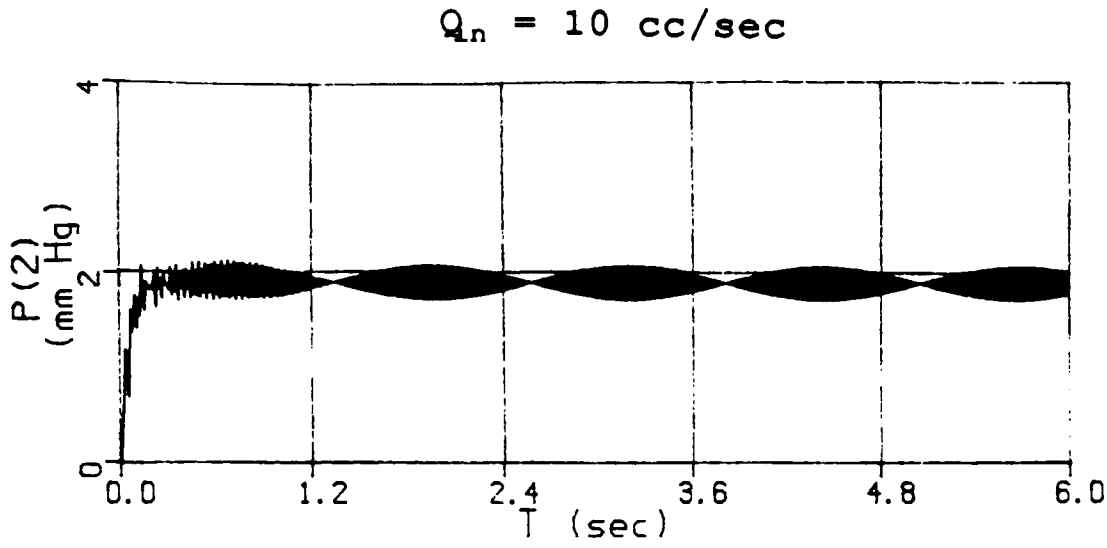

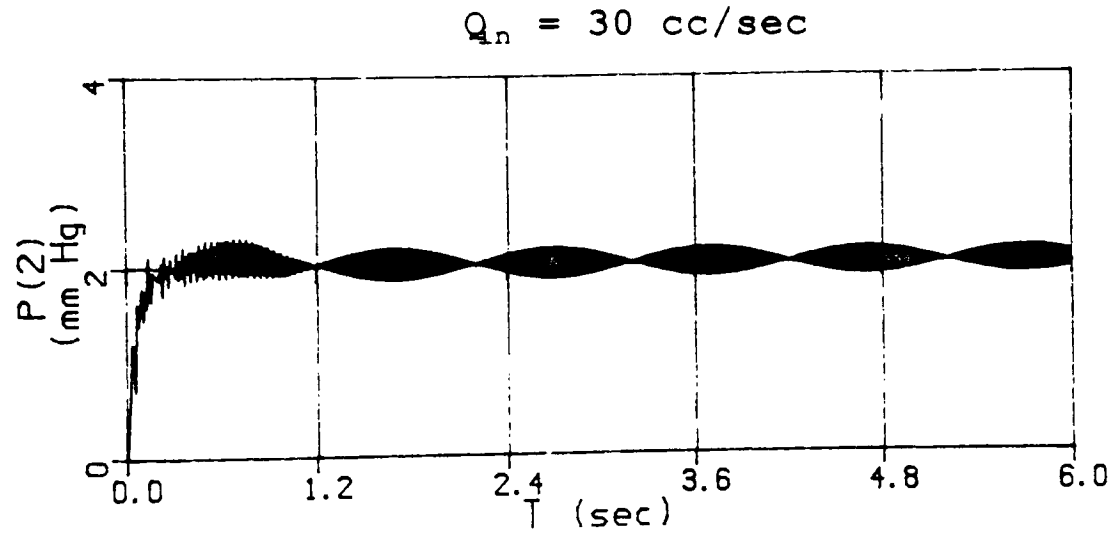

FIGURE 36 - Model 2: 5 element comparison of pressure responses for input flow rates of 10 cc/sec and 30 cc/sec

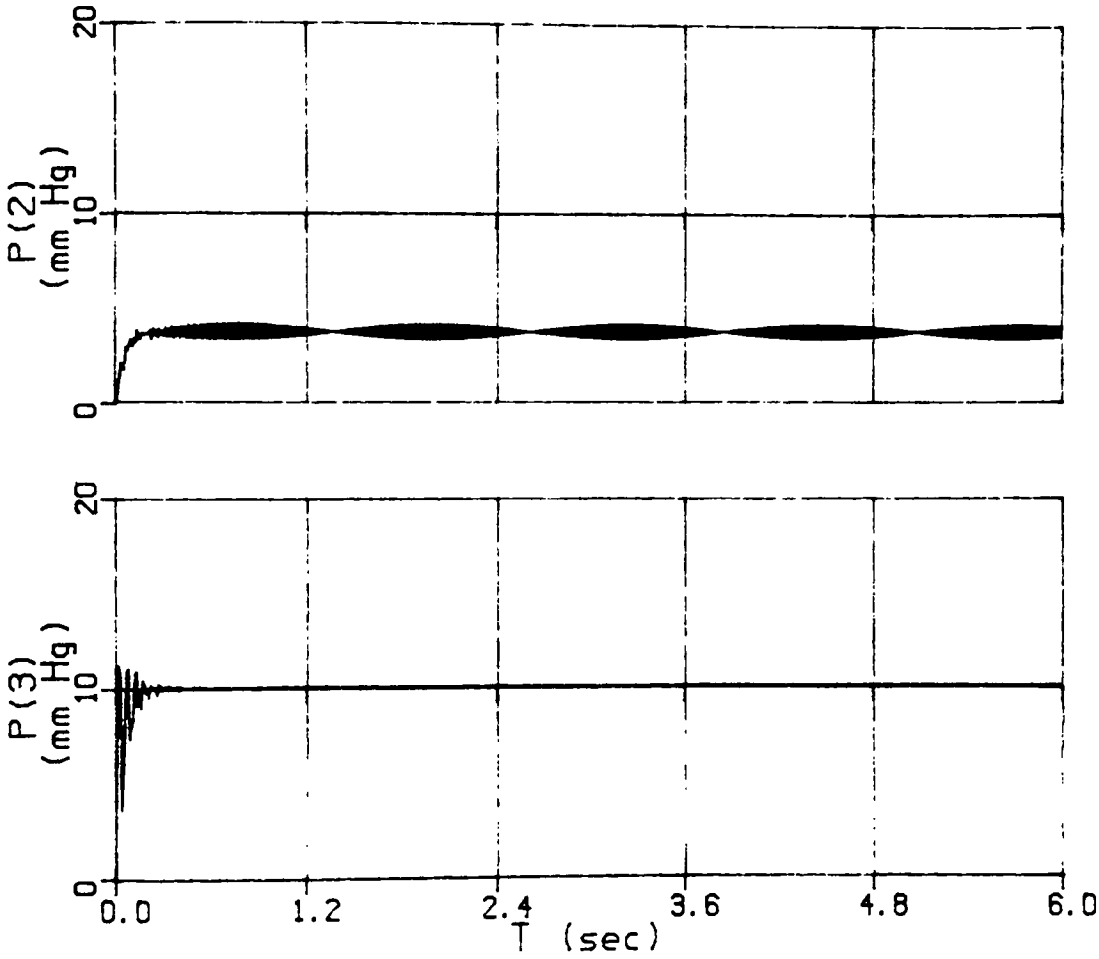

FIGURE 37 - Model 2: 5 element effect of increased outflow resistance on internal pressure

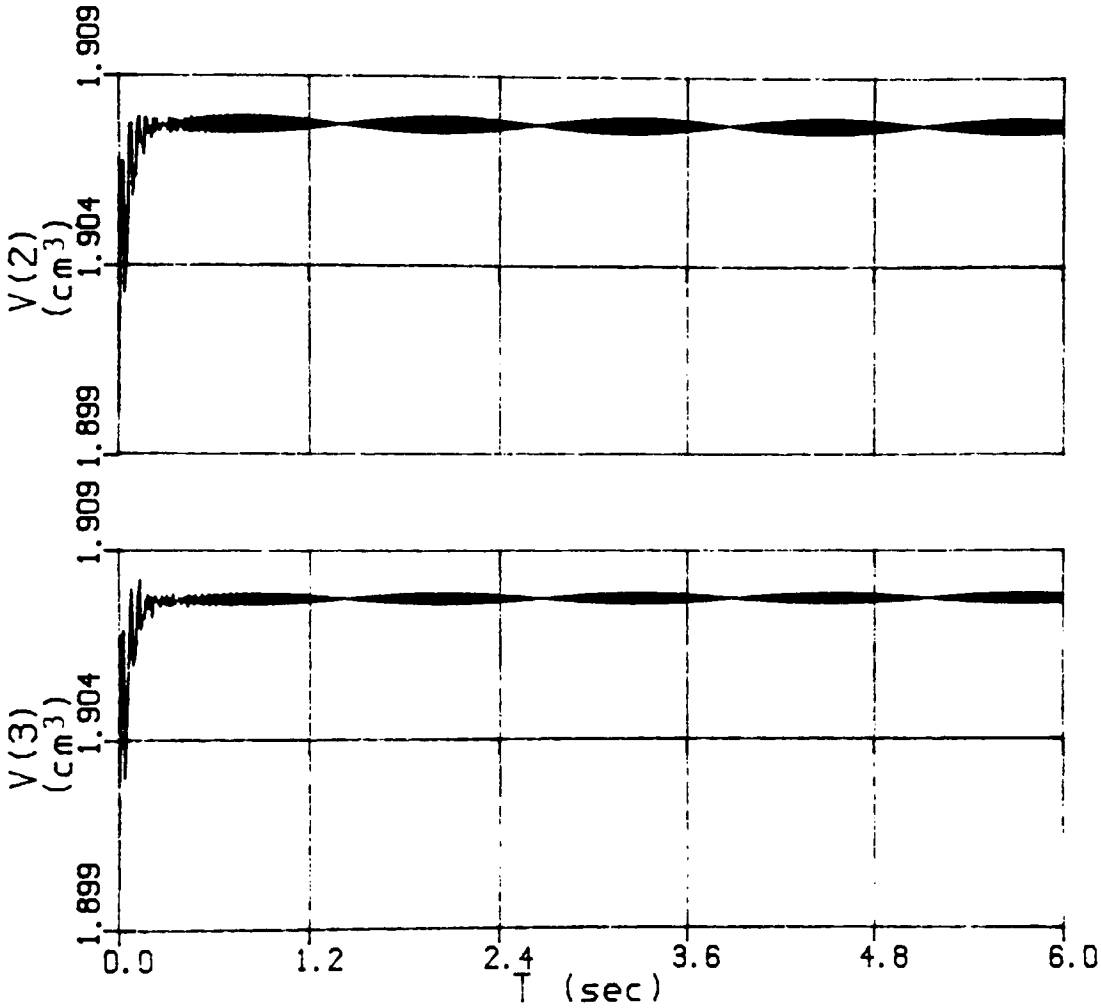

FIGURE 38 - Model 2: 5 element effect of increased outflow resistance on volume

Finally, the effect of increasing the external pressure, P_e, was investigated. In order to resolve numerical instabilities, the outflow resistance had to be increase to 0.125 mm Hg/(cc/sec) for an external pressure of 10 mm Hg. The effects on internal pressure and volume, depicted in Figures 39 and 40, respectively, show a damped oscillation envelope to steady-state conditions. An increase the external pressure, accompanied by the required increase in outflow resistance, increases the amplitude of the initial oscillations the system undergoes before reaching steady state condition. The frequency of these oscillations is, however, reduced. The same response was found in Model 1, as seen by comparing Figures 12 and 22. In addition, this increased external pressure significantly reduces the steady state volume, and has a variable effect on the internal pressure. The steady state internal pressure in segment 2 is increased, while the internal pressure in segment 5 is decreased. This seems to indicate that there may be some ideal combination of external pressure and outflow resistance which will produce a constant internal pressure throughout all segments of the tube, consistent with empirical protocol and data. Unfortunately, the number of possible combinations is endless, and the correct values were not discovered in this study. With regard to the envelope oscillations, the increase in external pressure increased their frequency, and while the amplitude was initially higher, it immediately began decreasing.

To verify that alternate segments of the tube still behaved

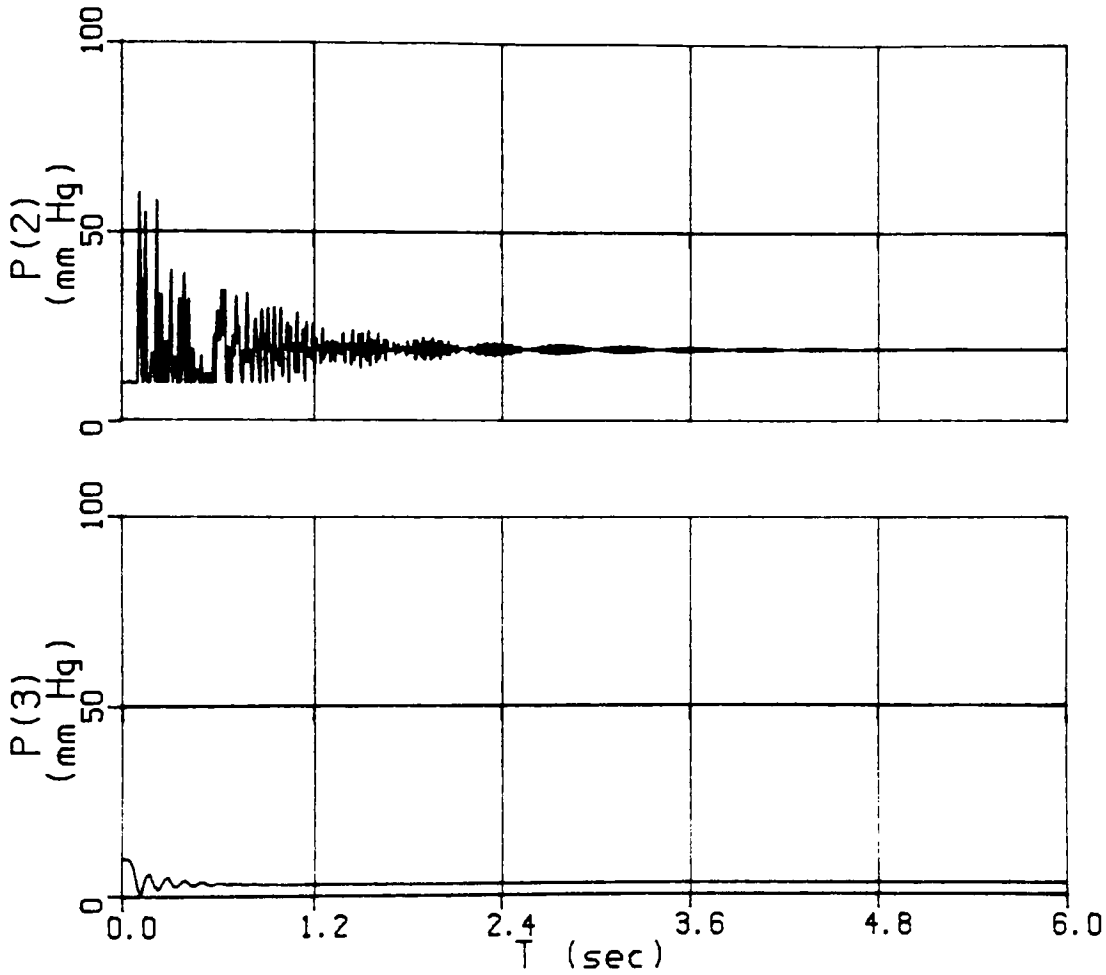

FIGURE 39 - Model 2: 5 element effect of increased external pressure on internal pressure

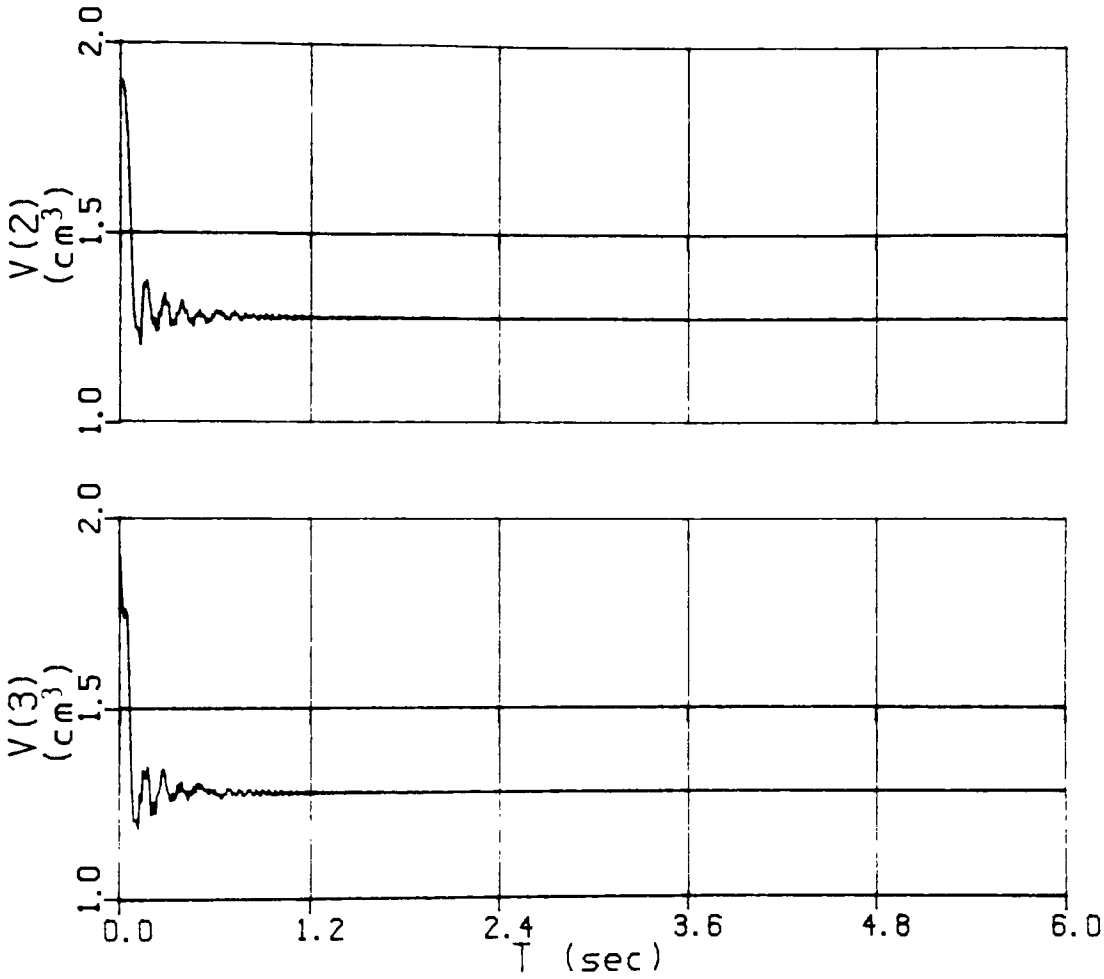

FIGURE 40 - Model 2: 5 element effect of increased external pressure on volume

in a similar fashion, the pressure responses from segments 4 and 5 are shown in Figure 41. Upon examination, it is clear that the behavior discussed above does indeed still hold. It is interesting to note, however, that the internal pressure in segment 4 is less than that of segment 2, and that the internal pressure of segment 5 is less than that of segment 3. Since segment 5 pressure is less than segment 1 pressure, a loss of pressure along the length of the tube is predicted, just as one would expect.

The major inconsistency with this model compared to any experimental apparatus is the shape of the collapsible tube at steady state. A typical tube configuration is shown below.

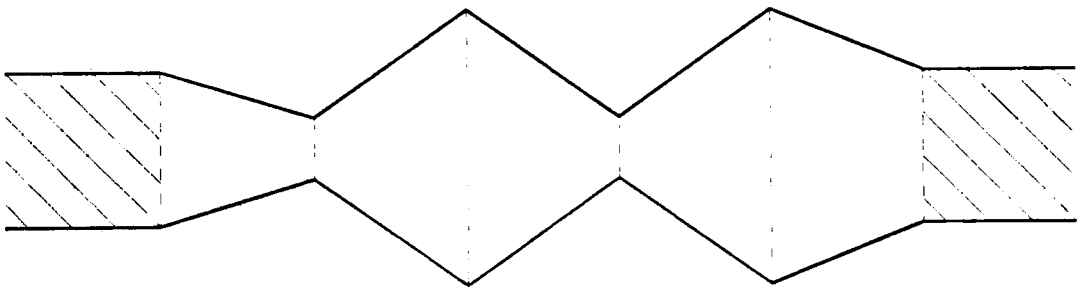

If the steady state areas of the nodes are examined, one finds that there is no slope continuity between the segments. This is because the state equations are not second order, thus the system has no control over the slope at each node. This problem was not resolved in this investigation.

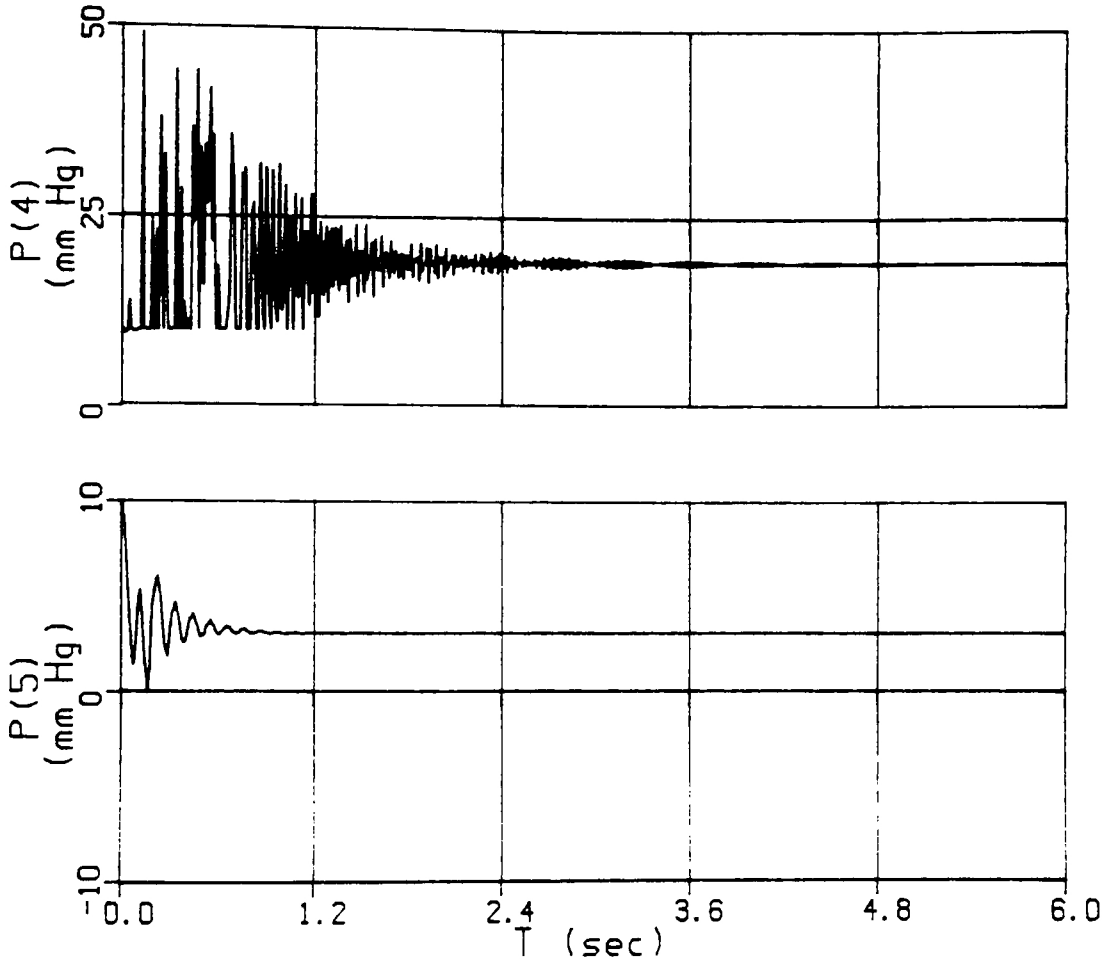

FIGURE 41 - Model 2: 5 element effect of increased external pressure on internal pressures of segments 4 and 5

5.0 SUMMARY

Although neither mathematical model was able to reproduce many of the numerous experimental results of Lyon [37] due to the manner in which her results were provided, some trends were matched. Both models showed that as the outflow resistance increased, the pressure loss along the tube decreased, and outflow pressure increased. Model 1 was able to show that for "very high" outflow resistance, the pressure loss along the tube became independent of flow rate.

The models produced somewhat conflicting pictures of the pressure and volume responses to variations in certain parameters, such as input flow rate, downstream resistance, and external pressure.

Model 1 intuitively seems more accurate since it predicts the following for viscous flow:

1. increases in both steady state volume and internal pressure for increased flow rate
2. increases in both steady state volume and internal pressure for increased outflow resistance
3. decreased steady state volume and increased internal pressure for increased external pressure

Secondary oscillations, present in Model 2, were not present in Model 1.

Model 2 had the following results for inviscid flow:

1. increased flow rate has no effect on the magnitude of steady state volume or internal pressure, but increases the frequency of the secondary oscillations
2. increased outflow resistance had no effect on steady state volume, but increased internal pressure in every *other* segment (even numbered segments), and increases the amplitude of the secondary oscillations
3. increased external pressure decreased the steady state volume and increased the internal pressure, while at the same time increasing the frequency of the secondary oscillations and increasing then decreasing their amplitude

Improvements to either model could include the incorporation of the Bernoulli resistance, and verification of the tube law that is utilized. The highly sensitive nature of the system to the tube law seems to indicate that this is an area that needs further investigation.

6.0 BIBLIOGRAPHY

1 Arts, T., and R. S. Reneman. Interaction between intramyocardial pressure (IMP) and myocardial circulation. J. of BiomechanicalEngineering. 107:51-56, 1985.

2 Barclay, W. H., and S. Thalayasingam. Self-excited oscillations in thin-walled collapsible tubes. Med. and Biol. Eng. and Comput. 24:482-487, 1986.

3 Bertram, C. D., and C. J. Raymond. Measurements of wave speed and compliance in a collapsible tube during self-excited oscillations: a test of the choking hypothesis. Med. & Biol. Eng. & Comput. 29:493-500, 1991.

4 Bertram, C. D. The effects of wall thickness, axial strain and end proximity on the pressure-area relation of collapsible tubes. J. Biomechanics. 20.9:863-876, 1987.

5 Bertram, C. D. Unstable equilibrium behavior in collapsible tubes. J. Biomechanics. 19.1:61-69, 1986.

6 Beyar, R., and S. Sideman. Time-dependent coronary blood flow distribution in left ventricular wall. Am. J. Physiol. 252(Heart Circ. Physiol. 21):H417-H433, 1987.

7 Bonsignori, F., and M. Salvini. Unidimensional steady flow in collapsible tubes with applications to blood vessels. Il Nuovo Cimento. 6d(n4):317-333, 1985.

8 Bove, A. A., W. P. Santamore, and R. A. Carey. Reduced myocardial blood flow resulting from dynamic changes in coronary artery stenosis. Internation J. of Cardiology. 4: 301-313, 1983.

9 Braakman, R., P. Sipkema, and N. Westerhof. Steady state and instantaneous pressure-flow relationships: characterisation of the canine abdominal periphery. Cardiovasculare Research. 17:577-588, 1983.

10 Bruinsma, P., T. Arts, J. Dankelman, and J. A. E. Spaan. Model of the coronary circulation based on pressure dependence of coronary resistance and compliance. Basic Res. Cardiol. 83: 510-524, 1988.

11 Cancelli, C., and T. J. Pedley. A separated-flow model for collapsible-tube oscillations. J. Fluid Mech. 157:375-404, 1985.

12 Canty, J. M., and R. E. Mates. A programmable pressure control system for coronary flow studies. Amer. J. Physiol. 243(Heart Circ. Physiol. 12):H796-H802, 1982.

13 Canty, J. M., F. J. Klocke, and R. E. Mates. Pressure and tone dependence of coronary diastolic input impedance and capacitance. Am. J. Physiol. 248(Heart Circ. Physiol.17): H700-H711, 1985.

14 Conrad, W. A. Pressure-flow relationships in collapsible tubes. IEEE Trans. on Bio-Medical Eng. BME-16(4):284-295, 1969.

15 Davis, R. B., D. J. Schneck, and W. H. Gutstein. Pulsatile flow through a branching tube with collapsing walls: volumetric flow redistribution. ASME J. of Fluids Eng. 106:430-434, 1984.

16 Elad, D., R. D. Kamm, and A. H. Shapiro. Choking phenomena in a lung-like model. ASME J. of Biomechanical Eng. 109:1-9, 1987.

17 Elad, D., A. Foux, and Y. Kivity. A model for the nonlinear elastic response of large arteries. ASME J. of Biomechanical Eng. 110:185-189, 1988.

18 Elad, D., R. D. Kamm, and A. H. Shapiro. Tube law for the intrapolmonary airway. J. Appl. Physiol. 65(1):7-13, 1988.

19 Elad, D., R. D. Kamm, and A. H. Shapiro. Mathematical simulation of forced expiration. J. Appl. Physiol. 65(1):14-25, 1988.

20 Elad, D., D. Katz, E. Kimmel, and S. Einav. Numerical schemes for unsteady fluid flow through collapsible tubes. J. of Biomedical Eng. 13(1):10-18, 1991.

21 Flaherty, J. E., J. B. Keller, and S. I. Rubinow. Post buckling behavior of elastic tubes and rings with opposite sides in contact. SIAM J. Appl. Math. 23(4):446-455, 1972.

22 Fox, Robert W., and Alan T. McDonald. Introduction to Fluid Mechanics. New York: John Wiley & Sons, Inc., 1985.

23 Fung, Y. C., S. S. Sobin, H. Tremer, M. R. T. Yen, and H. H. Ho. Patency and compliance of pulmonary veins when airway pressure exceeds blood pressure. J. Appl. Physiol. : Respirat. Environ. Exercise Physiol. 54(6):1538-1549, 1983.

24 Higgins, D. R., W. P. Santamore, A. A. Bove, and P. Nemir, Jr. Mechanism for dynamic changes in stenotic severity. Amer. J. Physiol. 249(Heart Corc. Physiol. 18):H293-H299, 1985.

25 Hoffman, J. I. E., R. W. Baer, F. L. Hanley, and L. M. Messina. Regulation of transmural myocardial blood flow. ASME J. of Biomechanical Eng. 107:2-9, 1985.

26 Holt, J. P. The collapse factor in the measurement of venous pressure. Amer. J. Physiol. 134:292-299, 1941.

27 Jan, D. L., R. D. Kamm, and A. H. Shapiro. Filling of partially collapsed compliant tubes. ASME J. of Biomechanical Eng. 105:12-19, 1983.

28 Karnopp, D., and R. Rosenberg. System Dynamics: A Unified Approach. 2nd edition, New York: John Wiley and Sons, 1990.

29 Kimmel, E., R. D. Kamm, and A. H. Shapiro. Numerical solutions for steady and unsteady flow in a model of the pulmonary airways. ASME J. of Biomechanical Eng. 110:292-299, 1988.

30 Knowlton, F. P., and E. H. Starling. The influence of variations in temperature and blood-pressure on the performance of the isolated mammalian heart. J. of Physiol. 44:206-219, 1912.

31 Krams, R., C. T. A. van Haelst, P. Sipkema, and N. Westerhof. Can coronary systolic-diastolic flow differences be predicted by left ventricular pressure or time-varying intramyocardiol elastance? Basic Res. Cardiol. 84:149-159, 1989.

32 Ku, D. N., M. N. Zeigler, and J. M. Downing. One-dimensional steady inviscid flow through a stenotic collapsible tube. ASME J. of Biomechanical Eng. 112:444-450, 1990.

33 Lee, S. Y., and G. W. Schmid-Schönbein. Pulsatile pressure and flow in the skeletal muscle microcirculation. ASME J. of Biomechanical Eng. 112:437-443, 1990.

34 Lichtenstein, O., and U. Dinnar. Experimental analysis of pulsitile flow through elastic collapsible tubes: application to cardiac assist device. ASME J. of Biomechanical Eng. 112:75-79, 1990.

35 Lloyd, T. C. Jr. Effect of inspiration on inferior vena caval blood flow in dogs. J. Appl. Physiol.: Respirat. Environ. Exercise Physiol. 55(6):1701-1708, 1983.

36 Low, H. T., and Y. T. Chew. Pressure/flow relationships in collapsible tubes: effect of upstream pressure fluctuations. Med. & Biol. Eng. & Comput. 29:217-221, 1991.

37 Lyon, C. K. "Flow through collapsible vessels." M.S. thesis, Michigan State University. 1978.

38 Lyon, C. K., J. B. Scott, and C. Y. Wang. Flow through collapsible tubes at low Reynolds numbers. Circ. Res. 47(1):68-73, 1980.

39 Lyon, C. K., J. B. Scott, D. K. Anderson, and C. Y. Wang. Flow through collapsible tubes at high Reynolds numbers. Circ. Res. 49(4):988-996, 1981.

40 Matsuzaki, Y., and T. Matsumoto. Flow in a two-dimensional collapsible channel with rigid inlet and outlet. ASME J. of Biomechanical Eng. 111:180-184, 1989.

41 Permutt, S., and R. L. Riley. Hemodynamics of collapsible vessels with tone: the vascular waterfall. J. Appl. Physiol. 18(5):924-932, 1963.

42 Porenta, G., D. F. Young, and T. R. Rogge. A finite-element model of blood flow in arteries including taper, branches, and obstructions. ASME J. of Biomechanical Eng. 108:161-167, 1986.

43 Reyn, J. W. Multiple solutions and flow limitation for steady flow through a collapsible tube held open at the ends. J. Fluid Mech. 174:467-493, 1987.

44 Rooz, E., T. F. Wiesner, R. M. Nerem. Epicardial coronary blood flow including the presence of stenoses and aorto-coronary bypass-I: model and numerical method. ASME J. of Biomechanical Eng. 107:361-367, 1985.

45 Rosenberg, R. C., and D. C. Karnopp. Introduction to Physical System Dynamics, 1st edition, New York: McGraw-Hill Book Company, 1983.

46 Shapiro, A. H. Steady flow in collapsible tubes. ASME J. of Biomechanical Eng. 126-147, August 1977.

47 Siebes, M., and D. Z. D'Argenio. Mathematical model of flow through a partially collapsible coronary stenosis. UCLA, 1990.

48 Siebes, M., "Modeling and Simulations of a Compliant Coronary Stenosis During the Cardiac Cycle", Ph.D. Thesis, University of Southern California, 1989.

49 Sipkema, P., and N. Westerhof. Mechanics of a thin walled collapsible microtube. Annals of Biomedical Eng. 17:203-217, 1989.

50 Skalak, T. C., and G. W. Schmid-Schonbein. Viscoelastic properties of microvessels in rat spinotrapezius muscle. ASME J. of Biomechanical Eng. 108:193-200, 1986.

51 Spaan, J. A. E., N. P. W. Breuls, and J. D. Laird. Diastolic-systolic coronary flow differences are caused by intramyocardial pump action in the anesthetized dog. Circ. Res. 49(3):584-593, 1981.

52 Sun, Y., and H. Gewirtz. Characterization of the coronary vascular capacitance, resistance, and flow in endocardium and epicardium based on a nonlinear dynamic analog model. IEEE Trans. on Biomedical Eng. BME-34(10):817-825, 1987.

53 Sun, Y., and H. Gewirtz. Estimation of intramyocardial pressure and coronary blood flow distribution. Am. J. Physiol. 255(Heart Circ. Physiol. 24):H664-H672, 1988.

54 Thielheim, K. O. Solitons in distensible tubes. J. Appl. Physiol. 54(6):3036-3042, 1983.

55 Tozeren, A. Elastic properties of arteries and their influence on the cardiovascular system. ASME J. of Biomechanical Eng. 106:182-185, 1984.

56 Westerhof, N., P. Sipkema, and G. A. van Huis. Coronary pressure-flow relations and the vascular waterfall. Card. Res. 17:162-169, 1983.

57 Yin, F. C. P., J. M. Cohen, J. Tsitlik, B. Zola, and M. L. Weisfeldt. Role of carotid artery resistance to collapse during high-intrathoracic-pressure CPR. Am. J. Physiol. 243(Heart Circ. Physiol. 12):H259-H267, 1982.

58 Zhuang, F. Y., Y. C. Fung, and R. T. Yen. Analysis of blood flow in cat's lung with detailed anatomical and elasticity data. Am. J. Physiol.: Respirat. Environ. Exercise Physiol. 55(4):1341-1348, 1983.

APPENDIX A - Bond Graph for Model 1

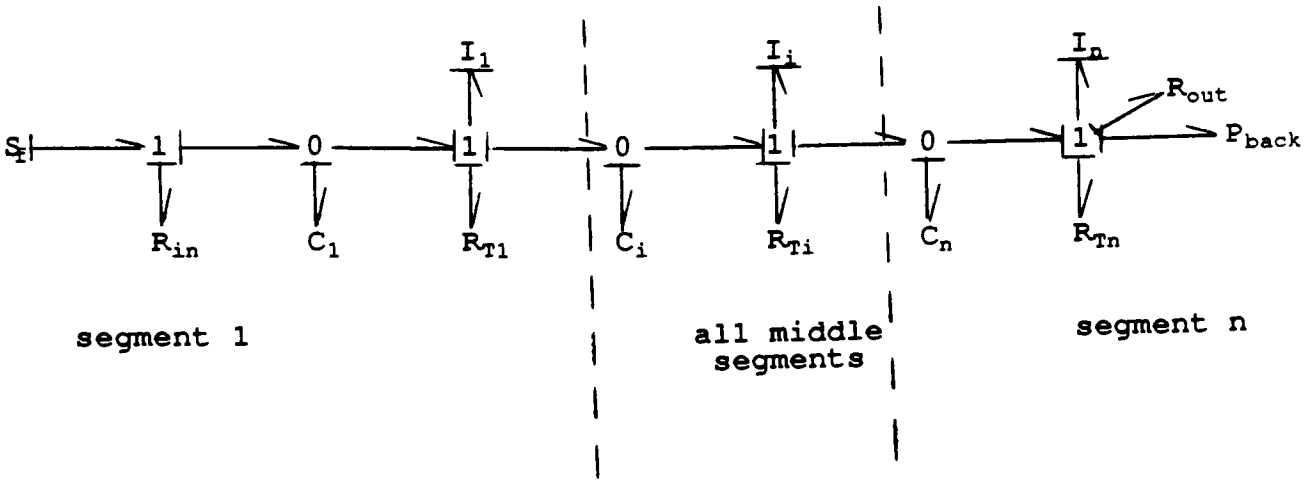

APPENDIX B - Model 1 Computer Program

```
program MODEL1

! PROGRAMMED BY:  Jennifer Lowdermilk
!
! DATE:  March 1992
!
! This program uses ACSL to predict the pressure-flow relationships
! of an incompressible, inviscid fluid in a collapsible tube, by
! examining the tube as an R-C-L circuit. The tube is divided into
! 'N' segments, each with the same tube properties.  Energy
! variables (volume and momentum) are calculated.
!
!   ARRAYS UTILIZED FOR EACH TUBE SEGMENT:
!
!        V.............volume of tube segment
!        VD............time rate of change of V
!        VIC...........initial condition of V
!        M.............momentum of fluid in tube segment
!        MD............time rate of change of M
!        MIC...........initial condition of M
!        P.............internal pressure of tube segment
!        Q.............fluid flow rate in tube segment
!        C.............capacitance of tube segment
!        I.............inductance of tube segment
!        R.............resistance of tube segment
!        AACT..........area capacitance acts on
!        A.............cross-sectional area of tube segment
!        AAVG..........average area of tube segment
!
!   CONSTANTS:
!
!        B.............magnitude of input fluid flow rate
!        LTOTAL........total length of collapsible tube
!        L.............length of individual tube segments
!        MU............fluid viscosity
!        RHO...........fluid density
!        E.............Young's Modulus of tube
!        NU............Poisson's ratio of tube
!        KP............circumferential bending stiffness of tube
!        H.............thickness of tube wall
!        RAD...........internal radius of tube
!        D0............nominal tube diameter
!        A0............nominal tube cross-sectional area
!        ROUT..........resistance of rigid tube downstream of
!                        collapsible tube
!        AMIN..........minimum allowable area of tube segment
!        AMAX..........maximum allowable area of tube segment
!        VMIN..........minimum allowable volume of tube segment
!        VENDMIN.......minimum allowable volume of either end segment
!        VMAX..........maximum allowable volume of tube segment
!        VENDMAX.......maximum allowable volume of either end segment
!        K.............constant used in capacitance calculations
!
!
!

        integer J,N,X

        constant N = 5
        parameter (maxn = 5)
        array V(maxn),VD(maxn),M(maxn),MD(maxn),...
              VIC(maxn),MIC(maxn),P(maxn),...
              Q(maxn),C(maxn),I(maxn),R(maxn),...
              AACT(maxn),A(maxn),AAVG(maxn)
```

```
        constant B = 10.0, TSTP = 6.0, PE = 0.0,...
              LTOTAL = 7.5, MU = 1.139E-5, ROUT = 0.0125,...
              RHO = 7.5E-4, E = 1200.12, NU = 0.5,...
              H = 0.032, RAD = 0.635, PI = 3.1415927

        cinterval cint = 0.01
        maxterval maxt = 0.001
        nsteps nstp = 1

! use second order Runge-Kutta method
!
        IALG = 4

initial  ! set initial conditions

        KP = (1.0/12.0)*E*((H/RAD)**3)/(1.0-(NU**2))
        A0 = PI*(RAD**2)
        L = LTOTAL/N
        D0 = 2.0*RAD
        V0 = A0*L
        K = 2.0*H*E*PI*L/D0
        VMIN = 0.08*V0
        VMAX = 4.0*V0
        VENDMIN = 0.54*V0
        VENDMAX = 2.5*V0

        X=N-1

        do 10 J=1,N
                P(J) = 0.0
                V(J) = V0
                M(J) = 0.0
                VIC(J) = V0
                MIC(J) = 0.0
                Q(J) = 0.0
                AACT(J) = PI*D0*L
        10..continue

end ! of initial


derivative

procedural

        QIN = B                                          ! step input flow rate

! segment 1

        C(1) = (AACT(1)**2)/K
        C(2) = (AACT(2)**2)/K
        P(1) = ((V(1)-V0)/C(1)) + PE
        P(2) = ((V(2)-V0)/C(2)) + PE

        A2 = AREA(P(2),PE,KP)
        A(2)=A2
        AAVG(1) = (A0+A(2))/2.0

        "I(1) = RHO*L/AAVG(1)"                           ! non-linear inductance
        I(1) = RHO*L/A0                                  ! constant inductance
        "R(1) = (8.0*MU*L*PI)/(AAVG(1)**2)"              ! non-linear resistance
        R(1) = (8.0*MU*L*PI)/(A0**2)                     ! constant resistance

        Q(1) = M(1)/I(1)
        VD1 = QIN - Q(1)
```

```
        VD(1) = VD1
        MD1 = P(1) - R(1)*Q(1) - P(2)
        MD(1) = MD1

! segments 2 through N-1

        X=N-1

        do 50 J=2,X

        C(J+1) = (AACT(J+1)**2)/K
        P(J+1) = ((V(J+1)-V0)/C(J+1)) + PE

        AJ = AREA(P(J+1),PE,KP)
        A(J+1) = AJ
        AAVG(J) = (A(J)+A(J+1))/2.0

        "I(J) = RHO*L/AAVG(J)"                    ! non-linear inductance
        I(J) = RHO*L/A0                           ! constant inductance
        "R(J) = (8.0*MU*L*PI)/(AAVG(J)**2)"       ! non-linear inductance
        R(J) = (8.0*MU*L*PI)/(A0**2)              ! constant resistance

        Q(J) = M(J)/I(J)
        VDJ = Q(J-1) - Q(J)
        VD(J) = VDJ
        MDJ = P(J) - R(J)*Q(J) - P(J+1)
        MD(J) = MDJ

        50..continue

! segment N

        PBACK = ROUT*Q(N)                    ! resistance of rigid tube

        AAVG(N) = (A(N)+A0)/2.0

        "I(N) = RHO*L/AAVG(N)"                    ! non-linear inductance
        I(N) = RHO*L/A0                           ! constant inductance
        "R(N) = (8.0*MU*L*PI)/(AAVG(N)**2)"       ! non;linear resistance
        R(N) = (8.0*MU*L*PI)/(A0**2)              ! constant resistance

        Q(N) = M(N)/I(N)
        VDN = Q(N-1) - Q(N)
        VD(N) = VDN
        MDN = P(N) - R(N)*Q(N) - PBACK
        MD(N) = MDN

! integrate

        V=INTVC(VD,VIC)
        M=INTVC(MD,MIC)

! check min/max volume restraints

        if (V(1) .le. VENDMIN) then
                V(1) = VENDMIN
        elseif (V(1) .gt. VENDMAX) then
                V(1) = VENDMAX
        endif

        do 100 J=2,X
            if (V(J) .le. VMIN) then
                V(J) = VMIN
            elseif (V(J) .gt. VMAX) then
                V(J) = VMAX
            endif
```

```
        if (V(N) .le. VENDMIN) then
                V(N) = VENDMIN
        elseif (V(N) .gt. VENDMAX) then
                V(N) = VENDMAX
        endif

        TERMT (T .ge. TSTP)

end   ! of procedural
end   ! of derivative
end   ! of program


      REAL FUNCTION  AREA(PIN,PE,KP)

C       Tube law that computes the area of the collapsible tube,
C       given the tube properties and the internal and external
C       pressures.
C
        real PIN,PE,A0,KP,AMIN,AMAX

        A0 = 1.2668
        PI = 3.1415927

        AMIN = 0.08*A0
        AMAX = 4.0*A0

        if (PIN .lt. PE) then
           AREA = A0 * (1.0/(((1.0 - ((PIN-PE)/KP))**2)**0.33333))
        else
           AREA = (PI/4.0)*((((PIN-PE)*0.000634)+(sqrt(4.0*A0/PI)))**2)
        endif

        if (AREA .lt. AMIN) AREA = AMIN
        if (AREA .gt. AMAX) AREA = AMAX

        return
        end
```

APPENDIX C - Model 2 Computer Program

```
program MODEL2
!
! PROGRAMMED BY:  Jennifer Lowdermilk
!
! DATE:  March 1992
!
! This program uses ACSL to predict the pressure-flow relationships
! of an incompressible, inviscid fluid in a collapsible tube,
! using the state equations of Shapiro [46].  The tube is divided
! into 'N' segments, each possessing the same tube properties.
! Power variables (area and velocity) are calculated.
!
!   ARRAYS UTILIZED FOR EACH TUBE SEGMENT:
!
!       U.............fluid velocity in tube segment
!       UD............time rate of change of U
!       UIC...........initial condition of U
!       A.............cross-sectional area of tube segment
!       AD............time rate of change of A
!       AIC...........initial condition of A
!       P.............internal pressure of tube segment
!       Q.............volumetric fluid flow rate in segment
!       V.............volume of tube segment
!
!   CONSTANTS:
!
!       B.............magnitude of input fluid flow rate
!       P(1)..........upstream internal pressure
!       LTOTAL........total length of collapsible tube
!       L.............length of individual tube segments
!       MU............fluid viscosity
!       RHO...........fluid density
!       E.............Young's Modulus of tube
!       NU............Poisson's ratio of tube
!       KP............circumferential bending stiffness of tube
!       H.............thickness of tube wall
!       RAD...........internal radius of tube
!       D0............nominal tube diameter
!       A0............nominal tube cross-sectional area
!       ROUT..........resistance of rigid tube downstream
!                       of collapsible tube
!       AMIN..........minimum allowable area of tube segment
!       AMAX..........maximum allowable area of tube segment
!       VMIN..........minimum allowable volume of tube segment
!       VENDMIN.......minimum allowable volume of either end segment
!       VMAX..........maximum allowable volume of tube segment
!       VENDMAX.......maximum allowable volume of either end segment
!
!
!
      integer J,N,X,Y

      constant N = 5
      parameter (maxn = 6)
      parameter (maxm = 5)
      array U(maxn),UD(maxn),A(maxn),AD(maxn),...
            UIC(maxn),AIC(maxn),V(maxm),P(maxm),...
            Q(maxn),AAVG(maxm)

      constant B = 10.0, TSTP = 10.0, TEND = 1.0,...
            LTOTAL = 7.5, AVISC = 7.5E-6, ROUT = 0.125,...
            RIN = 0.50, RHO = 7.5E-4, E = 1200.12, NU = 0.5,...
            H = 0.032, RAD = 0.635, PI = 3.1415927,...
            PE = 10.0
```

```
        cinterval cint1 = 0.01
        maxterval maxt1=0.001
        nsteps nstp1=1

initial         ! set initial conditions

        w = PI
        "KP = (1.0/12.0)*E*((H/RAD)**3)/(1.0-(NU**2))"
        "KP = 0.85326"
        KP = 1.70652
        "KP = 3.0"
        D0 = 2.0*RAD
        A0 = PI*(RAD**2)
        S = PI*D0
        L = LTOTAL/N
        V0 = A0*L
        AMIN = 0.08*A0
        AMAX = 4.0*A0
        PATM = 0.0
        PORIG = 0.0

        X = N-1
        Y = N+1

        do 10 J=1,N
                P(J) = PORIG
                U(J) = 0.0
                V(J) = V0
                A(J) = A0
                UIC(J) = 0.0
                AIC(J) = A0
                Q(J) = 0.0
        10..continue

        U(Y) = 0.0
        A(Y) = A0
        UIC(Y) = 0.0
        AIC(Y) = A0
        Q(Y) = 0.0
        PBACK = PORIG

end  ! of initial


derivative

procedural

        ! feathered ramp input flow rate

        if (T .le. TEND) then
                QIN = (B/2.0)*(cos((w*T)+PI) + 1.0)
                U(1) = QIN/A0
                UD0 = (-1.0/A0)*(B/2.0)*w*sin((w*T)+PI)
        else
                U(1) = B/A0
                UD0 = 0.0
        endif

        do 20 J=2,N
           if (A(J) .le. AMIN) then
                A(J) = AMIN
           else if (A(J) .ge. AMAX) then
                A(J) = AMAX
           endif
```

```
! check minimum/maximum area requirements

        AAVG(1) = (A0 + A(2))/2.0
        do 30 J = 2,X
          AAVG(J) = (A(J)+A(J+1))/2.0
        30..continue
        AAVG(N) = (A(N) + A0)/2.0

! compute segment's volumes and flow rates

        V(1) = AAVG(1)*L
        Q(1) = U(1)*A0
        do 40 J=2,N
           V(J) = AAVG(J)*L
           Q(J) = U(J)*A(J)
        40..continue
        Q(Y) = U(Y)*A0

! segment 1

        AD(1)=0.0
        P(1) = 10.0
        P(2) = ((PVSA(A(2)/A0))*KP)+PE
        UD1=(((RIN*A0*U(1))-P(2))/(2.0*RHO*L))+ &
             ((U(1)*(U(1)-U(2)))/(2.0*L))
        UD(1) = UD1

! segments 2 - N-1

        do 50 J=2,X

          ADJ = ((A(J)/(2.0*L))*(U(J-1)-U(J+1)))+ &
                ((U(J)/(2.0*L))*(A(J-1)-A(J+1)))
          AD(J) = ADJ
          P(J+1)=((PVSA(A(J+1)/A0))*KP)+PE
          UDJ=((P(J-1)-P(J+1))/(2.0*RHO*L))+ &
               ((U(J)*(U(J-1)-U(J+1)))/(2.0*L))
          UD(J) = UDJ

        50..continue

! segment N

        ADN = ((A(N)/(2.0*L))*(U(X)-U(Y)))+ &
              ((U(N)/(2.0*L))*(A(X)-A0))
        AD(N) = ADN
        PBACK = (ROUT*A0*U(6)) + PATM
        UDN=((P(N-1)-PBACK)/(2.0*RHO*L))+ &
             ((U(N)*(U(N-1)-U(N+1)))/(2.0*L))
        UD(N) = UDN

! end conditions

        UDY=((P(N)-PATM)/(2.0*RHO*L))+ &
             ((U(Y)*(U(N)-U(Y)))/(2.0*L))
        UD(Y) = UDY
        AD(Y) = 0.0

! integrate

        U=INTVC(UD,UIC)
        A=INTVC(AD,AIC)

! calculate pressure loss along tube length
```

```
        PLOSS = P(1) - PBACK

        TERMT (T .ge. TSTP)

end   ! of procedural
end   ! of derivative
end   ! of program

      real function PVSA(AR)


C       This functions uses the tube law to determine the
C       pressure difference between internal and external
C       pressure given the area ratio

        if (AR .le. 1.0) then
                PVSA = 1.0 - (1.0/(sqrt(AR**3)))
        else
                PVSA = 1016.5743*(AR - 1.0)
        endif

        return
        end
```